Improving Power System Voltage Regulation: A Capacitive Ladder-based Power Electronic AC Voltage Regulator

By

Abolfazl Babaei

A Thesis submitted to the Faculty of Graduate Studies of

The University of Manitoba

in partial fulfilment of the requirements of the degree of

Winnipeg, Manitoba

Doctor of Philosophy

Department of Electrical and Computer Engineering

University of Manitoba

Winnipeg, Manitoba

Use of Copyright Material

Author's Declaration

I hereby declare that I am the sole author of this thesis. This is a true copy of the thesis, including any required final revisions, as accepted by my examiners. I understand that my thesis may be made available to the public electronically.

Abstract

This thesis proposes a new circuit topology for a capacitive ladder-based electronic voltage regulator (CL-EVR) which is a substitute for an electromechanical tap changer in power transformers. The proposed CL-EVR employs a combination of capacitors and TRIACs to generate voltage steps that can be added or subtracted from the grid voltage to achieve voltage regulation. In comparison to traditional on-load tap changers (OLTC), the CL-EVR is much faster and also eliminates arcing while increasing the speed of the voltage regulation, thereby potentially increasing the operating lifetime of transformers and reducing failures. Other advantages over conventional OLTCs are the elimination of di/dt limiting reactors and numerous tap changer contact leads to a potentially lower cost.

The thesis begins with an examination of traditional approaches to voltage regulation such as electromechanical and solid-state tap changing transformers. Improved models for the change-over switch are introduced and used to design a better change-over switch. The focus then shifts to the *pièce de résistance* which is an entirely new topology. A converter-based on-load tap changer (COLTC) is proposed to be used as a substitute for the traditional tap changers. The proposed COLTC improves the transient behaviour, arcing, and response time as compared to the traditional tap changers.

The proposed design includes a new failure detection method that detects a failed TRIAC switch and isolates it from the circuit not only to prevent further damage to the other CL-EVR elements but also to continue the voltage regulation, albeit with a slightly reduced capacity.

To ascertain its performance and stability over the operating range, the thesis conducts a comprehensive theoretical analysis encompassing the steady state and transient

performance of a simplified system consisting of the CL-EVR connected to resistive or inductive loads.

A series of Electromagnetic Transient (EMT) simulations are conducted in order to investigate the CL-EVRS operation over a wider operating range and to fine-tune the component values and to coordinate the various control loops and to select the control system parameters. EMT simulation is also used to ensure the successful operation of the failure detection and protection strategy.

Finally, a single-phase leg rated at 33 kVA of the full three-phase 100 kVA design was prototyped in the laboratory and successfully tested under inductive and resistive loads. The results prove that the proposed CL-EVR can apply different voltage levels properly without significant overshoot during the transition from one level to the other.

Acknowledgments

I would like to extend my sincere gratitude to my advisor Prof. Aniruddha Gole for the continuous support, valuable comments, and amazing five years that I had under his supervision.

I would like to extend my appreciation to Dr. Waldemar Ziomek for the valuable comments and guidance throughout the course of this work.

I would also like to thank other members of advisory committee, Dr. Matt Khoshdarregi and Prof. Brian Johnson, for their comments and feedback on my thesis.

I would like to thank PTI Transformers LP for the generous support of my Ph.D. project.

Dedication

I would like to dedicate this thesis to my wife, Zahra, and my son, Nick, for bearing with me during this hard journey. Without their support, I would never succeed.

I would like to thank my family, especially my mother, for their support and encouragements.

Table of Contents

List of Tables

List of Figures

Chapter 1: Introduction and Literature Review

1.1 Introduction

The electricity generated in power plants is transmitted over a transmission system at high voltage levels. At distribution substations, transformers are used to step down the voltage to a smaller magnitude suitable for the different loads within the distribution network. Voltage regulation is very important since an increasing share of intermittent and highly variable renewable energy generation connected at the distribution level leads to larger and more frequent voltage fluctuations in distribution systems. Thus, utilizing on-load tap changers (OLTC) in transformers operating in power systems is becoming more necessary, as distribution systems with large amounts of renewable energy generation become more commonplace [1-3].

The OLTC as a voltage regulator is widely used in existing power delivery systems, such as HVdc, HVac, Renewable Energy connections, and power transformers. Currently, conventional electromechanical type OLTCs for power transformers are commonly

utilized, as they enable under-load operations, i.e. change of the output voltage under load, without interrupting the load current [3-5]. However, there are some downsides associated with electromechanical tap changers. A significant issue in these electromechanical tap changers is that there is always an arc generated during operation between tap contacts. This arcing process causes the deterioration of transformer oil. As far as the lifetime of the electromechanical tap changers is concerned, they have a relatively long lifetime – around 10 to 15 years – and this is mostly due to the lower number of tap changing operations. A small number of taps is a disadvantage for mechanical taps, as the voltage fluctuation is larger and faster in today's distribution networks due to the increasing share of distributed renewable energy sources. Therefore, OLTC transformers need to perform many more switching operations than before. This results in much higher maintenance requirements, and a more limited lifetime. Apart from electromechanical tap changers, other types of electronic tap changers have been introduced to the market [1]. They use solid-state electronic switches, such as thyristors, instead of electromechanical taps to regulate the output voltage level. Although the electronic tap changers could solve arcing problems present in mechanical tap changers, there are still issues, such as:

- the generation of harmonics
- voltage level change speeds, the soft start of the regulator,
- lack of failure detection of solid-state switches
- volume demands of regulators that need to be considered

Although improvements in voltage and current control methods have been proposed in the previous research, there are still issues in the solid-state transformers yet to be solved. Those challenges will be discussed in chapter 2.

This thesis proposes a new fully electronic voltage regulator which can be used as a substitute for electromechanical and solid-state tap changers for transformers. The presented voltage regulator can solve the aforementioned problems associated with the electromechanical and solid-state tap changers.

1.2   Literature Review

Overall, several published studies and patents worked on conventional tap changing transformers, converter-based transformers, and the transient behaviour of tap changing transformers. Also, two IEEE standards for transformers have been investigated. The key ones are summarized below.

In [1-9], two important IEEE standards for transformers, IEEE STDVUOD20810 and IEEE C57.12.59, have been investigated. Also, the popular structures of tap changing transformers and challenges in OLTCs were studied. Theoretical equations have been proposed. Also, standards for the tap changers are proposed under different applications have been released as well. The failure rate of the power transformer because of the failure of the tap changers is investigated [4].

In [10], an arc-less approach has been proposed for the tap changing transformer. This paper proposed a thyristor-assisted tap-changing transformer. Thyristors were used

instead of mechanical tap leads to increase the speed of switching between the tap voltage level.

In [11], a static on-load tap-changer is suggested as an alternative to the mechanical type of tap-changers. Without any phase shift, this method can control the load voltage variation.

In [12-13], a solid-state on-load tap changer with microcontroller-based controller is proposed to increase the speed of switching in the tap changer transformer as well improving the transient behaviour. Also, this paper ran a prototype by using insulated gate bipolar transistor (IGBT) switches.

In [14], an electronic tap changing transformer has been presented. The paper claimed that the proposed electronic tap changing transformer is more cost-effective than the conventional tap changer transformers.

In [15-17], an optimized approach for the electronic tap changing transformers has been proposed. This approach uses a new control method by which fewer thyristor switches will be used in a tap-changer transformer. This paper's method is claimed to be a cost-effective one.

In [18], this paper presents the design, theoretical analysis, and experimental approach for a quick OLTC regulator. The control system was programmed by a DSP, which claimed to be a fast response control system. Also, a two-step commutation method is used.

In [19-29], some popular electronic-assisted tap changer for distribution purposes is proposed. The physical layout of the proposed structures is unique and meant to

improve the dielectric withstand. Also, different control methods are proposed to enhance the transient behaviour of the electronic-assisted tap-changer transformers.

Publications [30-34] investigate the switching methods to eliminate any interruption in the output voltage while changing from one voltage level to the other. The acoustic signal and empirical mode decomposition algorithm were utilized to identify the switching state. The proposed methods are fast and remove the effect of circulating current.

In [35-40], mechanical taps were removed and solid-state switches such as thyristors were proposed in on-load tap changers. The proposed methods in these papers reduce the arc in the tap changer to a large extent. However, the literature did not consider the transient effect of the change-over switch.

In [41], the transient behaviour of the OLTC during change-over operation. The result of [41] shows that the change-over switch in the conventional tap changing transformers is experiencing a high-level transient voltage, which can cause full transformer failure.

In [42], a voltage regulation approach suitable for the distributed generation (DG) was proposed. The voltage regulation was performed based on the reactive power adjustment. The proposed approach was examined under a wide range of balanced and unbalanced loads in [43-44].

Using converters as a substitute for the conventional tap changers has been proposed a solution to manage the issues corresponding to electro-mechanical tap changers. Different converters have been investigated. In [45-69], different structures of multilevel inverters have been proposed. Those papers have tested the multilevel

inverters in different applications such as photovoltaic systems, wind generation, DC-AC conversion, etc. The switching strategies and harmonic studies have been investigated in [45-60]. The transient behaviour, reliability studies, and power capability have also been studied.

In [61], a high switching frequency 10 kV solid-state transformer with soft switching is presented. The dead time has been improved in this method, so there is no interruption in the output voltage. Also, the high-frequency design reduces the size of the transformer to a large extent.

In [70], a converter-based solution has been proposed in order to remove the transient effect of the change-over switch and remove the need for the tie-in resistor. The result of the paper was validated by a simulation in PLECS software. The proposed converter in [70] could maintain the load voltage in an acceptable range in resistive and inductive load conditions.

1.3 Gaps in Existing Research

- Although various improvements to electromechanical tap changer transformers have been proposed, they all assume the same transformer topology. The electromechanical tap changers have the issues of arcing and pitting on contacts, low response time, high transient voltage and current, and high maintenance cost. The solution to the electromechanical tap changer is to replace the mechanical switches by semiconductor devices such as Insulated Gate Bipolar Transistors (IGBT), Triode for Alternating Current (TRIAC), and Gate Turnoff Thyristors (GTO) in order to improve the speed of operation. Optimization is carried out to improve arcing by controlling power factor and thus enhancing reliability. However, there are still yet-to-be solved issues

associated with solid-state voltage regulators including high-stress voltage on the power devices, high harmonic level, and lack of failure detection method.

- In the previous methods, the transient behaviour of the change-over switch has not been considered, although the change-over switch when passing through a neutral tap is under high-level transient voltage driven by capacitive coupling of a tap winding to neighbouring winding(s) and grounded components.

- The power electronic switches, such as TRIACs are under high transient voltage in a tap changing transformer, and no failure detection method is proposed if the power switches fail. Therefore, under the failure of one switch, the tap changer transformer will shut down. Considering the mentioned points, failure detection and the self-healing process are missing points in the previous literature.

1.4 Objectives and Procedures of the Research

This thesis proposes a new voltage regulator that can be used as a substitute for the existing tap-changer transformers. In order to prove the capability and robustness of the proposed voltage regulator, the following steps will be addressed in particular.

- Electromagnetic Transient (EMT) modelling and study to determine the suitable circuit and control coordination are proposed.

- A comprehensive analysis of the overall system, i.e. theoretical calculation, transient studies, and experimental tests will be performed.

1.5 Thesis Organization

The contents of this thesis are organized in the following manner:

Chapter 2 provides deep insight into the background of electromechanical, solid-state, and converter-based tap-changer transformers. Chapter 3 provides a new model to investigate the transient behaviour of the OLTC during the change-over switch operation. Chapter 4 discusses a new model for a converter-based OLTC (COLTC). In Chapter 5, the detailed descriptions, theoretical analysis, EMT simulation, and experimental results are discussed. Finally, in chapter 6, the contributions, conclusions and future works will be discussed.

Chapter 2: Background to Voltage Regulators in Power Systems

2.1 Transformers equipped with tap changers

One of the commonly applied ways to regulate voltage in the power system was the use of tap-changer transformers. A tap changer is a device fitted to power transformers for regulation of the output voltage to required levels. This can be obtained by changing the ratios of the transformers by changing the number of turns in one winding of the appropriate transformer. The main goal of using a tap-changer transformer is to maintain the voltage within an acceptable range.

Tap changers can be either on-load or off-load. On-load tap changers have been used in the power distribution industry for over 90 years. They typically include a selector switch and a diverter switch which are responsible for transferring current from one voltage level to the other.

1. Three-limb core
2. LV Winding
3. HV Winding
4. Tapped Winding
5. Tap Leads
6. LV Bushings
7. HV Bushings
8. Clamping Frame
9. On-Load Tap Changer
10. Motor Drive
11. Tank
12. Conservator
13. Radiators
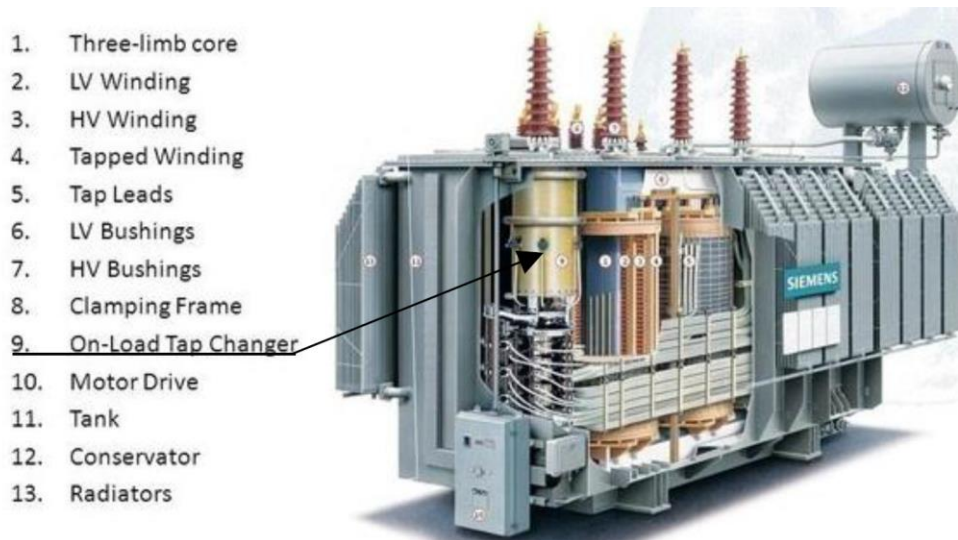
Figure 2.1: The general layout of the transformer with on-load tap-changer [71].

Figure 2.1 shows a general layout of the power transformer with an On-load Tap Changer (OLTC). On-load tap-changers may include a diverter switch and tap selector. The tap selector provides an elementary selection of the requested tap which is then connected to the dead side of the diverter switch. The subsequent diverter switch operation can result in this tap then taking on the operating current. During the tap-change operation, the functions of the diverter switch and tap selector are therefore coordinated [1-4].

Sometimes, a "change over switch" is used to reverse the polarity of the injected voltage to obtain a larger voltage range without adding more windings.   Figure 2.2 shows a delta-connected transformer with the tap winding having a change-over switch.
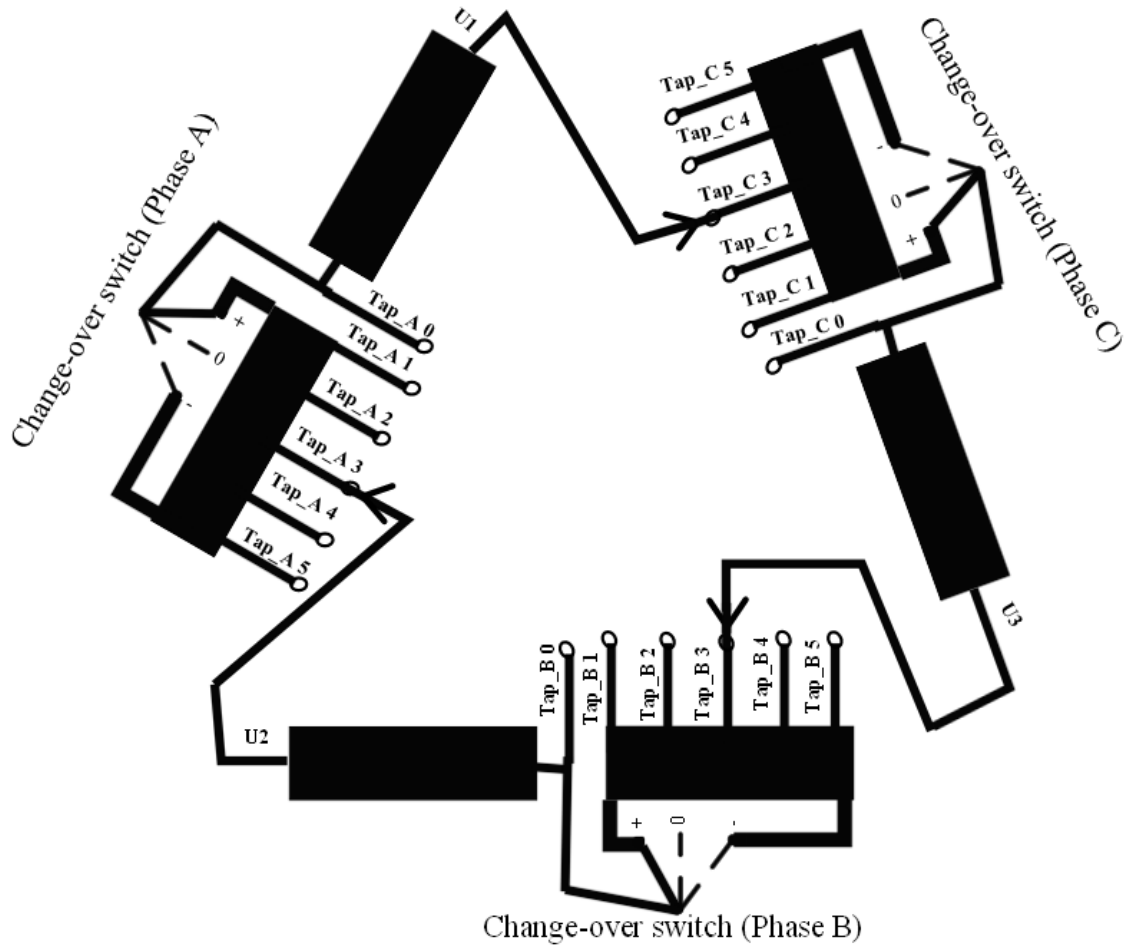
Figure 2.2: A delta-connected transformer with a tap changer having a change-over switch [41].

2.2   Solid-state tap changers

The mechanical tap changers have some significant downsides such as mechanical losses, more time for switching between taps, arc issues, and need for frequent maintenance [11-23]. The development of power electronic solid-state switches helped the operations of the tap changing transformer have been enhanced to a significant extent [1]. The different types

of semiconductors devices used include MOSFET[1], TRIAC[2], GTO[3], and IGBT[4]. Utilizing the solid-state semiconductors in tap-changer transformers removes arcing issues, increases the switching speed, and reduces the requirement for frequent and expensive maintenance for the transformers required frequent tap operation. A hybrid configuration is also proposed by numerous researchers, as this configuration can be a protection against fault currents. Figure 2.3 shows a hybrid configuration of three-phase delta-connected tap changing transformers. In this figure, tap leads are connected to thyristors.
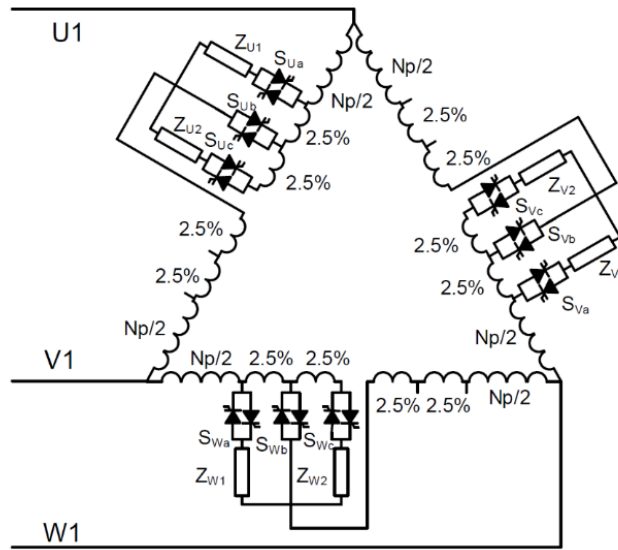
Figure 2.3: The hybrid configuration of a three-phase delta connected tap changing transformers [9].

In the power system, transformers are one of the most expensive parts. If any damage happens to the power transformer, the distribution system may shut down. Winding faults

---

[1] Metal oxide field-effect transistor
[2] triode for alternating current
[3] gate turn off thyristor
[4] insulated gate bi-polar transistor

and load tap changers are the major contributors to power transformer failures. According to the results shown in [4], OLTCs are the most significant contributor to the failure of the power transformers. Different approaches have been taken to reduce the possible failure of the tap-changer transformers by studying the transient behaviour of OLTCs [72-78]. An excessive rate of rise in transient voltage $\left(\frac{dv}{dt}\right)$ or current $\left(\frac{di}{dt}\right)$ is a major reason for the failure of the OLTCs. R-C snubber circuits are an effective solution to this issue as they limit the rate of voltage rise across the delicate semiconductor device. In [79], the snubber circuit has been added to the OLTC's circuit to manage the transient voltage and current. The results showed that the transient response of the OLTCs was improved to a large extent.

2.3   Problems with the change-over switch

Another reason for the failure of the tap winding is the change-over switch because there is a transient associated with operating the change-over switch at a neutral tap position, as its operation discharges parasitic capacitance. However, previous literature did not investigate the transient behaviour of the change-over switch. Considering this, a model is proposed in the next chapter of the thesis to predict the transient voltage and current of the OLTC [41].

2.4   Converter-based voltage regulators

Recently, Voltage Sourced Converters (VSC) have also been used as a substitute for conventional tap changers [70]. Multilevel inverters convert the DC voltage to AC voltage of selectable magnitude. The literature discusses several different types of VSC topologies

such as the diode-clamped, cascaded h-bridge, flying capacitor, etc. Figure 2.4 shows one configuration of the converter-based OLTC where a five-level inverter is used to convert DC voltage generated by solar cells to AC voltage, and then this voltage is in series with the grid voltage through a tapped winding. If the grid voltage changes to a certain limit, the converter-based OLTC applies the voltage to compensate for that change and to maintain the load voltage in an acceptable range.
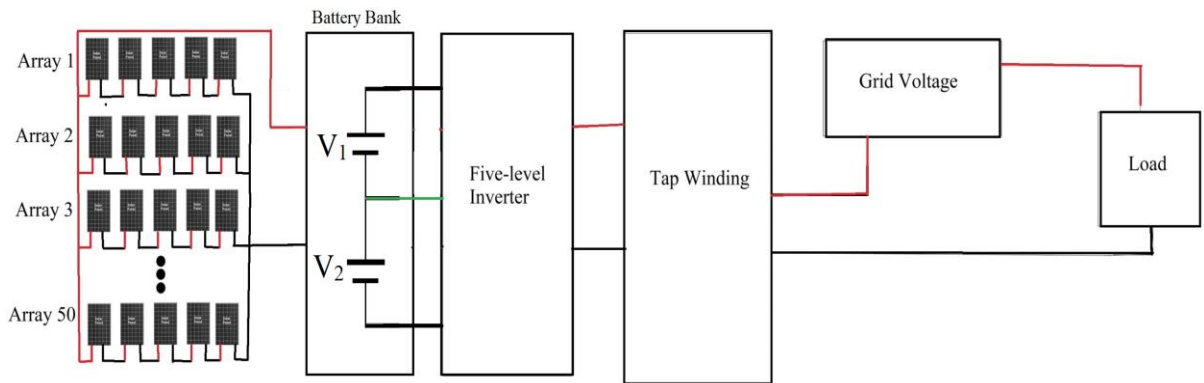
Figure 2.4: The Topology of a converter-based OLTC [61].

2.4.1   Benefits of the converter-based solution

- The converter-based OLTC can intrinsically inject subtractive or additive voltages. This eliminates the need for the change-over switch and tie-in resistor.

- The presence of the Multilevel Inverter (MLI) facilitates connection to photo-voltaic solar generators [70].

2.4.2   The problems with the converter-based tap changers

The converter-based OLTC (or COLTC) still has some drawbacks:

- high implementation cost, especially for higher currents.

- Needs a LC filter to make the MLI output purely sinusoidal

- Not easy to detect failures of the solid-state switching elements, which adds more cost for the detection circuit.

The thesis also investigates a VSC-based solution for the OLTC where a VSC is connected via a booster winding in series with the main transformer winding to provide an injection of variable magnitude voltage thereby mimicking the operation of a tapped winding. The VSC-based tap changer will be discussed in chapter 4.

Chapter 3: Change-over switch transient behaviour

3.1 Introduction

This thesis aims to come up with an improved voltage regulator. Hence, I started first by trying to improve existing topologies such as the electromechanical or solid-state tap changers. A central problem with the device is a transient associated with operating the change-over switch at a neutral tap position which creates arcing and loss of useful life.

In the previous chapter, a background for the on-load tap-changer transformer was provided. In addition, the different types of electromechanical tap-changer were introduced as well. In addition, the basic definition of OLTC was discussed, and also the reasons for the failure of the tap changer were mentioned as well. In this chapter, a model is provided to study the transient characteristics of OLTC during the change-over operation.

The operation of OLTCs corresponds to a sequence of switching events within defined timing intervals. The main goal of these switching operations is to compensate over and under voltages stemming from load variations [1]. The high-reliability operation of power

transformers is crucial, as it can reduce the number of power outages and costs associated with maintenance. Typically, OLTCs are one of the most expensive and vulnerable parts of transformers with the majority of power transformer failures occurring due to a defect in its windings [2]-[3]. The winding failures can be mechanical in origin, initiated by a current surge that causes the winding structure to deform. However, the transients related to OLTC tap changing are not so critical, as modern tap changers use vacuum interrupter technology. When the vacuum interrupter opens while changing the taps, the created arc is fully contained in the vacuum chamber and does not contaminate the oil with the products that result from an arc in the oil. So far, existing research has proposed ways to decrease the adverse effects of surge currents and voltages on the OLTCs. For example, publications [4-7], discuss optimized switching so that the switching from one tap to another does not create a break in a circuit which has an inductive characteristic.

Acoustic signals have also been employed to determine the switching state of the mechanical tap changer. This method is sufficiently fast to enable the protection unit to avoid any long-time circulating current and open-circuit voltages. In [8], solid-state switches such as thyristors were used in the tap changer transformer to change the position of the tap. Although [8] paper did not consider the transient response of the change-over selector during its operation, the authors state that the proposed design could decrease the arc to a large extent, which reduces the maintenance cost.

Tap changing transformers may include a "change-over" switch which permits the tap changing winding portion to be inserted with either positive or negative polarity so that the tap voltage can added or subtracted from the main winding voltage as in Figure 3.1 (b). The change-over switch is always operated in the zero-voltage position (tap A_0) so that

its operation does not create a voltage magnitude change. Once in this position, the OLTC taps are increased to increase (or decrease) the output voltage.

The earlier literature discusses the management of potential issues related to OLTC operation but not consider the effects of transients due to the change-over switch operation, due to the belief that the operation of the change-over switch is always done at zero tap position and the output voltage does not change when the change-over switch is operated. However, there is a transient associated with the change-over switch, as its operation discharges parasitic capacitance across the winding as shown in Figure 3.1 (b). This chapter investigates this transient. The change-over switch in Figure 3.1 (a) is not instantaneously moved from the "+" to the "-" position but is maintained in the electrically floating condition so that any arc associated with the capacitive discharge can be effective in the creation of high transient voltage.

This chapter provides a model for the transient behaviour of the change-over selector by considering two factors – namely the recovery voltages and the magnitude of the currents in the contacts. After transferring the current, the gap between the contacts stressed during the change-over must be capable of withstanding the recovery voltage and switch currents.

 In this chapter, a mathematical model for the change-over operation is developed, and the recovery voltages and switch currents are investigated in 3.2. Section 3.3 shows the arc characteristics used in this chapter. Then, a model to simulate the transient characteristics of the change-over selector is presented. Section 3.4 demonstrates the simulation results of the recovery voltages and the switch currents. The effect of the tie-in resistor will be modelled and investigated in section 3.5. In section 3.6, the conclusion will be provided.

3.2   Phasor analysis

The tap winding is galvanically isolated from the main winding by the change-over selector during the transition from the "+" to the "–" contact when the tap winding is electrically floating. Then, a recovery voltage V_{R+} exists between the stationary contact (+) and Tap_A0 resulting from the potential of the adjacent windings and winding coupling capacitances as shown in Figure 3.1 (b). Similarly, V_{R-} exists when the change-over selector switches from the "-" to the "+" contact. Note that the current I_{Switch}, interrupted during this change-over is capacitive and depends on the coupling capacitances of the tapped winding [1] and [41].

Figure 3.1 (a) shows a three-phase delta-connected OLTC structure with the change-over selector. Figure 3.1 (b) shows one phase of the studied winding. As shown, the coupling capacitance effects are considered in the circuit by C_1 and C_2. Simplifying the effect of capacitive coupling by two capacitors can help us is sufficient enough for the low frequency applications. However, for the high frequency transformers, the proposed model in this chapter will not work because the circuit structure must be much more complicated. C_1 is the capacitance of the tap winding (measured from the central coil of each winding) to the adjacent winding, and C_2 is the capacitor to the ground. V_{R+} is the voltage of the stationary contact (+) with respect to Tap_A0. Likewise, V_{R-} is the voltage of the stationary contact (-). Also, U_1 and U_2 represent the voltage of the adjacent winding.

As shown in Figure 3.1 (b), the change-over switch is always operated in the zero-voltage position (tap A_0), so that its operation does not create a voltage magnitude change, whether changing from "+" to "–" or from "–" to "+" [1] and [41].

In [1], it is shown that the recovery voltages and switch currents can be calculated by

using the equivalent circuit shown in Figure 3.2 (a). The voltage V_Y represents the voltage (w.r.t. ground) of the change-over selector contact "0", which is connected to the end of the HV winding. Although the switching is a transient process, a relatively good idea of the recovery voltage and switches current can still be obtained from a phasor calculation [1]. From Figure 3.2 (b), V_Y represents the voltage difference between the ground of capacitor C_2 and the ground of point one in Figure 3.2 (a) and (b). V_Y can be calculated by (3-1).

$$V_Y = \frac{-V_{HV}}{2} + j\frac{V_{HV}}{2\sqrt{3}} \qquad (3\text{-}1)$$

Change-over selector moving from position "+" to "-" gives different results for the recovery voltages and switch currents compared to the results for moving from "-" to "+". The reason is that the value of the voltage across capacitor C_2 is different for V_{R+} and V_{R-}. This is because of the sign of $\frac{V_{Tap}}{2}$ is positive when determining V_{R+} and negative for V_{R-} as shown in Figure 3.2 (b). Likewise, for the switch currents.

The value of the recovery voltage can be calculated by equations (3-2) and (3-3) [1], where V_{R+} and V_{R-} are the values of recovery voltage when transitioning from "+" to "–" and from "–" to "+", respectively.

$$|V_{R+}| = \sqrt{2} \times \left[\sqrt{(\frac{V_{HV}}{2} + \frac{V_{Tap}}{2})^2 + (\frac{V_{HV}}{2\sqrt{3}} \times \frac{C_2}{C_1 + C_2})^2} \right] \qquad (3-2)$$

$$|V_{R-}| = \sqrt{2} \times \left[\sqrt{(\frac{V_{HV}}{2} - \frac{V_{Tap}}{2})^2 + (\frac{V_{HV}}{2\sqrt{3}} \times \frac{C_2}{C_1 + C_2})^2} \right] \qquad (3-3)$$

V_{HV} is the voltage of the HV winding I_F is the forward current, and V_{Tap} is the voltage

across the tap winding.

According to Figure 3.2 (b), the peak value of the switch current for the "+" contact is shown in (3-4), and its peak value for the "-" contact can be found by employing (3-5) [1].

$$|I_{Switch}| = \sqrt{2} \times \left[\omega \sqrt{\left(\frac{V_{HV}}{2\sqrt{3}} \times C_2 \right)^2 + \left(\left(\frac{V_{HV} + V_{tap}}{2} \times (C_1 + C_2) \right)^2 \right)} \right] \qquad (3-4)$$

$$|I_{Switch}| = \sqrt{2} \times \left[\omega \sqrt{\left(\frac{V_{HV}}{2\sqrt{3}} \times C_2 \right)^2 + \left(\left(\frac{V_{HV} - V_{tap}}{2} \times (C_1 + C_2) \right)^2 \right)} \right] \qquad (3-5)$$

where ω is the angular frequency.

Figure 3.1: The winding arrangement of (a) a three-phase structure (b) a one-phase structure [1] and [41].
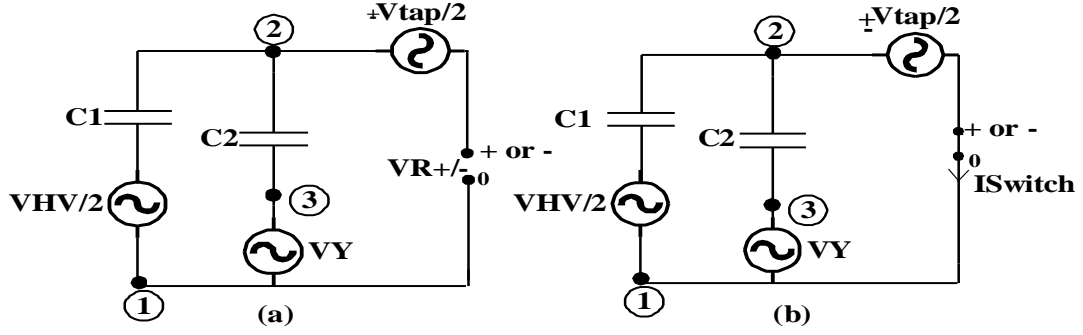
Figure 3.2: The equivalent circuit to calculate (a) the recovery voltage and (b) the switch currents [1].

3.3   Arc model simulation

In literature, Mayr's [81] and Cassie's [82] models are two widely used models for arcs with non-linear electric conductance, where the instantaneous arc conductance is a function of power. Mayr's model, which is better for simulating a low current arc (as is the case for the change-over selector in oil), is used in this chapter. The Mayr arc model behaves as a non-linear conductance, and it is described by equation (3-6) [80-81].

$$\frac{d \ln (g)}{dt} = \frac{1}{t_{au}} \times \left(\frac{u_{arc} \times i}{P} - 1 \right) \qquad (3-6)$$

Where g is the instantaneous conductance value, t_{au} represents the Mayr's time constant, u_{arc} is the arc voltage, i represents the arc current, and P is the cooling power.

To simulate the breaker with arc, Mayr's model block in the MATLAB Simulink is employed [83]. This block considers a constant value for t_{au} and cooling power, P. In this chapter, the default values for these two parameters are considered which are $t_{au} = 0.3 \times 10^{-6}$ and $P = 30900$ W[83]. Figure 3.3 shows the Mayr's control block in MATLAB Simulink.
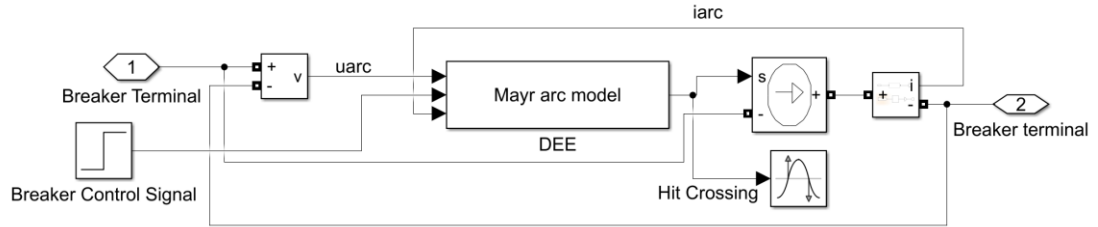
Figure 3.3: The breaker with the Mayr's arc model in MATLAB Simulink [82].

As shown in Figure 3.3, the breaker control signal is employed to control the contact separation of the breaker. The voltage of the control signal is from a value of zero to one at the determined contact separation time. When the contacts are closed, the differential equation shown in (3-7) is solved [83].

$$\frac{d \ln (g)}{dt} = 0 \qquad\qquad (3-7)$$

Therefore, the arc model behaves as a conductance with the value g(0) which corresponds to a short circuit. In the MATLAB Simulink simulation $g(0) = 10^4$ S (or 0.0001Ω). Then, beginning from the contact separation time, the Mayr arc model equation shown in (6) is incorporated using the Simulink DEE (Differential Equation Editor) block. Also, the output of the Mayr arc model is a current determined from "u_{arc}" and g(t), which is injected at the breaker terminal.

3.4   Proposed Transient Model of Change-over Process

The model used to investigate the transient characteristic of the OLTC's change-over selector operation is shown in Figure 3.4. As one may see in this figure, the primary winding (LV) is star-connected, and the secondary winding (HV) is delta-connected. The tap winding is delta-connected. Also, the effects of coupling capacitances, represented by the capacitors, C_1 and C_2, are considered in the model. To model the changeover process,

we represent the two fictitious breakers Breaker1 and Breaker2 as shown in Figure 3.4. If the Breaker1 is activated it means that the change-over selector is initially connected to the "+" contact. Likewise, if the Breaker2 is on, the change-over selector is initially connected to the "-" contact. When moving "+" to "-" VR+ is initially 0, and its value indicates the recovery voltage across the selector as it is moving to the "-" contact. Likewise, for VR- when moving from "-" to "+".
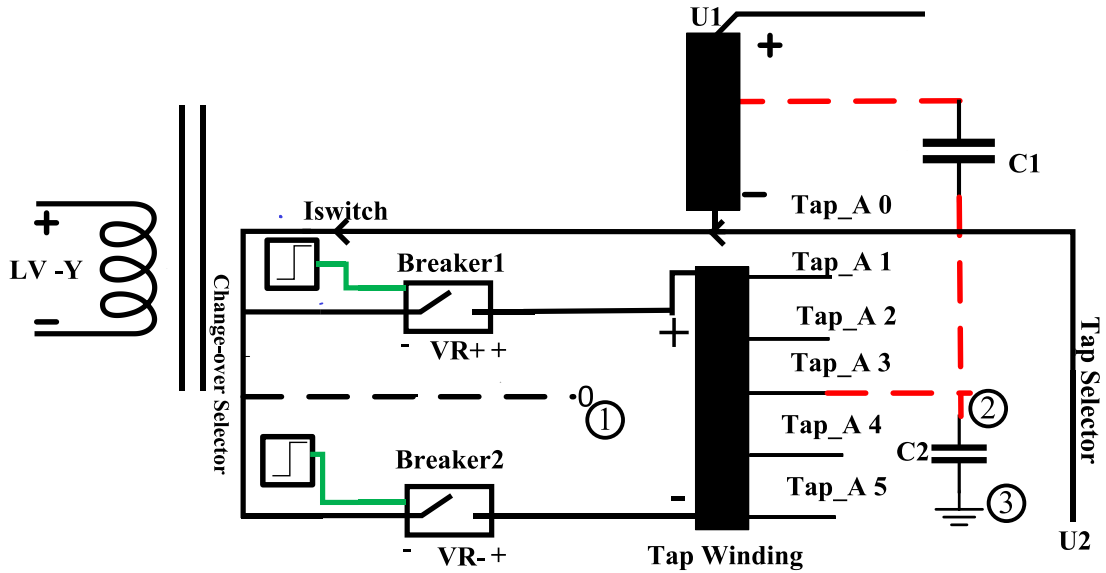
Figure 3.4: The arrangement of the proposed model [41].

3.5   Simulation and calculation results

The proposed circuit with the arc model was simulated in MATLAB Simulink software with transformer parameters as shown in Table 3.1. The duration of the simulation is one second. In order to continue an additive connection of the tap winding to the HV winding, the change-over selector is connected to the "+" contact for the first 0.4 second of simulation so Breaker1 is in the on state. During this time, the voltage across the "+" contact, V_{R+}, will be zero as the structure shown in Figure 3.5 (a). Exactly at 0.4 second

into the simulation, the change-over selector starts to move to the - contact, and two stationary contacts (+ and -) which are connected to the tap winding are electrically floating for 200 ms during this time, as it is shown in Figure 3.5 (b). This causes a change in the value of V_{R+} and V_{R-}, This change in the voltages represents the value of recovery voltage and could be significantly larger than the steady-state voltage across the change-over selector contacts. It should be noted, that at the beginning of the movement of the change-over selector, there are re-strikes between moving contact and stationary contact (+) due to the coupling capacitances and adjacent winding voltages. At the end of the motion, there may be pre-strikes from a moving contact approaching the stationary contact "-". The processes of moving the change over-selector are shown in Figure 3.5.

Table 3.1: Transformer parameters [41].

Transformer MVA rating (nominal tap)	100 MVA
HV winding Voltage	230 kV (Delta)
LV winding Voltage	13.8 kV (Y)
C_1	10 nF
C_2	3 nF
Tap winding	15% of HV winding
Change-over time	200 ms

3.5.1 Changeover from the "+" to "-" position

As mentioned in section 3.2, the change-over form "+" to "-" gives different results for the recovery voltages and switch currents compared to the results while the change-over starts to move from "-" to "+". Considering this, the results of the recovery voltage, V_{R+},

and the switch current are investigated in this section. Figure 3.6 (a) and (b) show the simulation results for V_{R+} and the switch current I_{switch}, respectively. As shown, for the first 0.4s, i.e., before the change-over selector moves, the voltage of the stationary contact (+) is zero as Breaker1 is closed and the switch current is equal to 923 mA (pk). Exactly at 0.4s, the change-over selector starts moving towards the "-" contact, and Breaker1 is set to the "open" state, as the selector floats in between the contacts. There is a restrike which is due to the effects of the coupling capacitances and adjacent winding voltages from 0.4 s to approximately 0.47 s. The restrike extinguishes at around 0.47 s and the switch current becomes zero. V_{R+} has a very high initial peak of 330 kV but soon settles to 188.312 kV (pk) for the remainder of the selector crossover time. For the Reinhausen M-type (delta-connected) OLTC as is the case here, the limit for the recovery voltage is 50 kV (pk), and so this recovery voltage is not acceptable, indicating a necessity for a tie-in resistor which will be discussed in Section 3.6. At t=0.6s, the selector reaches the "-" contact signified by closing Breaker2, and V_{R+} now signifies the voltage on the stationary contact (+) and is equal to the voltage of the tap winding, which is 15% of the HV winding giving a value of 48.79 kV (pk). The switch current is now the current of the "-" contact, which is equal to 670 mA (pk), as Breaker2 is closed.

3.5.2 The change-over from the "- to "+" position

Now, in order to assess the results of the recovery voltage, V_{R-}, and switch current while the change-over selector moves from "-" contact to "+" contact, another simulation is performed. Figure 3.7 (a) and (b) show the simulation results for the recovery voltage and the switch current when the change-over selector is initially connected to the "-" contact.

for the first 0.4s, the voltage of the stationary contact (-) is zero as Breaker2 is closed and the switch current is equal to 670 mA (pk), which signifies the current of the stationary contact (-). At 0.4s, the change-over selector starts to move from the "-" contact to "+" contact and Breaker2 is set as "open", and the selector floats between "-" and "+" contacts. From 0.4 s to around 0.47 s, restrike happens and its amplitude is less than the restrike of the switch current when the selector moves from "+" to "-". Then, approximately at 0.47 s, the restrike is extinguished and the switch current is zero, and V_{R-} reaches 140.16 kV (pk) for the remainder of the selector crossover time, which again is not acceptable. At t=0.6s, the selector reaches the "+" contact signified by closing Breaker1, and V_{R-} now signifies the voltage on the stationary contact (-) and is equal to the voltage of the tap winding. The switch current is now 923 mA (pk) and is the current of the "+" contact.

Table 3.2 shows the comparison of the simulation and theoretically calculated results as calculated from equations (2), (3), (4), and (5). The results are very close, with a maximum error of 2.3%, for both the recovery voltages and the switch current. The simulation model, however, shows much more transient detail in the restrike waveforms. Nevertheless, the close agreement between the simulation waveforms after fast transients have decayed, and theoretically, calculated phasor values is an additional validation step for the simulation model.
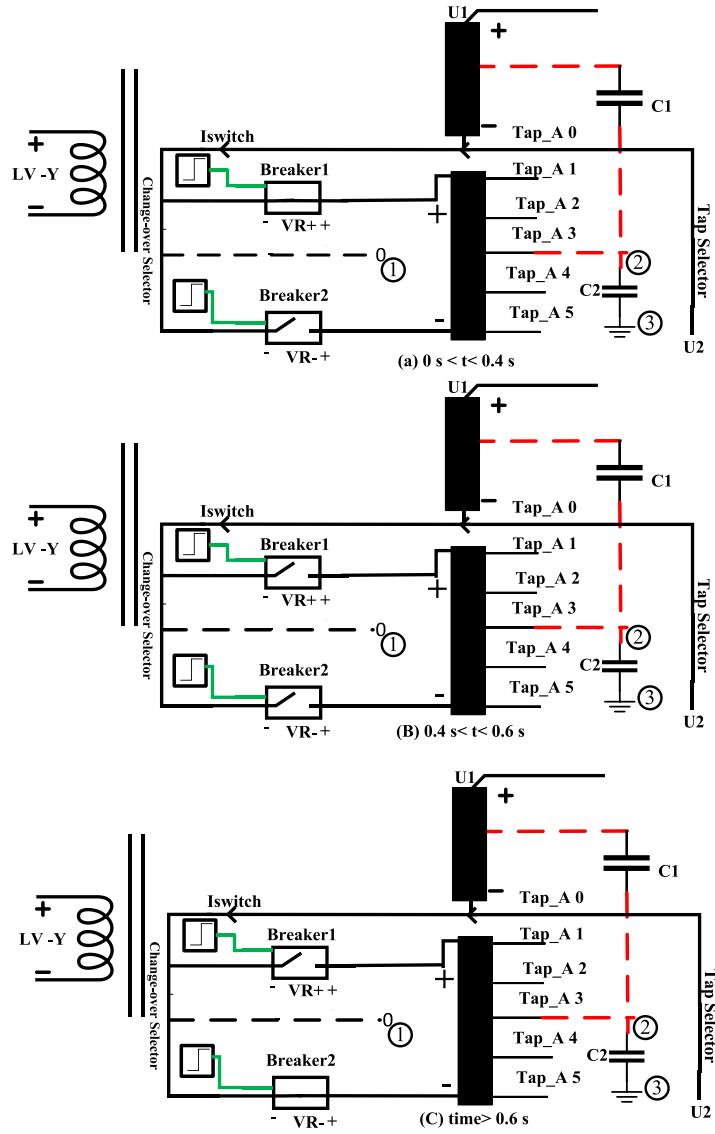
Figure 3.5:Change-over selector position during the simulation (i.e. 0 s <t< 1 s) [41].
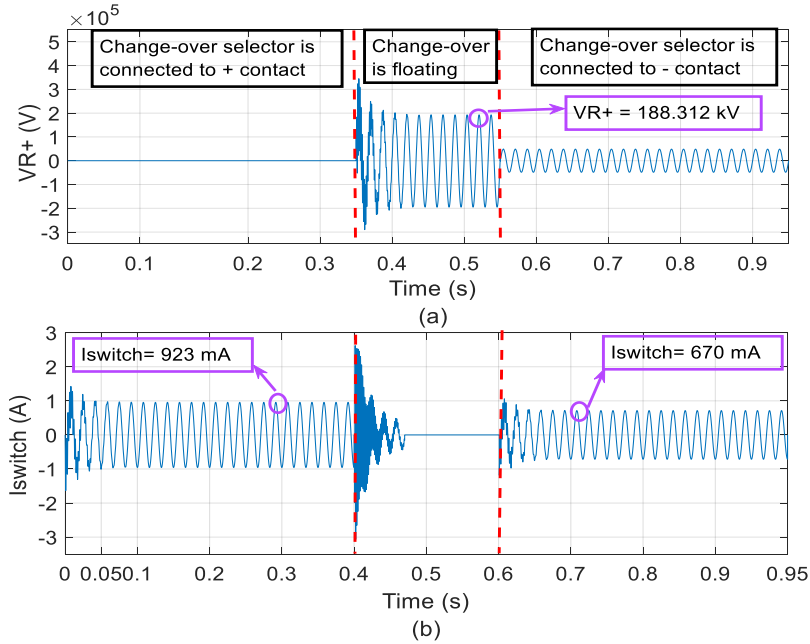
Figure 3.6: The simulation result for (a) V_{R+} and (b) I_{switch} while the change-over selector moves from "+" contact to the "-" contact [41].
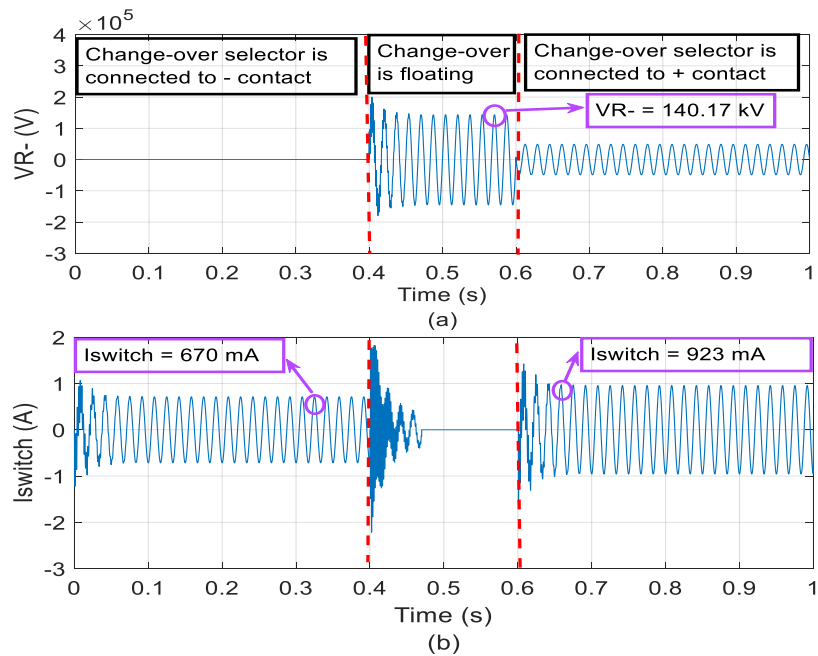
Figure 3.7:   The simulation result for (a) V_{R-} and (b) I_{switch} while the change-over selector moves from "-" contact to the "+" contact [41].

Table 3.2: the comparison of the simulation and calculation results [41].

Change-over from "+" to "-"			Change-over from "-" to "+"		
V_{R+} (pk)			V_{R-} (pk)		
Calculated value	Simulated value	|Error| %	Calculated value	Simulated value	|Error| %
188.28 kV	188.312 kV	0.017%	139.92 kV	140.17 kV	0.172
I_{Switch} (pk)			I_{Switch} (pk)		
Calculated value	Simulated value	|Error| %	Calculated value	Simulated value	|Error| %
922.7 mA	923 mA	0.033	685.7 mA	670 mA	2.29

3.6   Impact of the tie-in resistor

The tie-in resistor R_{tie} is used if the recovery voltage and switch current exceed the permissible equipment limits. As shown in Figure 3.8, the tie-in resistor is connected between the middle of the tap winding and tap selector, and significantly improves the transient response while the change-over selector is floating as it reduces the recovery voltage and current. Considering the results of the recovery voltages and switch current in section 3.5, using the tie-in resistor is a necessity, as the permissible recovery voltage for the change-over switch is less than 50 kV [1]. The tie-in resistor reduces the recovery voltage and so greatly reduces the gas-in-oil production during arc quenching. They also significantly reduce the audible sound level which is due to reduced arcing activity [1]. The resistance value is chosen in a way that the recovery voltage is limited to a permitted value which is stated in the technical guides for each tap-changer. In this simulation, the Reinhausen M-type (delta-connected) OLTC has been considered, the limit for the recovery voltage for this type is 50 kV (pk) [1]. Figure 3.9 (a) and (b) show the equivalent circuit of Figure 3.8 for the calculation of the switch current and recovery voltages. From

Figure 3.9 (a) and (b), the value of the (post-transient) switch current and recovery voltage can be calculated by phasor analysis. The recovery voltage can be calculated by (3-8). We keep the maximum allowable voltage to 48 kV (i.e., smaller than the 50 kV from [1]), giving a tie-in resistor value of 50 kΩ as shown in (3-9). Also, the switch current for "+" and "-" contact can be calculated by (3-10) and (3-11), respectively.
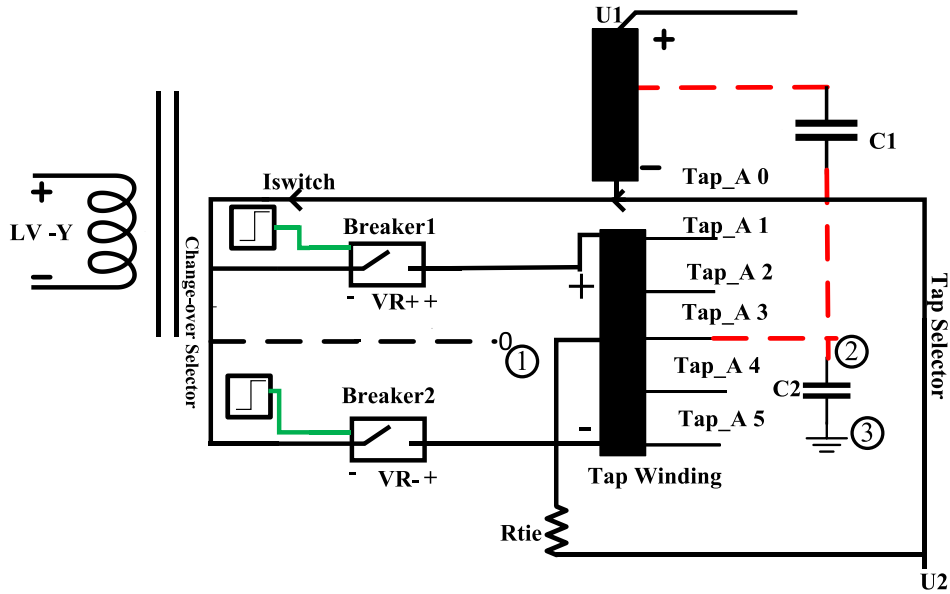
Figure 3.8:   The arrangement of the proposed model with the tie-in resistor [41].
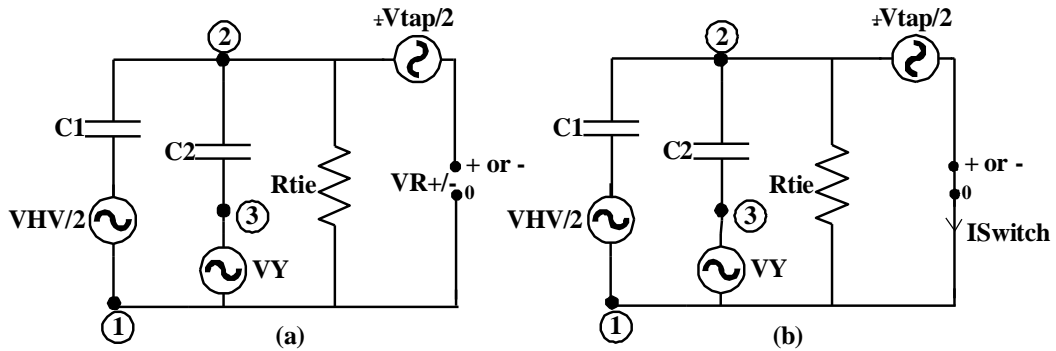
Figure 3.9: The equivalent circuit to calculate (a) the recovery voltage (b) the Switch currents with the tie-in resistor [41].

$$|V_{R\pm}| = \sqrt{2} \left| \frac{\frac{V_{HV}}{2}(R_{tie}||Z_{c2})}{(R_{tie}||Z_{c2}) + Z_{c1}} - \frac{\frac{V_Y}{2}(R_{tie}||Z_{c1})}{(R_{tie}||Z_{c1}) + Z_{c2}} \pm \frac{V_{Tap}}{2} \right| \qquad (3\text{-}8)$$

$$\text{Max}(|V_{R\pm}|) = 48 \text{ kV} \overset{\text{So}}{\rightarrow} R_{tie} = 50 \text{ k}\Omega \qquad (3\text{-}9)$$

$$|I_{Switch}| = \sqrt{2} \times \left| \frac{\frac{-V_{Tap}}{2} - \frac{V_{HV}}{2}}{Z_{c1}} + \frac{\frac{-V_{Tap}}{2} + \frac{V_Y}{2}}{Z_{c2}} + \frac{-\frac{V_{Tap}}{2}}{R_{tie}} \right| = 1092 \text{ mA} \qquad (3\text{-}10)$$

$$|I_{Switch}| = \sqrt{2} \times \left| \frac{\frac{V_{Tap}}{2} - \frac{V_{HV}}{2}}{Z_{c1}} + \frac{\frac{V_{Tap}}{2} + \frac{V_Y}{2}}{Z_{c2}} + \frac{\frac{V_{Tap}}{2}}{R_{tie}} \right| = 777 \text{ mA} \qquad (3\text{-}11)$$

The change-over is initiated at 0.4 s and takes 200 ms for the selector to move across the contacts. Figure 3.10 (a) and (b) show the simulation results for the V_{R+} and switch current with the tie-in resistor while the change-over selector moves from the "+" to "-" contact. For $t < 0.4$ s, V_{R+} is zero and I_{switch} of the "+" contact is 1100 mA (pk), which closely agrees with the theoretical calculation of 1092 mA (pk). Note that this is larger than the current of 923 mA without the tie-in resistor. It is marginally larger as the resistor adds a real component to the leading capacitor current. The initial high-frequency peak in the recovery voltage is now eliminated and V_{R+} attains a value of 47.8 kV which is much smaller than the 188.312 kV value without the tie-in resistor in Figure 3.6.(a). After selector cross-over (i.e., $t > 0.6$ s), the voltage of the stationary contact (+) is equal to the voltage of the tap winding of 48.79 kV (pk). Also, the switch current into the "-" contact is 800 mA (pk), (a calculated value of 777 mA). Similarly, the results for the switch current and V_{R-} are shown in Figure 3.11 (a) and (b) while the change-over switch moves from "-" contact to "+"

contact. Before switch-over (i.e. t< 0.4 s) the switch current (into the "-" contact) is 800 mA (pk). The transient part is improved significantly for the switch current and the recovery voltage. The recovery voltage value, V_{R-}, settles at 36 kV (pk) (i.e., below the 50 kV limit) which is also much smaller than the 140.2 kV (pk) without the tie-in resistor in Figure 3.7 (a). After changeover (i.e. t>0.6 s), the switch current is 1100 mA (pk), and the voltage of the "-" contact will be equal to the tap winding voltage of 48.79 kV (pk).
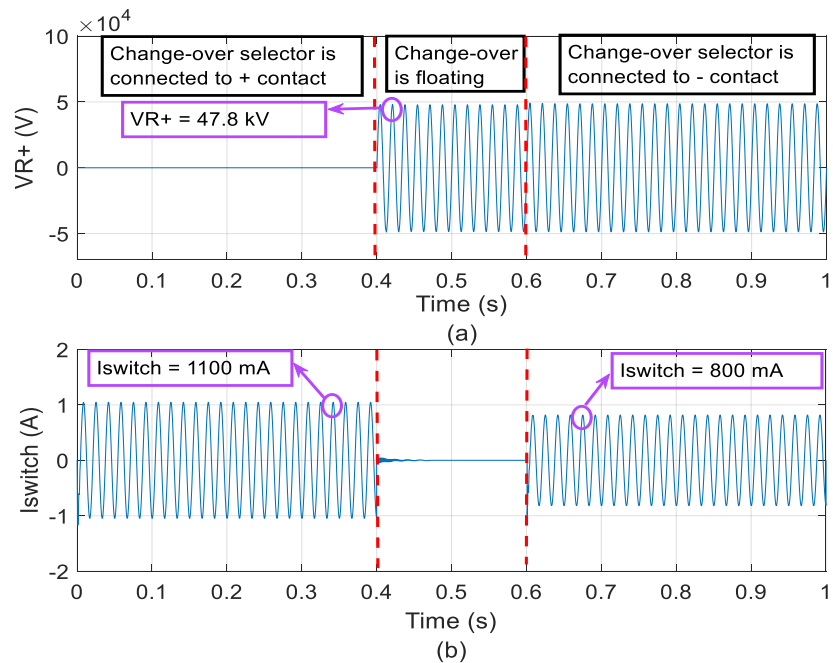
Figure 3.10: The simulation results for (a) V_{R+} and (b) I_{switch} with the tie-in resistor while the change-over selector moves from "+" contact to the "-" contact [41].
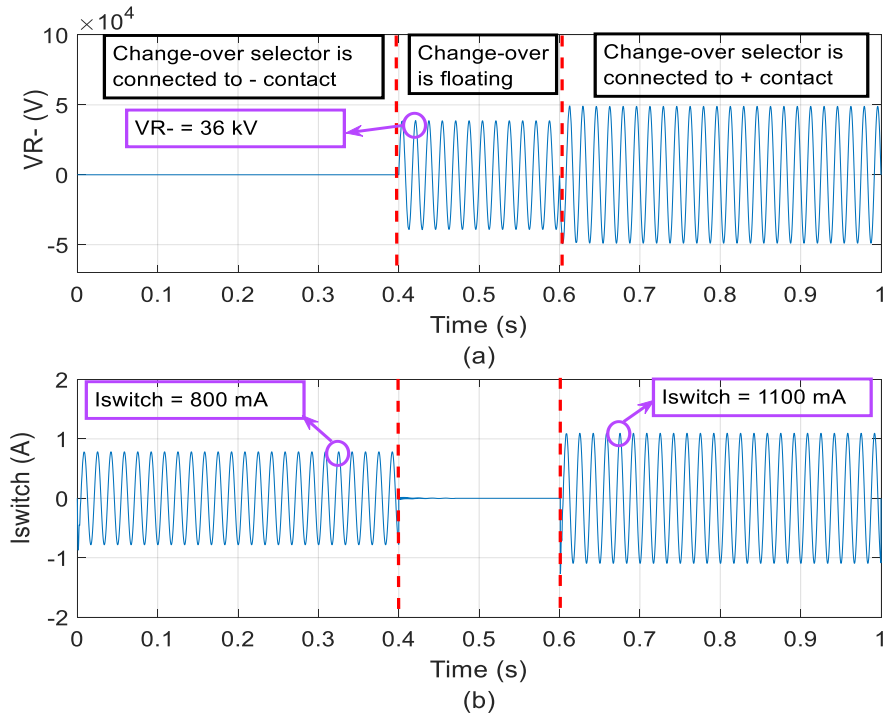
Figure 3.11: The simulation results for (a) V_{R-} and (b) I_{switch} with the tie-in resistor while the change-over selector moves from the "-" contact to the "+" contact [41].

3.7   Chapter conclusion

Chapter 3 showed that the proposed model in this thesis can provide the information for transient behaviour of the change-over switch. Also, the model proved that the transient voltage of the change-over switch is much higher than the steady-state voltage and it can create some challenges. To mitigate the transient voltage of the change-over switch, the tie-in resistor is one solution which improves the transient response to a large extent. However, there are still some challenges associated with the electromechanical tap changers for transformers in which power switches, such as TRIAC or Thyristors, fail because of a transient voltage or current. According to the above-mentioned challenges

associated with electromechanical tap-changers for transformers, one solution is to use a converter-based tap-changer for the transformer. The converter-based system can work with either AC or DC input. In the next chapter of this thesis, the converter-based tap changing transformer is utilized with a DC input, and the DC voltage comes from a photovoltaic system. This solution is new and enables the power transformer industry to retrofit their existing electromechanical tap changers with the converter-based solution which is more environmentally friendly.

Chapter 4: A converter-based tap changing transformer

Copyright Note: ©2021 IEEE. Reprinted, with permission, from Abolfazl Babaei, Waldemar Ziomek, and Aniruddha Gole, "A Multi-level Inverter Based On-load Tap Changer Transformer Topology for Harnessing Photo-voltaic Energy," 2021 IEEE Electrical Power and Energy Conference (EPEC), 2021, pp. 237-242.

4.1 Introduction

The previous chapter discussed the change-over switch operation as a source of the transient in OLTCs. A model was implemented which could predict the transient behaviour of the change-over switch close to the calculated results. However, there are still yet-to-be-solved issues including the high value of arc and high maintenance cost associated with the electromechanical and solid-state based tap changers. This chapter discusses one of the solutions to be used as a substitute for the electromechanical tap changer which improves the transient behaviour to a large extent. The topology uses a booster winding in series with the main transformer winding to provide an injection of variable magnitude voltage thereby mimicking the operation of a tapped winding as shown in Figure 4.1.

Various modifications to the tap changer have been proposed recently. In [20], a compensation transformer is used along with the solid-state tap changers to improve the power capability. The solid-state transformers can work under higher power levels similar

to those of the transformers with mechanical OLTCs. In [20-23], IGBT-based OLTCs are proposed.
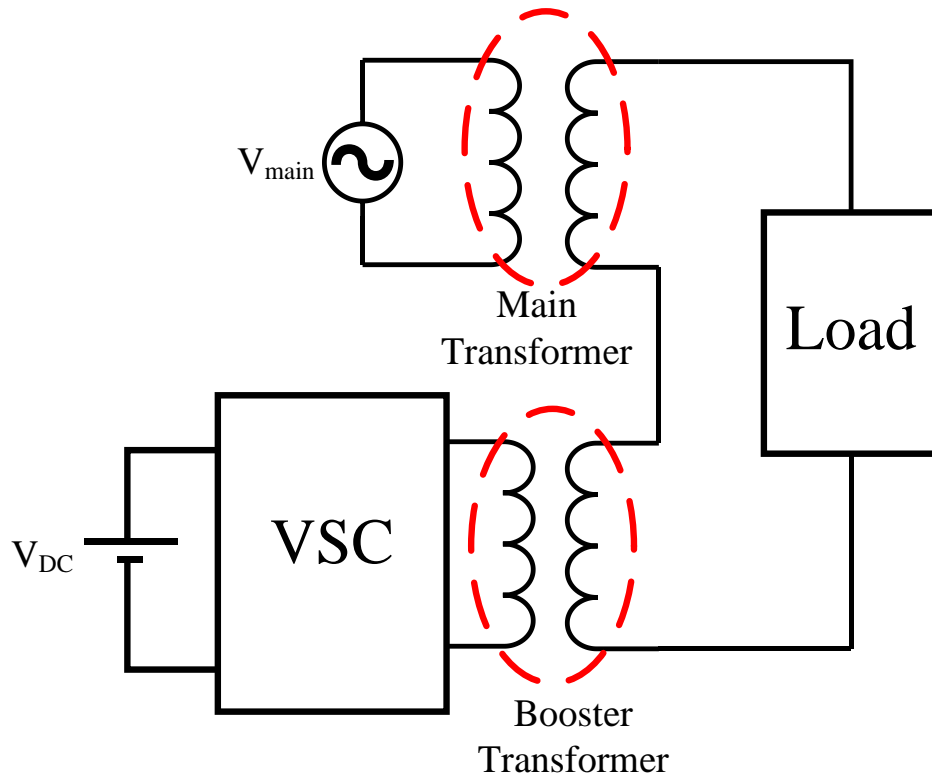
Figure 4.1: The converter-based tap changer's topology.

After thoroughly investigating previous literature, this chapter proposes a new approach for the converter-based OLTC with a completely different topology.

The proposed converter-based OLTC solution can overcome the drawbacks associated with the electromechanical tap changing transformers outlined in the previous chapter. The proposed model is also suitable for connecting to a photovoltaic voltage source which make the OLTCs more environmentally friendly. It will be shown that the proposed solution will limit the arcing between contacts, which increases the lifetime of the system.

In the power distribution system, applications of grid-connected renewable energy sources are increasing. Renewable energy sources are asynchronous with the frequency of the grid.

Therefore, using a power converter to synchronize the frequency is a requirement, especially for wind energy. In [57-59], dc-ac power converters are used with the same goals. In [60], two dc-ac converters are used with an OLTC to increase the reliability and power capability of the system. Photovoltaic (PV) grid-connected dc renewable energy sources are also becoming widely used. To convert the dc voltage to ac, multilevel inverters are used. Multilevel inverters are now widely used in the photovoltaic system [46-54]. In [61], a 10 kV soft-switching and high-frequency solid-state transformer is proposed. The presented circuit uses a current-source inverter bridge, and the proposed soft-switching technique can successfully remove the dead-time and overlap states between IGBTs switches. This approach increases the reliability of the proposed system. Also, the number of components and the filter size is improved in [61].

In this chapter, a topology using dc power generated by the solar panel array is connected to the grid through a modified on-load tap changer (OLTC). An existing multilevel structure is used to convert the dc power to ac and replaces the change-over switch in the traditional OLTC. This also improves the OLTC operation as the transients from the electromechanical switch operation are eliminated and also the tie-in resistor in the mechanically switched transformers is no longer necessary. After the multilevel inverter, a tapped winding with four taps is used. The tap winding is in series with grid voltage to compensate for the load voltage changes. TRIACs are used in series with each tap of the transformer to add or subtract a ratio of the voltage to the grid voltage. The TRIACs also change the tap position faster than the mechanical tap. Also, an L-C filter is employed to make the output voltage of the tap winding purely sinusoidal.

Although the tapped windings could themselves have been replaced by a single winding, as the multi-level converter can control voltage by itself, having the tap allows for lower voltage ratings of the power electronic components. It also allows for bidirectional voltage injection, for bucking or boosting the grid voltage. The idea here was to retrofit existing OLTCs so that they could also be used as a port for importing solar PV power.

A simulation is performed in PLECS software to validate the claims. The results show that the output voltage of the tap winding is purely sinusoidal, and the load voltage remains in an acceptable range, the system will have an excellent performance with either resistive or inductive load, and the transient behaviour of the voltage is improved.

4.2   Multilevel inverter

4.2.1   SPWM Modulation

In previous literature, a large number of modulation techniques have been presented to make the inverter voltage near a pure sinusoidal waveform. Several modulation techniques have been proposed, such as Selective Harmonic Elimination (SHE), SPWM, Space Vector Control (SVC), and Space Vector Modulation (SVM) and used in the multilevel inverters. Among these, SPWM is widely used in multilevel inverters because it is simple to implement [45-47]. The SPWM has two different types: phase shift and level shift as illustrated in Figure 4.2. The total harmonic distortion (THD) of phase-shifted modulation is much higher than the level-shifted technique therefore, level-shifted modulation is considered in this chapter [45] and [49].
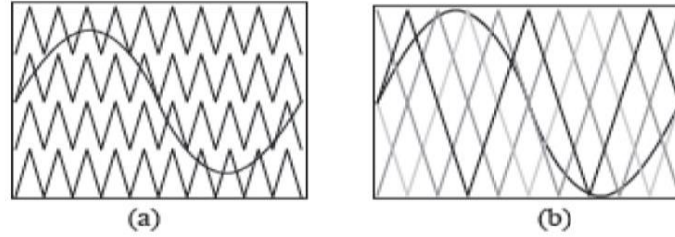
Figure 4.2: The SPWM with (a) amplitude-shift (b) phase-shift [39].

4.2.2   Five-level diode-clamped inverter

There are different topologies used for multilevel inverters, such as diode-clamped, cascaded H-bridge (CHB), and flying capacitors. A popular topology in industrial applications [47] for converting the dc voltage generated by a photovoltaic system to an ac voltage is the five-level inverter which is used in the proposed circuit in this chapter. The reason for this selection is that the diode-clamped converter provides a larger operating range and the ability to use fewer dc input voltages, and it has lower THD than the flying capacitor and cascaded H-bridge topologies [46-47]. Figure 4.3 shows a five-level diode-clamped inverter which has two dc inputs which are coming from a photovoltaic system. Figure 4.4 shows the conduction time for each level in a five-level multilevel inverter. Table 4.1 shows which switches are on at each level in the five-level inverter.

Table 4.1: the activated switches at each voltage level [39].

Level	S_{a1}	S_{a2}	S_{a3}	S_{a4}	S_{b1}	S_{b2}	S_{b3}	S_{b4}
2	on	on	off	off	off	off	on	on
1	off	on	on	off	off	off	on	on
0	off	off	on	on	off	off	on	on

-1	off	off	on	on	off	on	on	off
-2	off	off	on	on	on	on	off	off
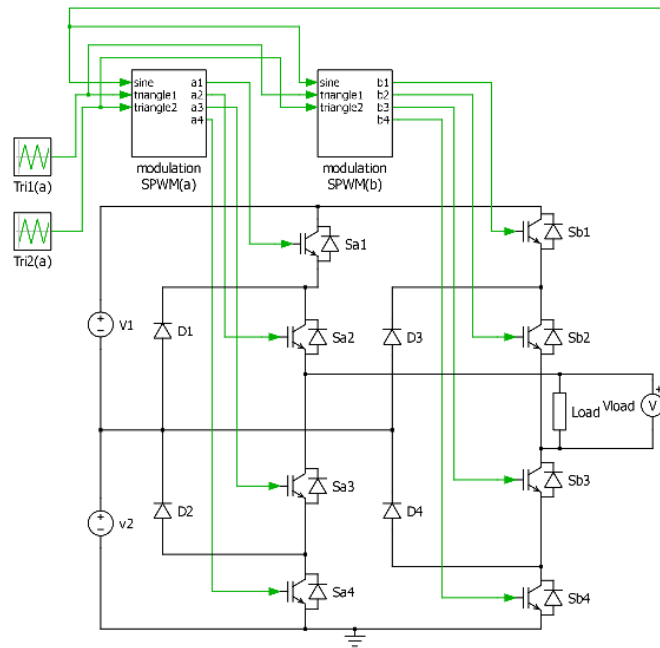
Figure 4.3: Schematic of a five-level diode-clamped multilevel inverter [47].
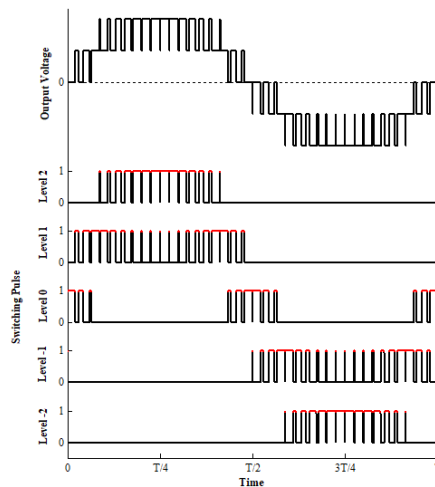
Figure 4.4: Conduction time for each level in a five-level inverter [47].

4.3 The proposed circuit

Figure 4.5 demonstrates the proposed structure. This structure includes (SN-M500W) solar panels rated 500W/48.6V connected with 5 in series and 50 in parallel which charge a battery bank that provides the dc voltage to the inverter. The output of the battery bank is connected to the five-level inverter. Then, the voltage output by the inverter is injected in series with the grid voltage via an OLTC. This idea is employed to retrofit the existing OLTC topology so that it could also be utilized as a port for injecting solar PV power into the grid. Figure 4.5 shows the proposed circuit. The battery bank is represented by two voltage sources, V_1 and V_2, in the circuit shown in Figure 4.6. If the grid voltage increases, the control system puts the applied voltage from the multilevel inverter in a subtractive condition. Similarly, for an additive condition, the multilevel inverter applies a voltage with the same phase angle of the grid voltage to compensate for the decrease in the load voltage. The additive or subtractive voltage level depends on the compensation which is required to keep the load voltage level approximately constant. To do so, one of the TRIAC switches in series with the tap winding (S_5, S_6, S_7, or S_8) is turned on. When S_9 is in the on-state, zero voltage will be injected as well, which means the grid voltage itself is in the acceptable range and no compensation is required. Also, in Figure 4.5, the grid voltage is represented by a voltage source, and the grid voltage is connected in series with the output voltage of the multilevel inverter after an L-C filter. Although the tapped windings could themselves have been replaced by a single winding, as the multi-level converter can control voltage by itself, having the TRIAC-controlled tap allows for lower voltage ratings of the power electronic components.
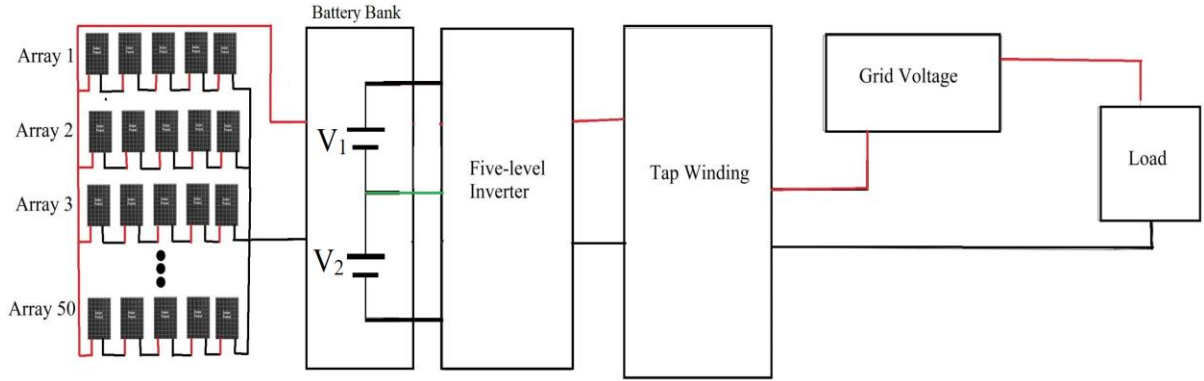
Figure 4.5: The block-base representation of the proposed circuit [70].
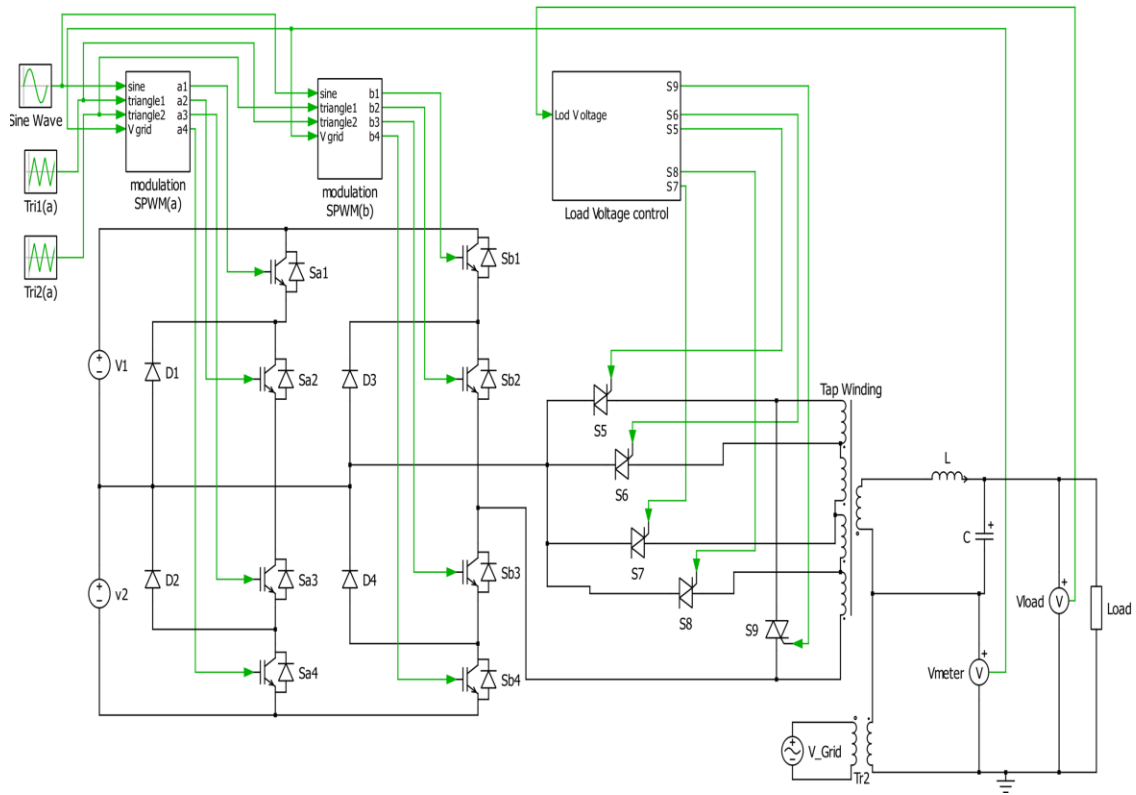
Figure 4.6: The schematic of the proposed circuit [70].

4.4   Simulation results

The proposed structure is simulated in PLECS software. Table 4.2 shows the simulation parameters. Figure 4.7 demonstrates the output voltage of the five-level inverter. Figure

4.8 shows the tap winding voltage after the L-C filter, and this voltage is purely sinusoidal, which shows the effectiveness of the filter. Also, Figure 4.9 shows the multilevel inverter and grid voltage in either additive or subtractive conditions. Figure 4.9 (a) illustrates the additive condition, and Figure 4.9 (b) shows the subtractive condition. As shown in Figure 4.9, the proposed structure can provide a voltage which can have same phase angle or can have 180^0 phase shift to the grid voltage.

Figure 4.10 (a) illustrates the grid voltage which is changing during the simulation time. Also, in Figure 4.10, the red line represents the desired grid voltage, which is 100kV. Figure 4.10 (b) demonstrates the output voltage of the tap winding. This voltage is changing with respect to the variations in the grid voltage. The tap winding voltage can be either in an additive or subtractive state. If the grid voltage is higher than the desired voltage, the proposed topology provides a sinusoidal voltage having 180^0 phase shift with the grid voltage. Likewise, if the grid voltage decreases to a value less than 100 kV, the presented structure will apply a voltage which has the same phase angle with the grid voltage. This approach can keep the load voltage to an acceptable limit. Figure 4.10 (c) illustrates the load voltage which is almost constant under a resistive load. The proposed structure can apply zero voltage by turning the switch S_9 on as well, and this situation happens when the grid voltage is around 100kV. Considering this, the injected voltage from the tap winding is zero for the first one second as shown in Figure 4.10 (b). Figure 4.11 illustrates the results under an inductive load. Figure 4.11 (a) shows the grid voltage which is changing between 90 kV to 110 kV. Figure 4.11 (b) demonstrates the tap winding voltage. The load voltage is shown in Figure 4.11 (c). The results of the inductive load are similar to the resistive

load, and this proves that the proposed structure can add or subtract the required range of

the voltage to the grid voltage under either resistive or inductive load.

Table 4.2: Simulation Parameters [70].

Parameter	Value	Parameter	Value
DC input voltages (V_1 and V_2)	240 V	Tap Winding	100 kVA
TRIACs (TD330N16KOFTIMHPSA1)	330A/1.4 kV	Tap winding Voltage Regulation(%)	10%
The maximum voltage of the tap winding	10 kV	Load Voltage	100 kV
Grid Voltage	100 kV	Grid power	1 MVA
Switching frequency	2 kHz	Input Current	208.33 A
IGBTs (CM400HA-24A)	400A/ 1.2 kV	Resistive load	10 kΩ
Inductive load	26.53 H	Simulation time	9 s
Additive time	0-5 s	Subtractive time	5-9 s
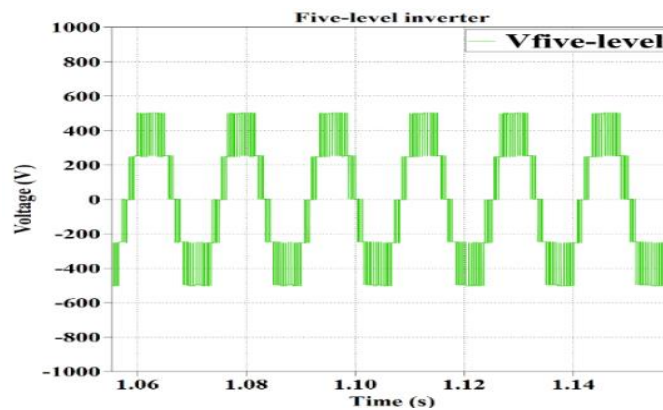
Figure 4.7: The output of the five-level diode-clamped multilevel inverter [70].
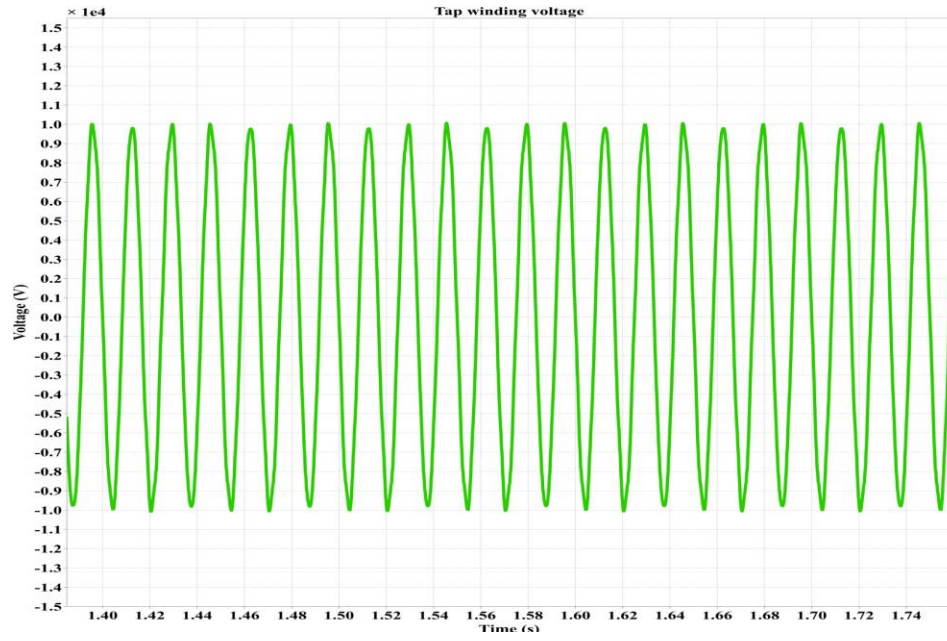
Figure 4.8: The output of the tap winding after the L-C filter [70].
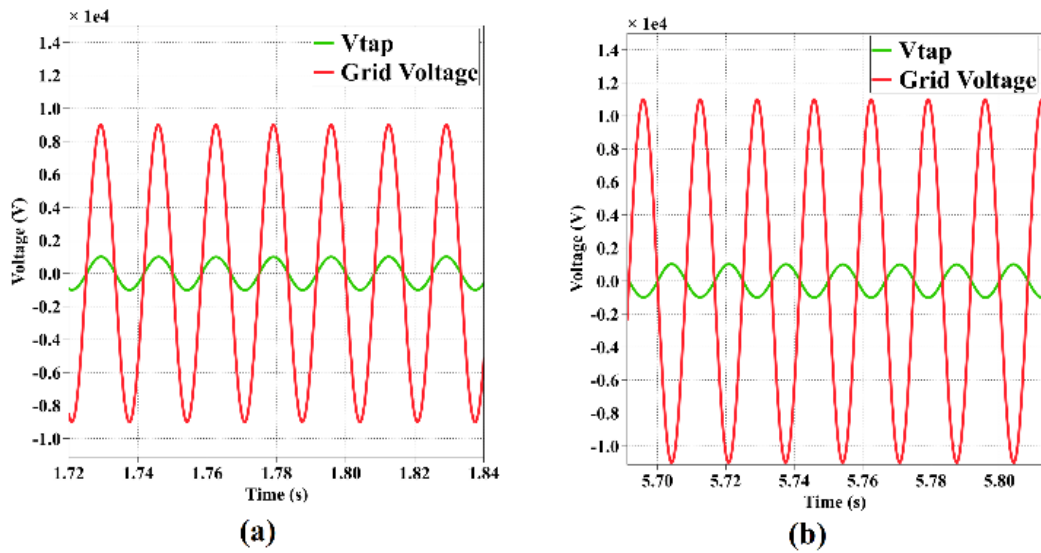
Figure 4.9: The simulation results for the tap voltage and the grid voltage: (a) additive

condition, (b) subtractive condition [70].
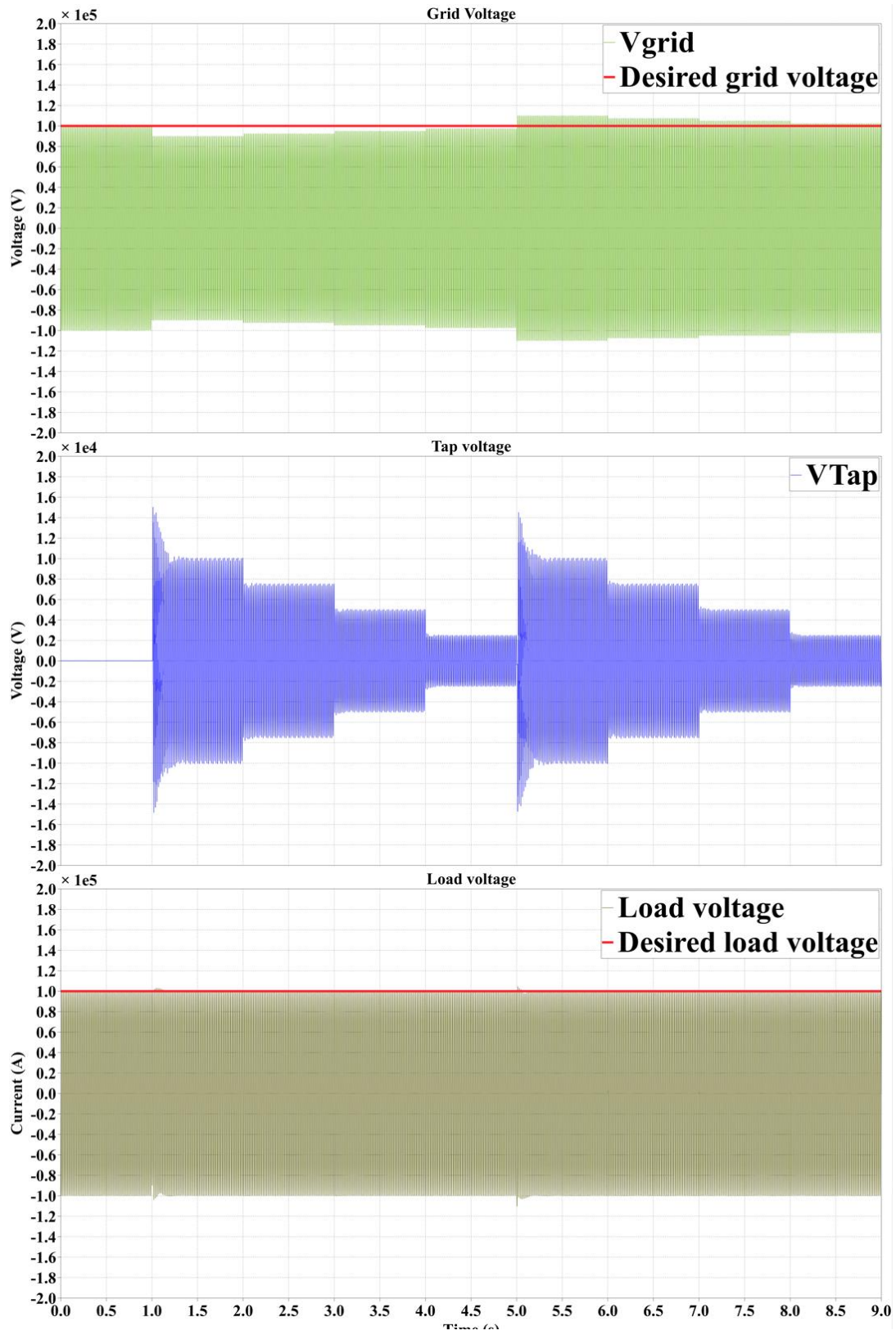
Figure 4.10: The voltages with unity power factor and R_L=10 kΩ [70].
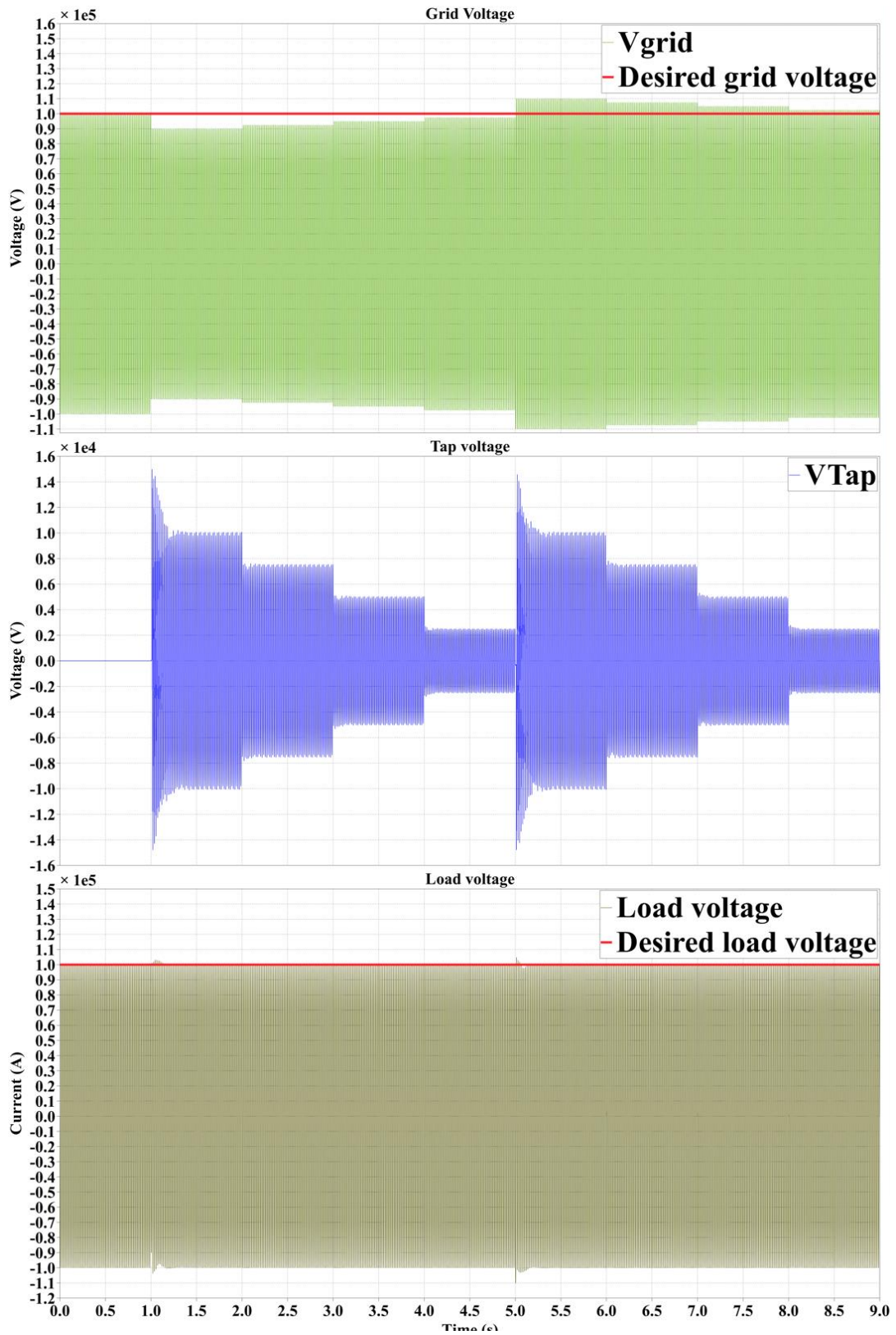
Figure 4.11: The voltages with the inductive load, Z_L=10 kΩ [70].

Figure 4.12 (a) shows the voltage of the tap winding under a variable inductive load. The impedance of the load is varied between 10 kΩ to 50 kΩ. Figure 4.12 (b) illustrates the load voltage under the same condition. Figure 4.12 (c) demonstrates the current of the load which is changing from 2A to 10A. As shown in Figure 4.12, the load voltage remains close to 100kV, meaning the voltage regulation process is well done under load changing condition. Figure 4.13 illustrates the transient behaviour of the tap winding voltage while changing from the additive to the subtractive state. There is a jump in the voltage which is around 14.5 kV. However, this transient voltage is far less than the transient voltage recorded in [41] as shown in Table 4.3. In Table 4.3, the transient results of the change-over switch voltage without a tie-in resistor in [41] are compared to the proposed structure. It shows that the transient voltage of the proposed structure is 1.45 times higher than the maximum voltage of the tap winding, but the transient voltage for a change-over switch under the conventional tap winding is 6.4 times higher than the tap winding voltage. This improvement means that the tie-in resistor can be removed from the structure of the tap winding. Figure 4.14 illustrates the load voltage variations with respect to the loads with different power factors. The results in this figure prove that the tap winding can make the load voltage almost constant.
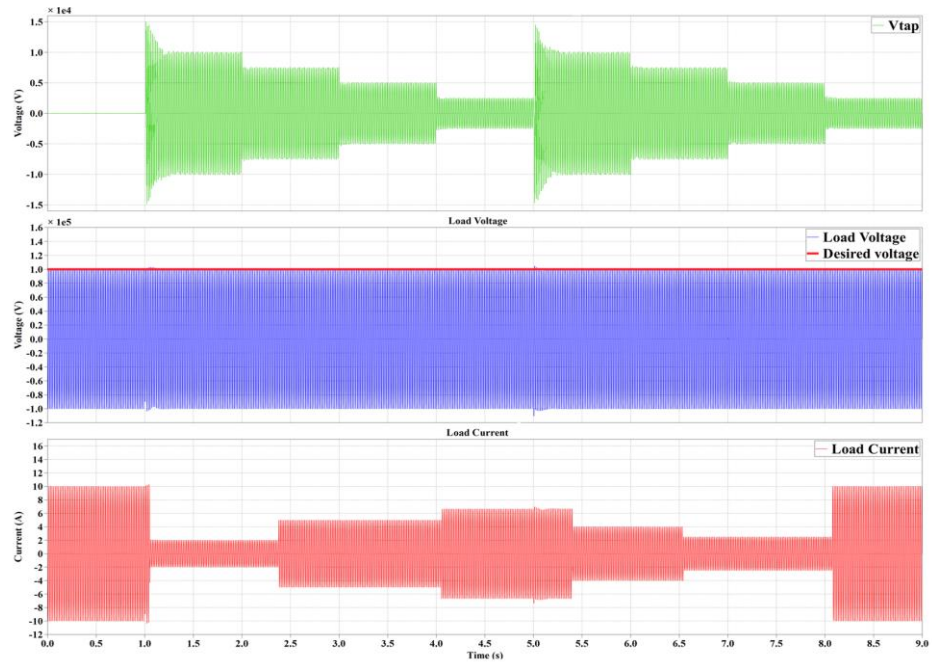
Figure 4.12: The tap voltage, load voltage, and load current with variable inductive loads

[70].
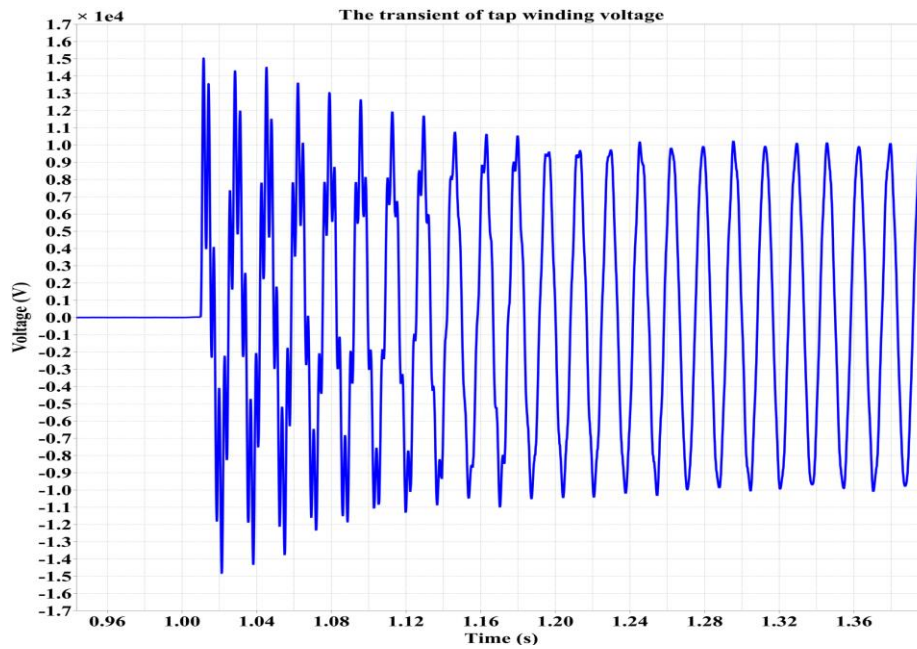
Figure 4.13: The transient behaviour of the tap voltage while changing from additive to

subtractive condition [70].

Table 4.3: Comparing maximum transient of the proposed structure and the results shown

in [41] while changing from additive to subtractive condition.

Load	Maximum value
Proposed Structure	$1.45 \times V_{Maximum\_tap}$
Results in [12]	$6.4 \times V_{Maximum\_tap\_in [14]}$
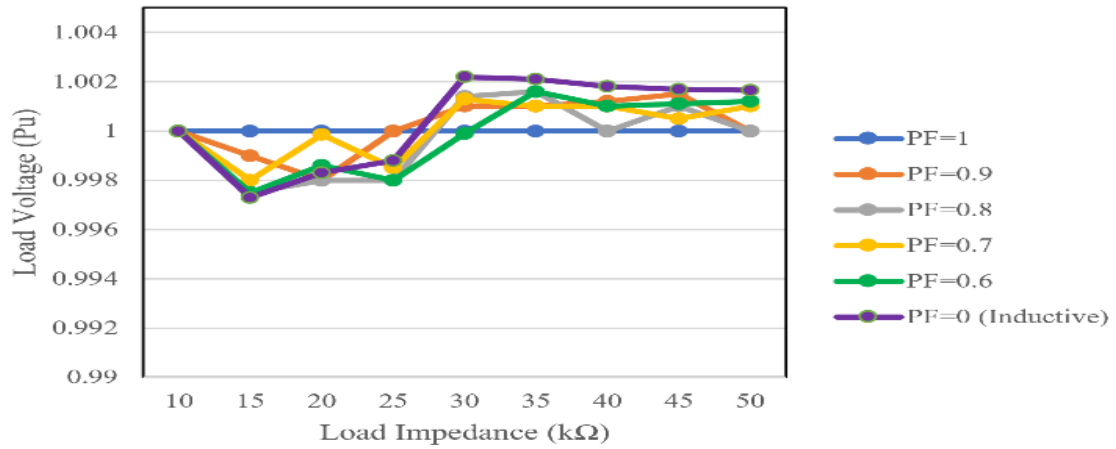
Figure 4.14: The load voltage variation with respect to the R-L load impedance with

different power factors [70].

4.5   Chapter conclusion

This chapter proposed a new topology in which the electromechanical tap changing arrangement is substituted with a variable voltage ac source derived using a multi-level converter transforming photovoltaic (PV) generated dc voltage. One of the ideas of this chapter is to retrofit the existing OLTCs to enable them to import solar power to the network. The proposed structure uses a five-level diode-clamped inverter. The output of the inverter is connected to an OLTC with four taps. At each tap, a TRIAC is used instead

of an electromechanical switch in the OLTC system to inject a voltage in series or series opposition with the grid voltage. Hence, the injection can compensate for any increase or decrease in the grid voltage. The arrangement reduces the voltage ratings on the multi-level converter semiconductor devices, as additional voltage control is available due to tap changing. The viability of the concept was demonstrated using EMT simulation and showed that the proposed structure has improved transient behaviour and eliminates the need for the change-over switch and its tie-in resistor used in the conventional OLTCs. The proposed structure is investigated under the resistive and inductive loads, and the results show that the proposed topology can maintain the load voltage at an acceptable limit in both load conditions.

Although the converter-based OLTC works well and has a better transient behaviour than the traditional tap changers, there are some disadvantages associated with the proposed converter in this chapter. They include the high implementation cost, high transient voltage across multilevel inverter solid-state switches, and complicated control systems. The alternative solution is to use the capacitor ladder method which will be proposed in chapter 5.

Chapter 5: An improved Solution: A capacitive ladder-based voltage regulator (CL-EVR)

5.1 Introduction

In the previous chapters, the challenges related to the electromechanical tap changers were discussed. Also, a multilevel inverter-based tap changer was proposed to be used as a substitute for the electromechanical tap changers. All the previous literature and proposed models for the OLTC have their drawbacks such as reliability issues, high implementation cost, and high transient voltage and current. In this chapter, a new fully-electronic tap changer is proposed. This tap changer overcomes the problems in previous OLTCs and proposes new features to the transformer industry. Also, the proposed method in this thesis is provisionally patented in [83-84].

In this chapter, the proposed circuit for the electronic voltage regulator is discussed firstly. The proposed circuit is simulated under loads with different power factors. Then, the specification of the circuit is discussed as well. The theoretical analysis of the proposed electronic voltage regulator is introduced. The resonant effects are considered, and the resonant frequency and loads are calculated. Also, to increase the reliability of the proposed

circuit, a new failure detection method is proposed to enable the CL-EVR to keep operating after the failure of a limited number of switches. Finally, the proposed design was prototyped in the laboratory and successfully tested under inductive and resistive loads.

The results prove that the proposed CL-EVR can apply different voltage levels properly without significant overshoot during the transition from one level to the other.

5.2 Proposed CL-EVR circuit

Figure 5.1 shows the proposed circuit which is in series with a transformer as a voltage regulator. The voltage of the proposed regulator, after selecting the voltage level from the capacitive ladder and using the H-bridge to define its sign, will be added or subtracted from the load winding through a booster transformer, in order to maintain the load voltage in an acceptable range. The input voltage of the electronic voltage regulator (CL-EVR) comes from the auxiliary winding, which has the same phase angle as the load winding voltage. Also, the presented regulator can compensate for 10% of the load winding voltage, 8kV. According to Figure 5.1, the proposed circuit includes a capacitor ladder to apply different voltage levels, the capacitor value is 300µF based on the theoretical analysis and reducing the voltage phase shift of the injected voltage from the CL-EVR. The capacitor ladder is used to be considered as a substitute for the mechanical taps used for electromechanical OLTCs. Each capacitor is connected to one TRIAC to apply the voltage to maintain the load voltage in an acceptable range. Also, each TRIAC is connected to an R-C snubber to ease the transient behaviour of the TRIAC. Also, H-bridge is used to apply the voltage in additive or subtractive mode. To isolate the proposed electronic voltage regulator from the high voltage side, a booster transformer is employed. The booster transformer is in series

with the main winding. If any change, up to 10% of rated voltage, happens to the main

winding voltage, CL-EVR applies voltage in either additive or subtractive mode to

maintain the load voltage in an acceptable range. Figure 5.2 shows the CL-EVR prototype

for the field test. Figure 5.3 shows the capacitor ladder implemented in the CL-EVR, and

Figure 5.4 displays the TRIAC in the prototyped CL-EVR.

In the next section, the simulation results for the proposed circuit will be discussed.
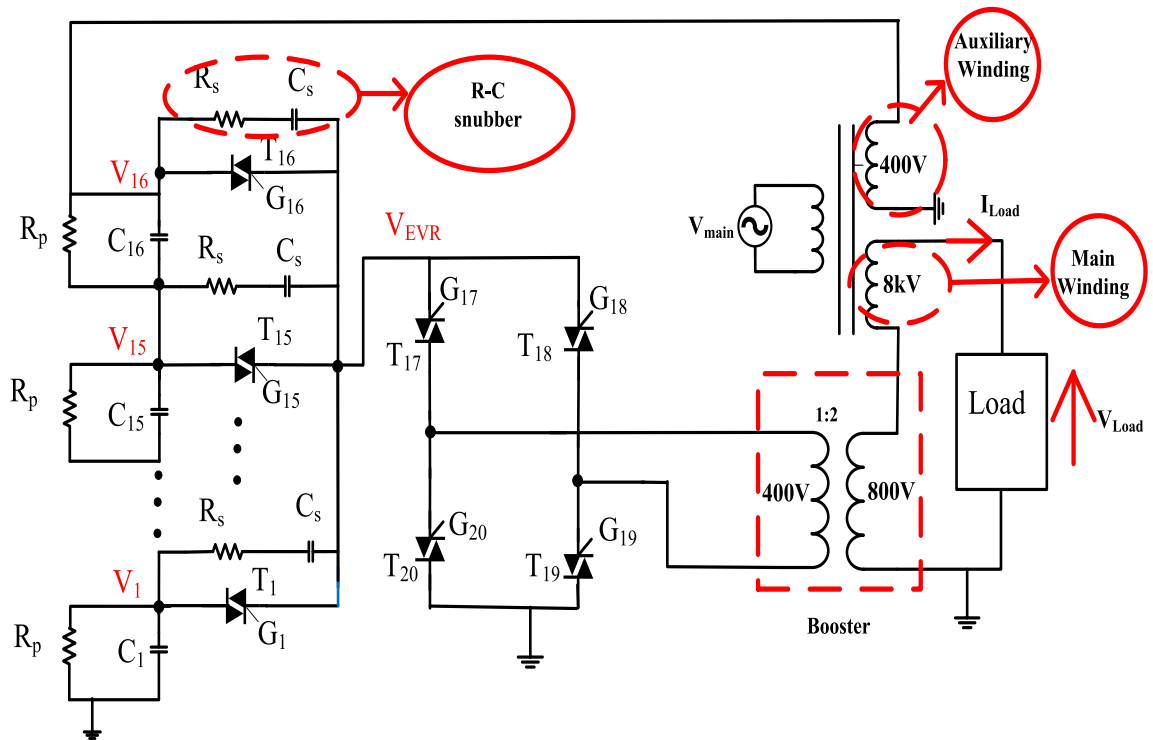
Figure 5.1: shows the proposed CL-EVR circuit, which is connected in series with a
transformer as a voltage regulator. [83-84].
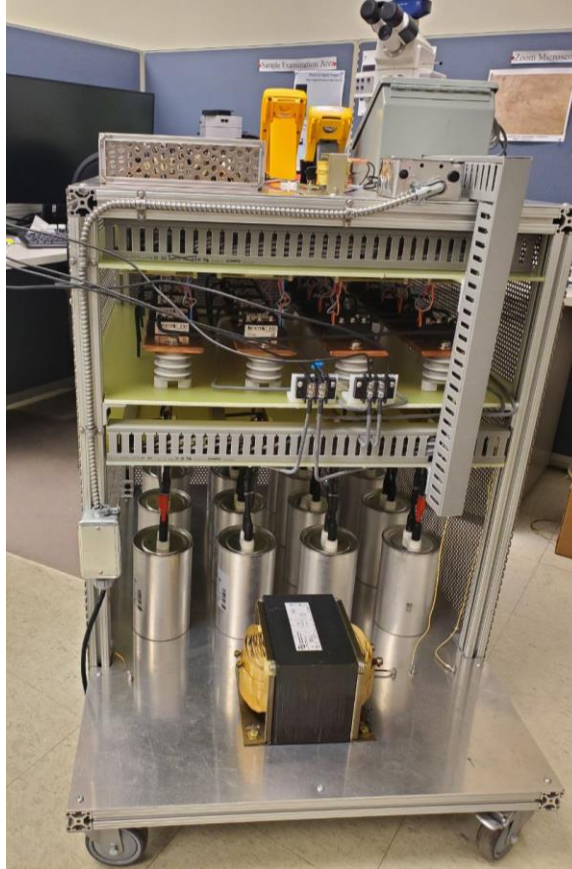
Figure 5.2: The general view of the prototyped CL-EVR [83-84].

Figure 5.3: The capacitor ladder implemented in the prototyped CL-EVR [83-84].

Figure 5.4: The TRIAC implemented in the prototyped CL-EVR [83-84].

5.3   Design refinement and Simulation results

The CL-EVR's performance was checked using an electromagnetic transient simulation program (PSCAD/EMTDC). This also allowed us to select appropriate ladder capacitor values that would work over the expected operating range of load currents and power factors. It also allows us to judge the transient performance and fine-tune the values of the grading resistor, Rp.

Table 5.1 shows the simulation parameters. The simulation has been performed under different load conditions. All the mentioned simulations are performed based on the fact that the load winding has a single-phase power of 33kVA and three-phase power of 100kVA.

Table 5.1: The EMT simulation parameters [83-84].

Component	Value
C_1- C_{16}	300µF
R_p	150Ω
R_s	3000Ω
C_s	0.1µF
Load Voltage	8kV
Main winding voltage	8kV $\pm$ 10%
The voltage ratio	400V:800V
Load power	33 kVA

5.3.1   Simulation results: resistive load

In this simulation, it is assumed that the main supply voltage is changing from 90% to 110% of the rated value. For the first 9s, the supply voltage is changing from 90% to the rated value, so the CL-EVR injects the voltage in additive mode during this 9s to maintain the load voltage in an acceptable range. From 9s to 16s, the supply voltage is changing up to 110% of the rated value. Figure 5.5 shows the CL-EVR output voltage. After that, it is assumed that the main winding voltage is changing from the rated value to 110% of the rated voltage, so the CL-EVR injects the voltage in subtractive mode.

Figure 5.6 (a), shows the capacitor voltages over the 16 s window, with a zoomed 1 s detail shown in Figure 5.6 (b). The capacitor voltage shows a transient overvoltage at the switching instant with a maximum peak of around 130V for about ½ cycle, which is well within the rating of 480 V for the capacitor for the prototype.

Figure 5.7 displays the gate signals of TRIAC (T_{16} to T1) during the simulation time.
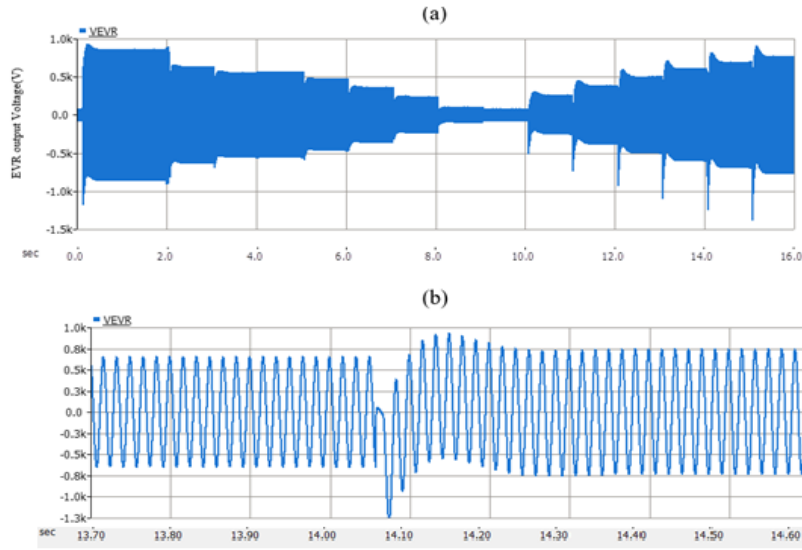
Figure 5.5: The output voltage of the proposed electronic voltage regulator (CL-EVR) (a)

for the whole simulation time (b) for one second.
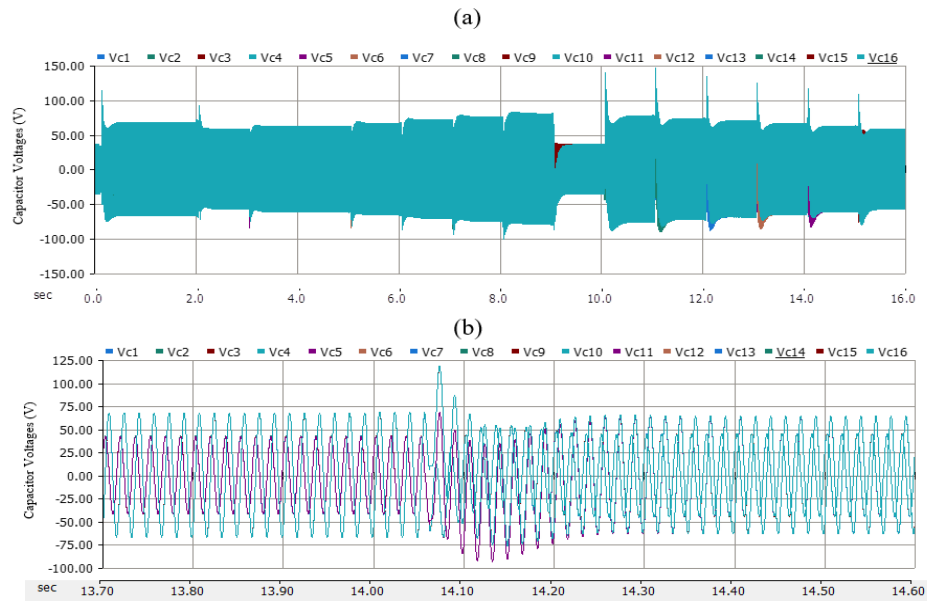
Figure 5.6: The voltage across each capacitor (C_1-C_{16}) (a) for the whole simulation time

(b) for one second.
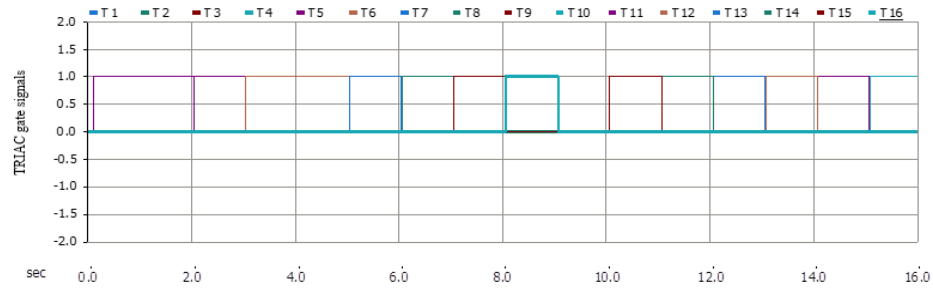
Figure 5.7: The gate signal for each TRIAC.

Figure 5.8 shows the load voltage and rated voltage (8kV rms). According to this figure, the load voltage is very close to the desired voltage (within 0.5%). This shows that the proposed electronic voltage regulator can keep the load voltage in an acceptable range. Figure 5.9 shows the load current which is almost constant all along the simulation time.
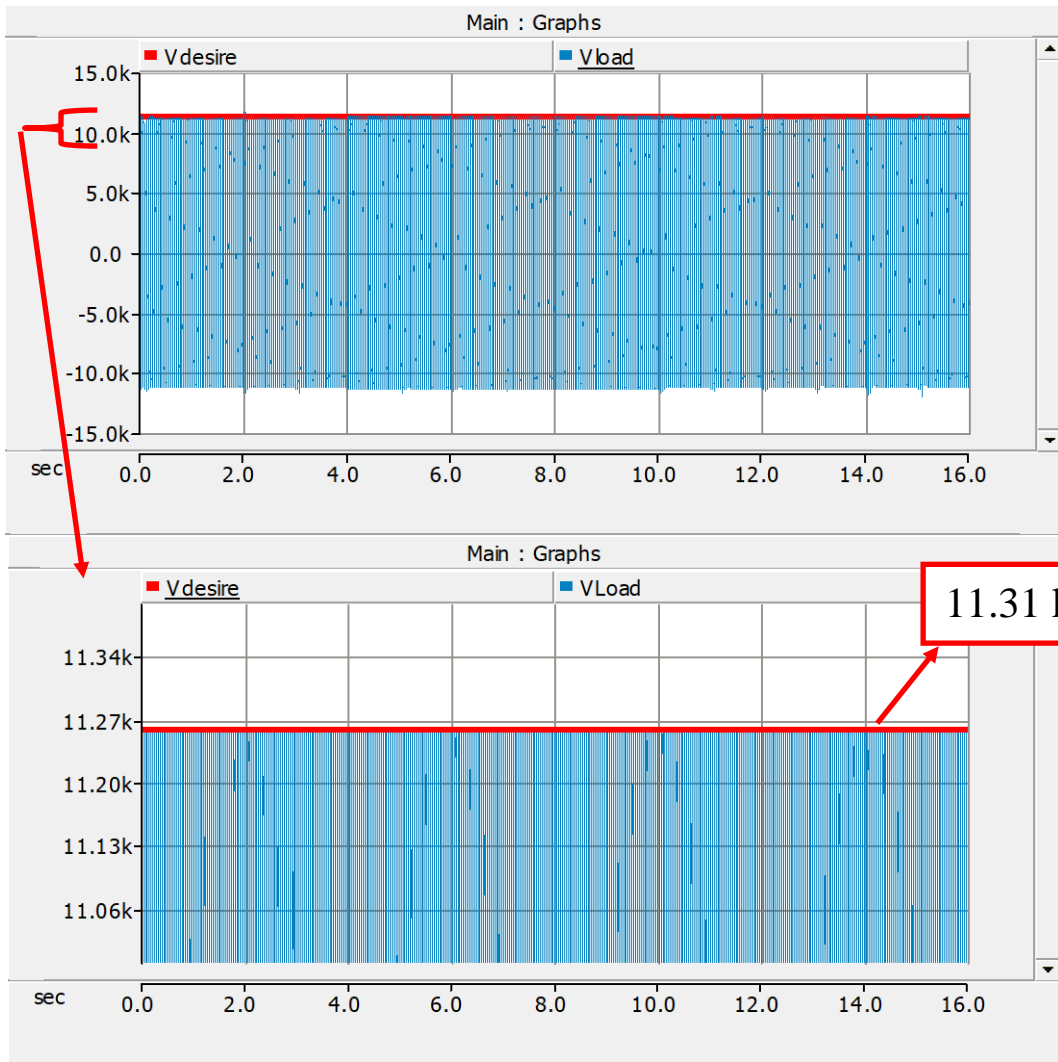
Figure 5.8: The load voltage under the resistive load.
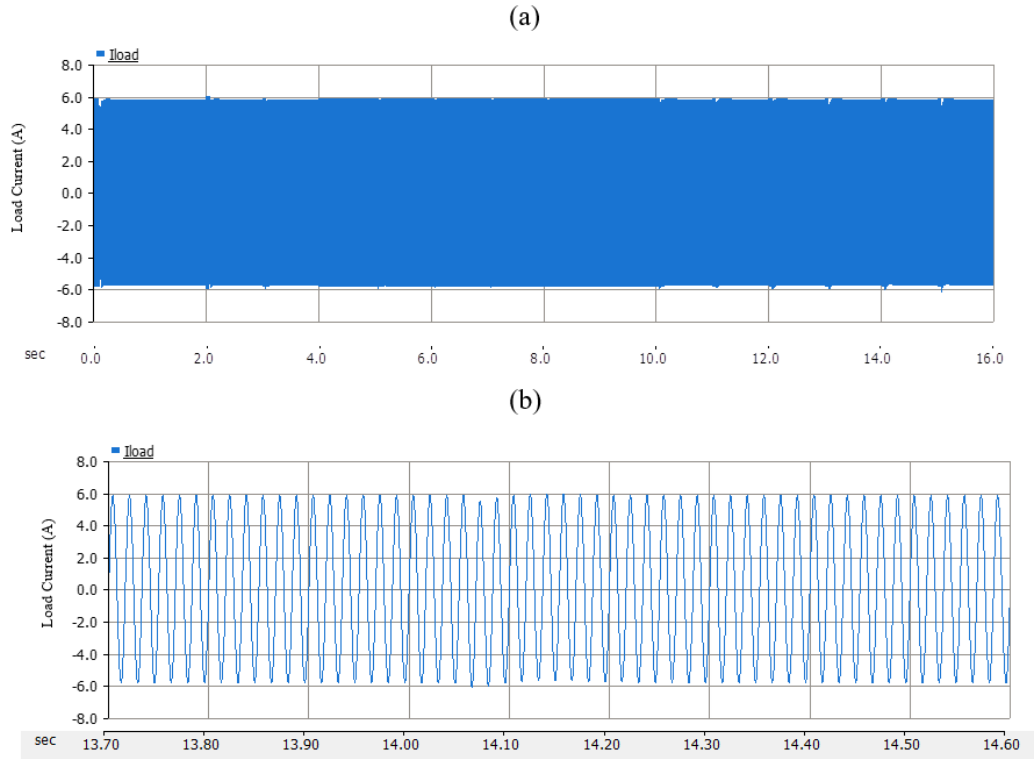
Figure 5.9: The current of the load (a) for the whole simulation time (b) for one second.

5.3.2 Simulation results: inductive load

In this simulation, it is assumed that the main supply voltage is changing from 90% to 110% of the rated value. For the first 9s, the supply voltage is changing from 90% to the rated value, so the CL-EVR injects the voltage in additive mode during this 9s to maintain the load voltage in an acceptable range. From 9s to 16s, the supply voltage is changing up to 110% of the rated value. Figure 5.10 shows the CL-EVR output voltage. After that, it is assumed that the main winding voltage is changing from the rated value to 110% of the rated voltage, so the CL-EVR injects the voltage in subtractive mode.

Figure 5.11 shows the capacitor voltages over the 16 s window. The capacitor voltage shows a transient overvoltage at the switching instant with a maximum peak of   around

200 V for about ½ cycle, which is well within the rating of 480 V for the capacitor for the prototype.
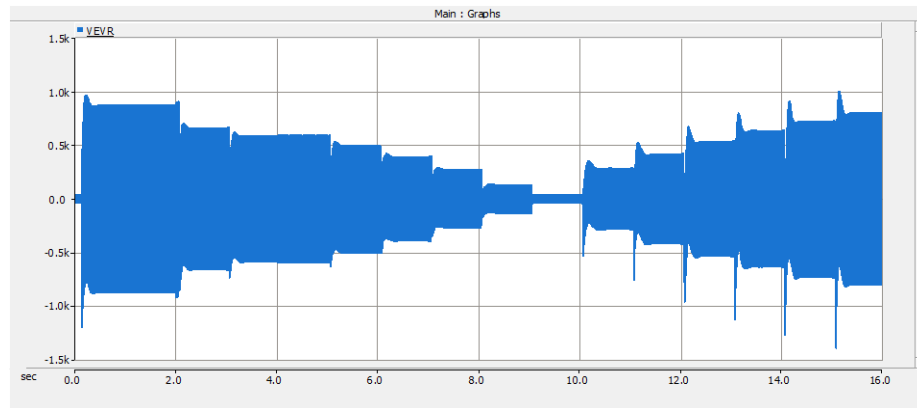
Figure 5.10: The output voltage of the proposed electronic voltage regulator (CL-EVR) (inductive load).
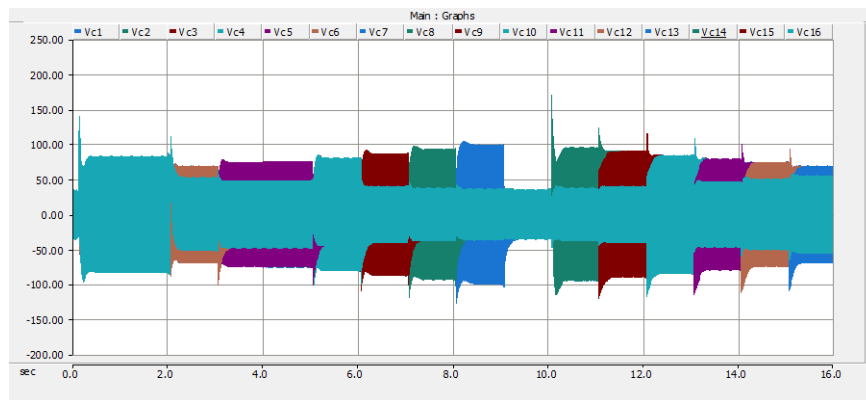
Figure 5.11: The voltage across each capacitor (C_1-C_{16}) (inductive load).

Figure 5.12 shows the load voltage and rated voltage (8kV rms). According to this figure, the load voltage is very close to the desired voltage (within 0.5%). This shows that the proposed electronic voltage regulator can keep the load voltage in an acceptable range.
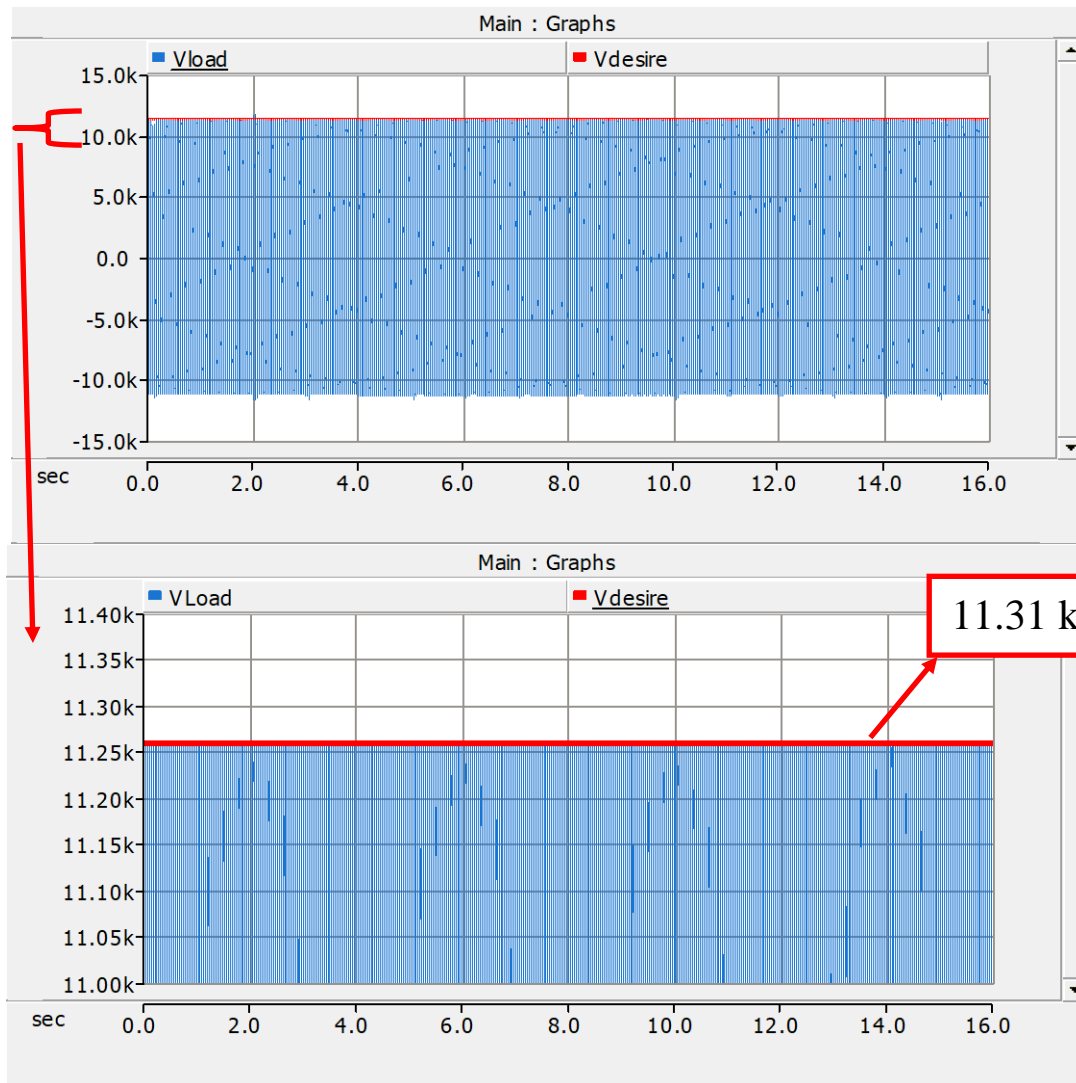
Figure 5.12: The load voltage (inductive load).

5.4   Theoretical Analysis (Phasor Analysis)

5.4.1   CL-EVR load Characteristics

In this part, the CL-EVR load characteristics under different load values are investigated. In order to evaluate the performance of the CL-EVR, it is assumed that the load is directly connected to the CL-EVR. Figure 5.13 shows the phasor equivalent circuit while the nth TRIAC is on. To simplify the calculation, the effect of the snubber is not considered. The input voltage is considered to be 120V and the load could be either inductive, resistive, or load with a power factor of 0.8.

Now, to find the impedance of the CL-EVR, Figure 5.13 is utilized. According to Figure 5.13, The load voltage can be calculated as (5-1). Then, if $Z_{parallel}$ is the parallel of load impedance and Z_B, the load voltage equation will be equal to (2). Z_A and Z_B can be calculated via (5-3) and (5-4).

$$V_{Load} = 120 \times \frac{Z_{Parallel}}{(Z_A)+(Z_{Parallel})} \tag{5-1}$$

$$Z_{Parallel} = \frac{(Z_{Load}||Z_B)}{(Z_{Load}+Z_B)} \tag{5-2}$$

$$Z_B = n \times (8.8266\angle - 86.626) \tag{5-3}$$

$$Z_A = (16 - n) \times (8.8266\angle - 86.626) \tag{5-4}$$

Where Z_A and Z_B are the total impedance of the capacitive and resistive elements above and below the nth level.
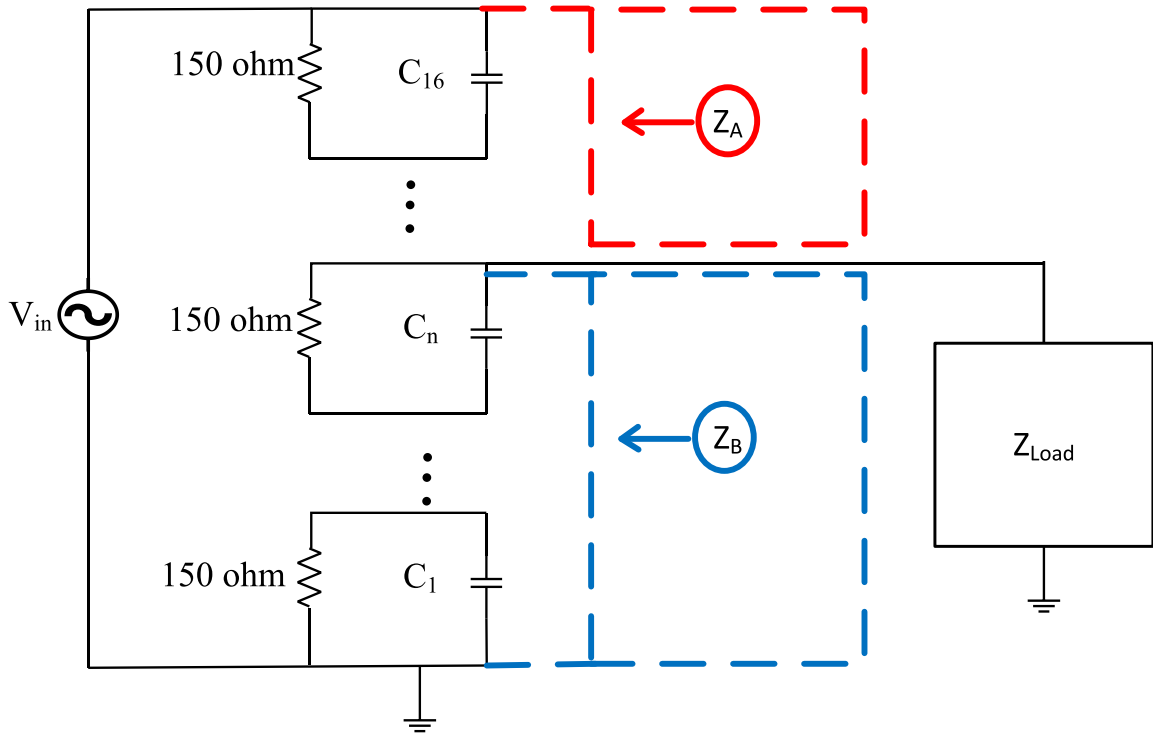
Figure 5.13: The phasor equivalent circuit of CL-EVR.

5.4.2 Theoretical analysis: resistive loads

The load values are shown in Table 5.2. Figure 5.14 shows the calculation results for the CL-EVR with the resistive loads under different loads.

Table 5.3 shows the numerical results of the load voltage under different resistive loads. As shown in

Table 5.3, there is no overshoot in the voltage of CL-EVR under the resistive load. In Tables 5.3, 5.5, and 5.7, V_L and I_L represent the load voltage and load current, respectively.

Table 5.2: The values of the resistive loads.

Impedance=Z (Ω) = a + j0 = R	|Z| (Ω)	Current (A)
1 + 0j	1	120
2 + 0j	2	60
3 + 0j	3	40
4 + 0j	4	30
5 + 0j	5	24
10 + 0j	10	12
15 + 0j	15	8
20 + 0j	20	6
25+ 0j	25	4.8

Table 5.3: The load voltage results of CL-EVR under different resistive loads.

Level	V_L @ I_L=120A	V_L @ I_L=60A	V_L @ I_L=40A	V_L @ I_L=30A	V_L @ I_L=24A	V_L @ I_L=12A	V_L @ I_L=8A	V_L @ I_L=6A
1	0.89	1.73	2.5	3.19	3.78	5.61	6.4	6.79
2	0.96	1.91	2.82	3.7	4.54	7.94	10.15	11.54
3	1.041	2.071	3.08	4.06	5.02	9.27	12.5	14.88
4	1.129	2.24	3.355	4.44	5.5	10.39	14.42	17.59
5	1.23	2.45	3.66	4.86	6.04	11.53	16.24	20.1
6	1.35	2.7	4.04	5.36	6.66	12.8	18.17	22.68
7	1.50	3	4.49	5.96	7.41	14.29	20.37	25.54
8	1.69	3.38	5.05	6.71	8.34	16.1	22.97	28.85
9	1.93	3.86	5.77	7.66	9.53	18.37	26.19	32.84
10	2.26	4.5	6.74	8.93	11.1	21.34	30.29	37.81
11	2.71	5.4	8.07	10.7	13.28	25.38	35.73	44.22
12	3.38	6.74	10.065	13.32	16.52	31.19	43.28	52.77

13	4.51	8.97	13.35	17.63	21.78	40.2	54.28	64.51
14	6.75	13.38	19.8	25.95	31.79	55.5	71.08	80.83
15	13.4	26.08	37.64	47.86	56.72	82.27	96.14	101.85
16	120	120	120	120	120	120	120	120
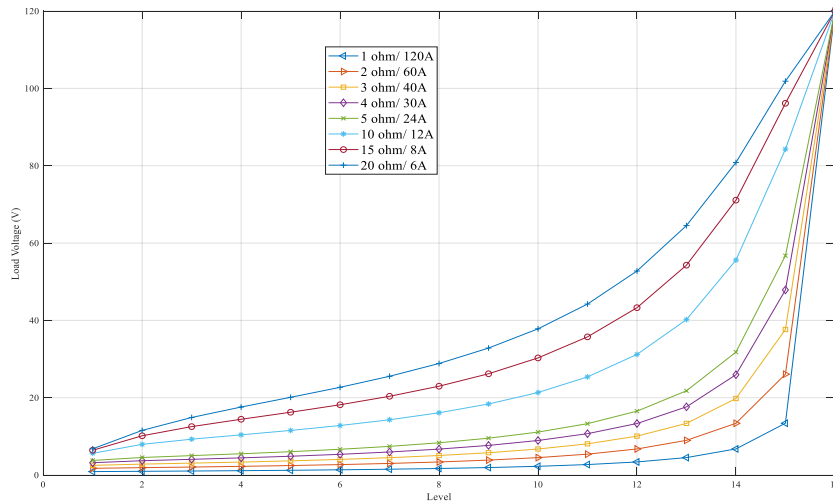
Figure 5.14: The load voltage results of CL-EVR under different resistive loads.

5.4.3 Theoretical analysis: inductive loads

The load values are shown in Table 5.4. Figure 5.15 shows the calculation results for the CL-EVR with the inductive loads. Table 5.5 shows the numerical results of the load voltage under different inductive loads. According to Figure 5.15, there are some overshoots in the voltage of CL-EVR, which shows the resonance.

Table 5.4: The values of the reactive loads.

Impedance=Z (Ω) = a + jb	|Z| (Ω)	|Current	(A)
0 + 1j	1	120
0 + 2j	2	60
0 + 3j	3	40

0 + 4j	4	30
0 + 5j	5	24
0 + 10j	10	12
0 + 15j	15	8
0 + 20j	20	6
0 + 25j	25	4.8
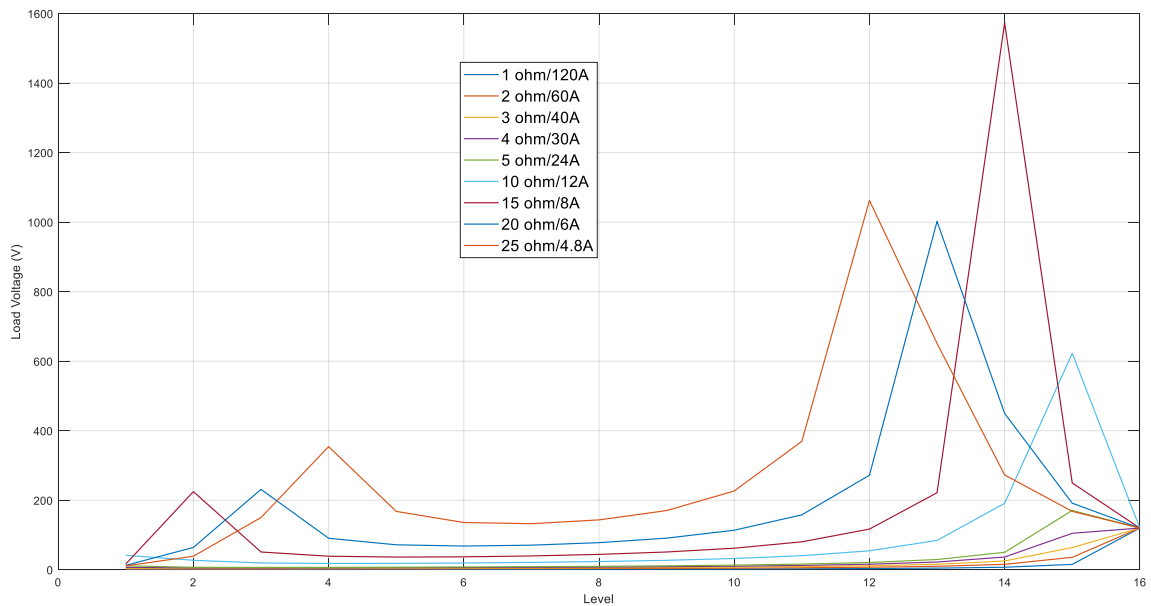
Figure 5.15: The load voltage results of CL-EVR under different reactive (inductive)

loads.

Table 5.5: The load voltage results of CL-EVR under different reactive loads.

Level	V_L @ I_L=120A	V_L @ I_L=60A	V_L @ I_L=40A	V_L @ I_L=30A	V_L @ I_L=24A	V_L @ I_L=12A	V_L @ I_L=8A	V_L @ I_L=6A	V_L @ I_L=4.8A
1	1.03	2.39	4.26	7.00	11.37	15.2	16.65	12.77	11.20
2	1.04	2.23	3.61	5.24	7.17	27.30	224.73	64.25	38.97
3	1.10	2.31	3.64	5.14	6.81	19.49	51.14	231.27	150.28
4	1.18	2.45	3.83	5.34	6.98	18.17	39.00	90.63	354.17

5	1.28	2.65	4.11	5.69	7.40	18.41	36.54	71.82	167.95
6	1.40	2.89	4.48	6.18	8.00	19.46	37.20	68.25	135.95
7	1.56	3.21	4.96	6.83	8.82	21.19	39.77	70.77	132.47
8	1.75	3.60	5.57	7.66	9.90	23.69	44.22	77.99	143.49
9	2.00	4.12	6.38	8.78	11.34	27.24	51.14	90.99	170.32
10	2.34	4.82	7.47	10.31	13.34	32.43	61.99	113.75	226.59
11	2.81	5.82	9.05	12.52	16.27	40.51	80.39	158.01	369.48
12	3.53	7.35	11.50	16.01	20.94	54.52	116.99	271.90	1062.52
13	4.75	9.99	15.79	22.26	29.50	84.44	221.59	1002.16	651.21
14	7.27	15.61	25.30	36.66	50.19	191.07	1573.10	449.73	272.78
15	15.46	35.83	63.88	104.94	170.62	622.84	249.74	191.50	167.95
16	120.00	120.00	120.00	120.00	120.00	120.00	120.00	120.00	120.00

Some values in Table 5.5 are highlighted in red. These values are even bigger than the input voltage. This jump in the voltage happens when the load is inductive. This change is very high under 8A load at level 14.

5.4.4   Theoretical analysis: R-L load with pf=0.8

The load values are shown in Table 5.6. Figure 5.16 shows the calculation results for the CL-EVR with the R-L loads. Table 5.7 shows the numerical results of the load voltage under different loads with the power factor of 0.8. According to Figure 5.16, there is no overshoot in the CL-EVR voltage when the load power factor is 0.8.

Table 5.6: The values of the R-L loads with pf=0.8.

Impedance=Z (Ω)	|Z| (Ω)	|Current | (A)
$0.9 + 0.432j$	1	120

1.802+0.865j	2	60
2.703+1.297j	3	40
3.604+1.73j	4	30
4.505+2.162j	5	24
9+4.324j	10	12
13.51+6.486j	15	8
18.02+8.649j	20	6
22.52+10.81j	25	4.8

As shown in Figure 5.16 and Table 5.7, the voltage profile is improved to a large extent when the load is not purely inductive, and there is no voltage higher than the input voltage, thereby no resonance under the load with the power factor of 0.8.
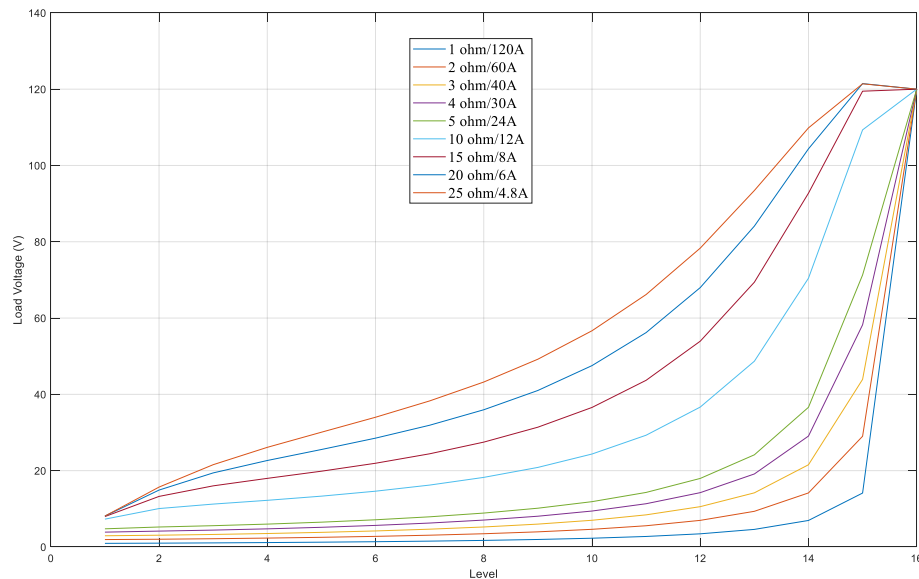
Figure 5.16: The load voltage results of CL-EVR under different loads with PF=0.8.

Table 5.7: The load voltage results of CL-EVR under different RL loads with pf=0.8.

Level	V_L @ I_L=120A	V_L @ I_L=60A	V_L @ I_L=40A	V_L @ I_L=30A	V_L @ I_L=24A	V_L @ I_L=12A	V_L @ I_L=8A	V_L @ I_L=6A	V_L @ I_L=4.8A
1	0.94	1.93	2.93	3.88	4.75	7.29	8.98	8.10	8.09
2	0.99	2.02	3.08	4.15	5.23	10.06	14.96	14.91	15.69
3	1.06	2.16	3.27	4.41	5.57	11.23	17.36	19.41	21.56
4	1.15	2.32	3.52	4.74	5.99	12.22	18.92	22.66	26.11
5	1.25	2.53	3.82	5.15	6.50	13.31	20.52	25.54	30.07
6	1.37	2.77	4.20	5.65	7.12	14.62	22.43	28.52	34.00
7	1.52	3.08	4.66	6.27	7.90	16.22	24.83	31.90	38.28
8	1.71	3.46	5.24	7.04	8.88	18.23	27.89	35.96	43.23
9	1.96	3.96	5.99	8.06	10.16	20.85	31.92	41.02	49.21
10	2.29	4.62	6.99	9.41	11.87	24.36	37.39	47.53	56.67
11	2.75	5.56	8.41	11.33	14.29	29.29	45.14	56.19	66.16
12	3.44	6.97	10.56	14.23	17.96	36.66	56.75	67.98	78.33
13	4.60	9.34	14.18	19.13	24.15	48.68	75.21	84.10	93.43
14	6.94	14.16	21.54	29.06	36.61	70.45	104.72	104.36	109.85
15	14.13	29.01	43.92	58.23	71.29	109.33	110.76	120.46	120.41
16	120.00	120.00	120.00	120.00	120.00	120.00	120.00	120.00	120.00

5.4.5　Resonant condition

The theoretical analysis of resonance is investigated. According to Figure 5.13, the impedance of capacitors, Z_B, at each level is found. Table 5.8 shows the impedance, Z_B value at each level.

Table 5.8: The impedance value at each level.

Level	Z_B (Ω)	Level	Z_B (Ω)
1	0.5194 - 8.8113j	9	4.674-79.3017j
2	1.0388-17.6226j	10	5.194-88.113j
3	1.5582-26.4339j	11	5.7134-96.9243j
4	2.0776-35.2452j	12	6.2328-105.7356j
5	2.597-44.0565j	13	6.752-114.546j
6	3.1164-52.8678j	14	7.271-123.358j
7	3.6358-61.6791j	15	7.791-132.1695j
8	4.155-70.4904j	16	8.3104-140.9808j

The resonance can happen if the imaginary part of $Z_{parallel}$ is cancelled by the imaginary part of the Z_A. Therefore, to find whether there could be a resonance at 60Hz frequency, $Z_{parallel}$ should be equal to the conjugate of the imaginary part of Z_A, which will be equal to $(16 - n)(j8.8113)$. Therefore,

$$Z_{parallel} = (16 - n)(j8.8113) \qquad (5\text{-}5)$$

By using equations (5-2) and (5-5), Z_{loadR} can be found as shown in equation (5-6). Z_{loadR} is the resonant impedance.

$$Z_{LoadR} = \left[\frac{(n-16) \times (j8.8113) \times n \times (0.5194 - j8.8113)}{(16) \times (j8.8113) - (n) \times (0.5194)} \right] \qquad (5\text{-}6)$$

Considering equation (7), Table 5.9 shows the Z_{loadR}, the impedance of resonance, value at each level.

Table 5.9: The resonance impedance Z_{loadR} values at each level.

Level	Z_{LoadR} (Ω)	Level	Z_{LoadR} (Ω)
1	-0.456+8.262j	9	-0.893+34.724j
2	-0.795+15.425j	10	-0.729+33.069j
3	1.0285+21.88j	11	-0.557+30.311j
4	-1.168+26.451j	12	-0.388+26.451j
5	-1.227+30.311j	13	-0.236+21.488j
6	-1.216+33.069j	14	-0.113+15.42j
7	-1.149+34.724j	15	-0.03+8.2627j
8	-1.037+35.275j	16	-----

At level 16, no resonant impedance is considered because the load voltage will be directly connected to the input voltage. In order to avoid any resonance to happen, the impedance seen by the CL-EVR when n^{th} level is activated should not be close to the resonance impedance at n^{th} level shown in Table 5.9.

The minimum CL-EVR current for the resonant creation is for level 8 which is around 12A. However, the operating current of CL-EVR is 8.25 A which is selected to avoid any resonance.

5.5   Theoretical analysis (Laplace transform)

This section provides the study on the transient behaviour of CL-EVR under different loads using theoretical analysis. Laplace transform is used to consider both transient and steady-state results. The results are used to validate the EMT simulation results.

In this study, CL-EVR is considered to be directly connected to the load. In CL-EVR, there are 16 different stages that each of them could be activated when the corresponding TRIAC is at on state. In this study, different calculations will be performed for all sixteen conditions. For example, if TRIAC T_1 is at on state, the output voltage of CL-EVR would be equal to the voltage of capacitor C_1 as shown in Figure 5.17. Then, the calculation will be performed accordingly.

Regarding the parameters of the calculation, Z_1 is the equivalent impedance between each capacitor (C_1- C_{16}) and parallel resistors. Z_2 is the impedance of the R-C snubber circuit. Z_1 and Z_2 can be calculated by equations (5-7) and (5-8).

$$Z_1 = \frac{R_p \times \frac{1}{sC_1}}{R_p + \frac{1}{sC_1}} = \frac{R_p}{1 + sR_pC_1} = \frac{150}{1 + s \times 150 \times 300 \times 10^{-6}} = \frac{150}{1 + 0.045s} \qquad (5\text{-}7)$$

$$Z_2 = R_s + \frac{1}{sc_s} = 3000 + \frac{1}{s \times 0.1 \times 10^{-6}} = 3000 + \frac{10^7}{s} \qquad (5\text{-}8)$$

For the theoretical analysis, the transfer function is calculated for each nth condition, which is equal to $H_n(s) = \frac{Vout(s)}{Vin(s)}$. Then the transfer function is multiplied by the input voltage to find the output voltage as shown in (5-9). The initial voltage values for the theoretical analysis are considered to be zero.

$$Vout(s) = H_n(s) \times Vin(s) \qquad (5-9)$$

Table 5.10 shows the theoretical calculation parameters:

Table 5.10: The theoretical analysis parameters [83-84].

Parameters	Value
Input Voltage	400V rms
R load	50 Ω
R-L load	R=38.09 Ω and L=0.07578 H
L load	0.1263 H
R_s	3000 Ω
C_0	0.1 µF
C_1-C_{16}	300 µF
CL-EVR output power	33 kVA

Now, the first condition in which T_1 is at on state. According to Figure 5.17, when T_1 is at on-state, the load voltage (V_{out}) is equal to the voltage of capacitor C_1. The equations of voltages are shown in (5-10) based on node analysis.
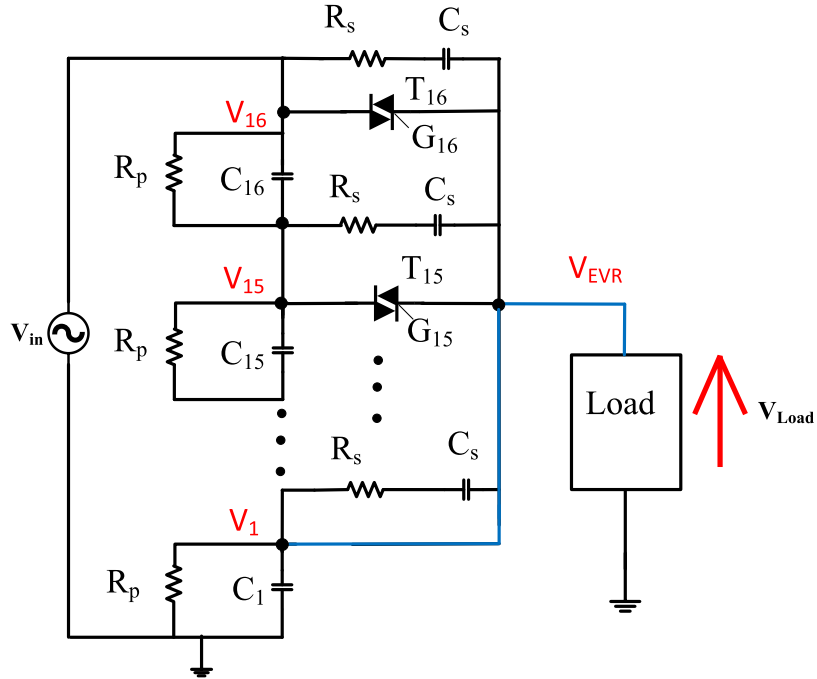
Figure 5.17: The 16-level CL-EVR when it is directly connected to the load and T_1 is at on-state [83-84].

$$(\frac{2}{Z1}+\frac{1}{Z2})V1-\frac{1}{Z1}V2-\frac{1}{Z2}Vout=\frac{1}{Z1}Vin$$
$$-\frac{1}{Z1}V1+(\frac{2}{Z1}+\frac{1}{Z2})V2-\frac{1}{Z1}V3-\frac{1}{Z2}Vout=0$$
$$-\frac{1}{Z1}V2+(\frac{2}{Z1}+\frac{1}{Z2})V3-\frac{1}{Z1}V4-\frac{1}{Z2}Vout=0$$
$$-\frac{1}{Z1}V3+(\frac{2}{Z1}+\frac{1}{Z2})V4-\frac{1}{Z1}V5-\frac{1}{Z2}Vout=0$$
$$-\frac{1}{Z1}V4+(\frac{2}{Z1}+\frac{1}{Z2})V5-\frac{1}{Z1}V6-\frac{1}{Z2}Vout=0$$
$$-\frac{1}{Z1}V5+(\frac{2}{Z1}+\frac{1}{Z2})V6-\frac{1}{Z1}V7-\frac{1}{Z2}Vout=0$$
$$-\frac{1}{Z1}V6+(\frac{2}{Z1}+\frac{1}{Z2})V7-\frac{1}{Z1}V8-\frac{1}{Z2}Vout=0$$
$$-\frac{1}{Z1}V7+(\frac{2}{Z1}+\frac{1}{Z2})V8-\frac{1}{Z1}V9-\frac{1}{Z2}Vout=0$$
$$-\frac{1}{Z1}V8+(\frac{2}{Z1}+\frac{1}{Z2})V9-\frac{1}{Z1}V10-\frac{1}{Z2}Vout=0$$
$$-\frac{1}{Z1}V10+(\frac{2}{Z1}+\frac{1}{Z2})V11-\frac{1}{Z1}V12-\frac{1}{Z2}Vout=0$$
$$-\frac{1}{Z1}V11+(\frac{2}{Z1}+\frac{1}{Z2})V12-\frac{1}{Z1}V13-\frac{1}{Z2}Vout=0$$
$$-\frac{1}{Z1}V12+\left(\frac{2}{Z1}+\frac{1}{Z2}\right)V13-\frac{1}{Z1}V14-\frac{1}{Z2}Vout=0$$

(5-10)

$$-\frac{1}{Z1}V13 + (\frac{2}{Z1} + \frac{1}{Z2})V14 - (\frac{1}{Z1} + \frac{1}{Z2})Vout = 0$$

$$-\frac{1}{Z2}V1 - \frac{1}{Z2}V2 - \frac{1}{Z2}V3 - \frac{1}{Z2}V4 - \frac{1}{Z2}V5 - \frac{1}{Z2}V6$$
$$-\frac{1}{Z2}V7 - \frac{1}{Z2}V8 - \frac{1}{Z2}V9$$
$$-\frac{1}{Z2}V10 - \frac{1}{Z2}V11 - \frac{1}{Z2}V12$$
$$-\frac{1}{Z2}V13 - (\frac{1}{Z2} + \frac{1}{Z1})V14 + (\frac{15}{Z2}$$
$$+\frac{2}{Z1} + \frac{1}{ZL})Vout = \frac{1}{Z2}Vi$$

(5-10) can be reduced to a single equation (5-11) relating the output voltage V_{out} to the input V_{in}.

$$Vout(s) = H_1(s) \times Vin(s) \qquad (5\text{-}11)$$

Similar transfer functions $H_2(s)$, $H_3(s)$ …$H_{16}(s)$ are derived (not shown) for the other 15 levels (Note: $H_{16}(s) = 1$).

Then, the transfer function $H_1(s)$ when T_1 is closed can be found as (5-12).

$$H_1(s)$$

$$
\begin{vmatrix}
\frac{2}{Z1}+\frac{1}{Z2} & -\frac{1}{Z1} & 0 & 0 & 0 & 0 & 0 & 0 & 0 & 0 & 0 & 0 & 0 & 0 \\
-\frac{1}{Z1} & \frac{2}{Z1}+\frac{1}{Z2} & -\frac{1}{Z1} & 0 & 0 & 0 & 0 & 0 & 0 & 0 & 0 & 0 & 0 & 0 \\
0 & -\frac{1}{Z1} & \frac{2}{Z1}+\frac{1}{Z2} & -\frac{1}{Z1} & 0 & 0 & 0 & 0 & 0 & 0 & 0 & 0 & 0 & 0 \\
0 & 0 & -\frac{1}{Z1} & \frac{2}{Z1}+\frac{1}{Z2} & -\frac{1}{Z1} & 0 & 0 & 0 & 0 & 0 & 0 & 0 & 0 & 0 \\
0 & 0 & 0 & -\frac{1}{Z1} & \frac{2}{Z1}+\frac{1}{Z2} & -\frac{1}{Z1} & 0 & 0 & 0 & 0 & 0 & 0 & 0 & 0 \\
0 & 0 & 0 & 0 & -\frac{1}{Z1} & \frac{2}{Z1}+\frac{1}{Z2} & -\frac{1}{Z1} & 0 & 0 & 0 & 0 & 0 & 0 & 0 \\
0 & 0 & 0 & 0 & 0 & -\frac{1}{Z1} & \frac{2}{Z1}+\frac{1}{Z2} & -\frac{1}{Z1} & 0 & 0 & 0 & 0 & 0 & 0 \\
0 & 0 & 0 & 0 & 0 & 0 & -\frac{1}{Z1} & \frac{2}{Z1}+\frac{1}{Z2} & -\frac{1}{Z1} & 0 & 0 & 0 & 0 & 0 \\
0 & 0 & 0 & 0 & 0 & 0 & 0 & -\frac{1}{Z1} & \frac{2}{Z1}+\frac{1}{Z2} & -\frac{1}{Z1} & 0 & 0 & 0 & 0 \\
0 & 0 & 0 & 0 & 0 & 0 & 0 & 0 & -\frac{1}{Z1} & \frac{2}{Z1}+\frac{1}{Z2} & -\frac{1}{Z1} & 0 & 0 & 0 \\
0 & 0 & 0 & 0 & 0 & 0 & 0 & 0 & 0 & -\frac{1}{Z1} & \frac{2}{Z1}+\frac{1}{Z2} & -\frac{1}{Z1} & 0 & 0 \\
0 & 0 & 0 & 0 & 0 & 0 & 0 & 0 & 0 & 0 & -\frac{1}{Z1} & \frac{2}{Z1}+\frac{1}{Z2} & -\frac{1}{Z1} & 0 \\
0 & 0 & 0 & 0 & 0 & 0 & 0 & 0 & 0 & 0 & 0 & -\frac{1}{Z1} & \frac{2}{Z1}+\frac{1}{Z2} & -\frac{1}{Z1} \\
0 & 0 & 0 & 0 & 0 & 0 & 0 & 0 & 0 & 0 & 0 & 0 & -\frac{1}{Z1} & \frac{2}{Z1}+\frac{1}{Z2} \\
-\frac{1}{Z2} & -\frac{1}{Z2} & -\frac{1}{Z2} & -\frac{1}{Z2} & -\frac{1}{Z2} & -\frac{1}{Z2} & -\frac{1}{Z2} & -\frac{1}{Z2} & -\frac{1}{Z2} & -\frac{1}{Z2} & -\frac{1}{Z2} & -\frac{1}{Z2} & -\frac{1}{Z2} & -\left(\frac{1}{Z2}+\frac{1}{Z1}\right)
\end{vmatrix}
$$

$$
=
\begin{vmatrix}
\frac{2}{Z1}+\frac{1}{Z2} & -\frac{1}{Z1} & 0 & 0 & 0 & 0 & 0 & 0 & 0 & 0 & 0 & 0 & 0 & 0 \\
-\frac{1}{Z1} & \frac{2}{Z1}+\frac{1}{Z2} & -\frac{1}{Z1} & 0 & 0 & 0 & 0 & 0 & 0 & 0 & 0 & 0 & 0 & 0 \\
0 & -\frac{1}{Z1} & \frac{2}{Z1}+\frac{1}{Z2} & -\frac{1}{Z1} & 0 & 0 & 0 & 0 & 0 & 0 & 0 & 0 & 0 & 0 \\
0 & 0 & -\frac{1}{Z1} & \frac{2}{Z1}+\frac{1}{Z2} & -\frac{1}{Z1} & 0 & 0 & 0 & 0 & 0 & 0 & 0 & 0 & 0 \\
0 & 0 & 0 & -\frac{1}{Z1} & \frac{2}{Z1}+\frac{1}{Z2} & -\frac{1}{Z1} & 0 & 0 & 0 & 0 & 0 & 0 & 0 & 0 \\
0 & 0 & 0 & 0 & -\frac{1}{Z1} & \frac{2}{Z1}+\frac{1}{Z2} & -\frac{1}{Z1} & 0 & 0 & 0 & 0 & 0 & 0 & 0 \\
0 & 0 & 0 & 0 & 0 & -\frac{1}{Z1} & \frac{2}{Z1}+\frac{1}{Z2} & -\frac{1}{Z1} & 0 & 0 & 0 & 0 & 0 & 0 \\
0 & 0 & 0 & 0 & 0 & 0 & -\frac{1}{Z1} & \frac{2}{Z1}+\frac{1}{Z2} & -\frac{1}{Z1} & 0 & 0 & 0 & 0 & 0 \\
0 & 0 & 0 & 0 & 0 & 0 & 0 & -\frac{1}{Z1} & \frac{2}{Z1}+\frac{1}{Z2} & -\frac{1}{Z1} & 0 & 0 & 0 & 0 \\
0 & 0 & 0 & 0 & 0 & 0 & 0 & 0 & -\frac{1}{Z1} & \frac{2}{Z1}+\frac{1}{Z2} & -\frac{1}{Z1} & 0 & 0 & 0 \\
0 & 0 & 0 & 0 & 0 & 0 & 0 & 0 & 0 & -\frac{1}{Z1} & \frac{2}{Z1}+\frac{1}{Z2} & -\frac{1}{Z1} & 0 & 0 \\
0 & 0 & 0 & 0 & 0 & 0 & 0 & 0 & 0 & 0 & -\frac{1}{Z1} & \frac{2}{Z1}+\frac{1}{Z2} & -\frac{1}{Z1} & 0 \\
0 & 0 & 0 & 0 & 0 & 0 & 0 & 0 & 0 & 0 & 0 & -\frac{1}{Z1} & \frac{2}{Z1}+\frac{1}{Z2} & -\frac{1}{Z1} \\
0 & 0 & 0 & 0 & 0 & 0 & 0 & 0 & 0 & 0 & 0 & 0 & -\frac{1}{Z1} & \frac{2}{Z1}+\frac{1}{Z2} \\
-\frac{1}{Z2} & -\frac{1}{Z2} & -\frac{1}{Z2} & -\frac{1}{Z2} & -\frac{1}{Z2} & -\frac{1}{Z2} & -\frac{1}{Z2} & -\frac{1}{Z2} & -\frac{1}{Z2} & -\frac{1}{Z2} & -\frac{1}{Z2} & -\frac{1}{Z2} & -\frac{1}{Z2} & -\left(\frac{1}{Z2}+\frac{1}{Z1}\right)
\end{vmatrix}
$$

(5-12)

So, the output voltage results when 400 V sinusoidal input is applied and T_1 is closed to the resistive, inductive, and pf=0.8 are shown in Figure 5.18, Figure 5.19, and Figure 5.20. Also, the PSCAD simulations are shown only for level 1 to show that the results are very close for both the transient and the steady-state condition.

(a)   (b)

Figure 5.18: The load voltage (resistive load) (a) PSCAD (b) theoretical.
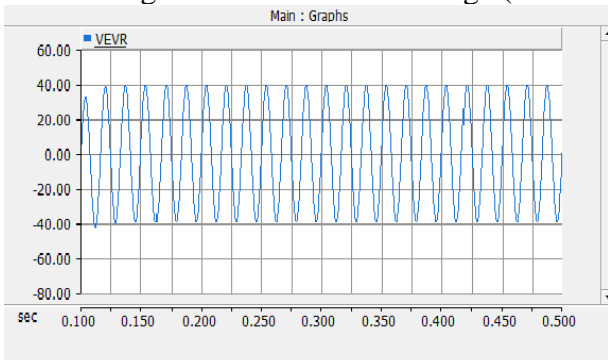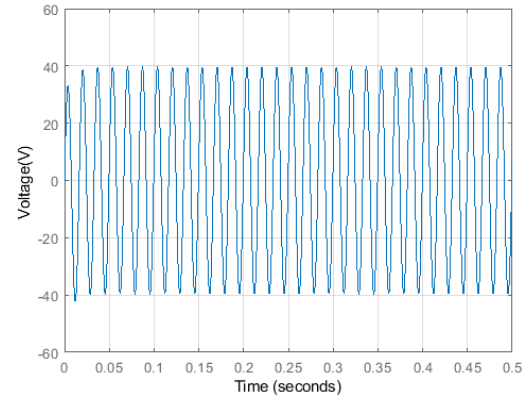
(a)   (b)

Figure 5.19: The load voltage (pf=0.8) (a) PSCAD (b) theoretical.
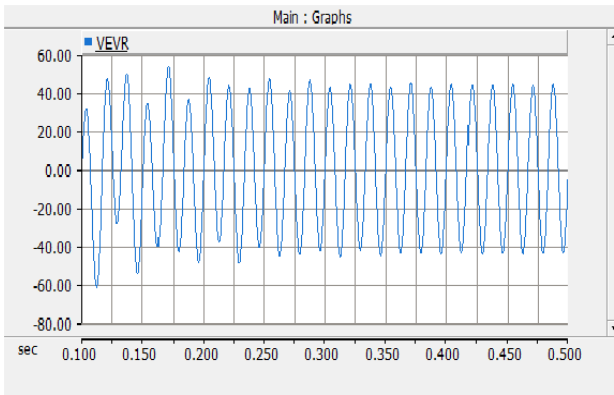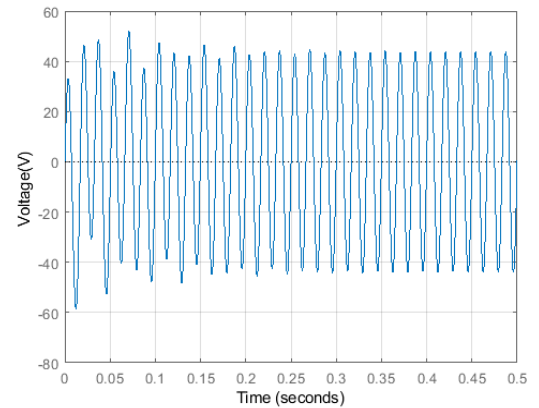
(a)   (b)

Figure 5.20: The load voltage (Inductive load) (a) PSCAD (b) theoretical.

5.5.1   Comparing EMT simulation and theoretical results:

Now, the EMT simulation results are compared with the theoretical result to check the validity of the simulations and calculations. Figure 5.1 is considered as a case study in this comparison. For the theoretical results, the effect of the main winding, load, and booster transformer is considered in Laplace transform as well. The load is 33 kVA (single-phase) in this study.   Figure 5.21 shows the comparison results for the steady-state condition between EMT simulation and theoretical analysis.
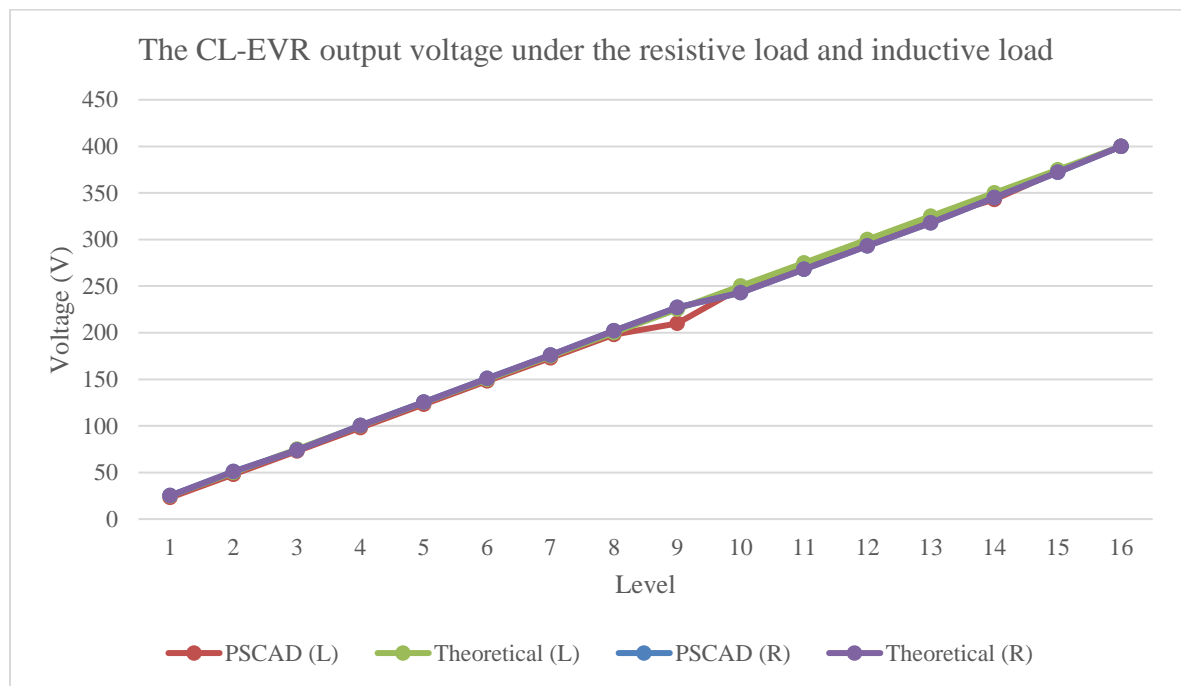
Figure 5.21: Comparing PSCAD and Theoretical Results (R and L loads)

5.6   Protecting the System: Failure detection methods

The TRIACs failure mode is a permanent short, which can create damaging currents in other TRIACs. Assume that the main ac voltage is rising and just before t =2 s, in which T_{16} is conducting. The increase in the main voltage requires a reduction in injected voltage or $V_{CL\text{-}EVR}$ so that the load voltage remains constant. This is achieved by stopping the gate

pulse to T_{16} at t = 2 s and applying a gate pulse to T_{15} 1 cycle later (i.e., at t =2.016s). However, T_{16} has failed during this interval in the shorted condition (i.e., continually conducting). Now without any protection circuitry, when T_{15} is commanded, a high circulating current would flow through T_{15} and capacitor C_{16}, which would cause this TRIAC and most likely C_{16} as well, to fail. Figure 5.22 shows the condition in which T_{16} fails. Different solutions have been proposed in the literature to detect a TRIAC failure and isolate the faulted TRIAC.
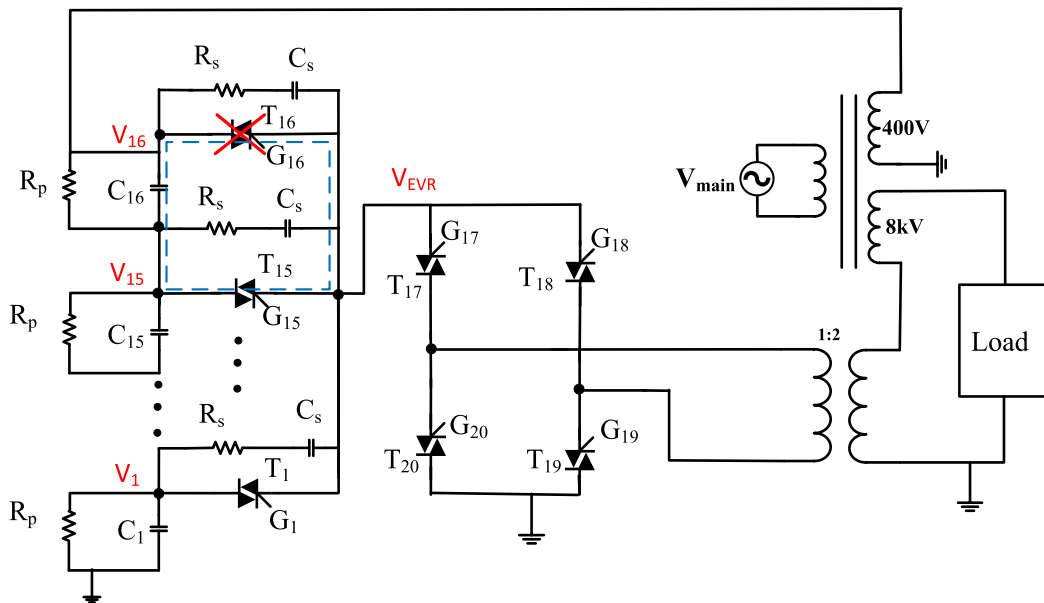
Figure 5.22: The schematic of the circuit used in the failure detection method.

5.6.1   Failure detection method

This section presents a new method [83-84] to protect the system. It detects and isolates the failed TRIAC from the CL-EVR so that the CL-EVR can still operate, albeit with a reduced number of levels.

Figure 5.23 shows the proposed control method when TRIAC T_{16} fails for ensuring that the failed TRIAC is removed from the circuit. The jth TRIAC T_j (j=1,2...16) are in series with

microswitch MS$_j$ which is responsible for removing the failed TRIAC from the CL-EVR circuit. The microswitch rating is 800V and 10A in the experiment. The TRIAC failure detection and isolation system are next described.

When a change of voltage level is ordered, i.e., when TRIAC T$_j$ is to be turned off and TRIAC T$_k$ is to be turned on, there is a one-cycle period when no gate pulses are given to any TRIAC. During this time, the CL-EVRs output voltage V$_{CL-EVR}$ would nominally drop to zero once the current in the TRIAC is extinguished at a zero-crossing. Hence, if V$_{CL-EVR}$ is larger than a certain threshold (found by simulation and experiment to be about 20 V for the proposed rating and structure of the circuit) it indicates that the last conducting TRIAC is faulted and not turned off. On TRIAC fault detection, the control system sends a "turn-off" signal to the microswitch in series with the failed TRIAC to isolate it so it is no longer in the circuit. The CL-EVR can still keep working without any interruption, although there is one-less level for the selectable voltage.

Figure 5.23: The proposed failure detection circuit.

5.6.2 Simulation results for the failure detection method

Figure 5.24 shows an EMT simulation demonstrating the operation of this detection and

isolation controller. Assume T_{16} is on, thereby applying the cumulative voltage across capacitors C_1 thru C_{16} at $V_{CL\text{-}EVR}$. At t=2 s, the gate pulses are discontinued and T_{15} is commanded to turn on (after a 1 cycle delay at t= 2.016s. During the one cycle as shown in Figure 5.24, the voltage of CL-EVR will be zero to keep the load voltage uninterrupted. After the fault is cleared, the CL-EVR voltage stays at level 15th voltage. Figure 5.24 shows the capacitor voltages during the fault time at which there is a transient voltage of 250V on capacitor C_{16}, which is less than the maximum rating of the capacitors, 480V, in the CL-EVR. Also, Figure 5.24 displays the load voltage during the fault and protection operation period. There is a slight momentary dip for about 1 Cycle, which is essentially uninterrupted and close to the rated value. Figure 5.25 shows the load voltage for where the supply voltage is changed from 90% to the rated value and back from 110% to the rated value. The CL-EVR output voltage continues to behave as required and the load voltage remains at the desired 8 kV setpoint during the simulation time. But of course, now there are only 15 steps of control instead of 16.
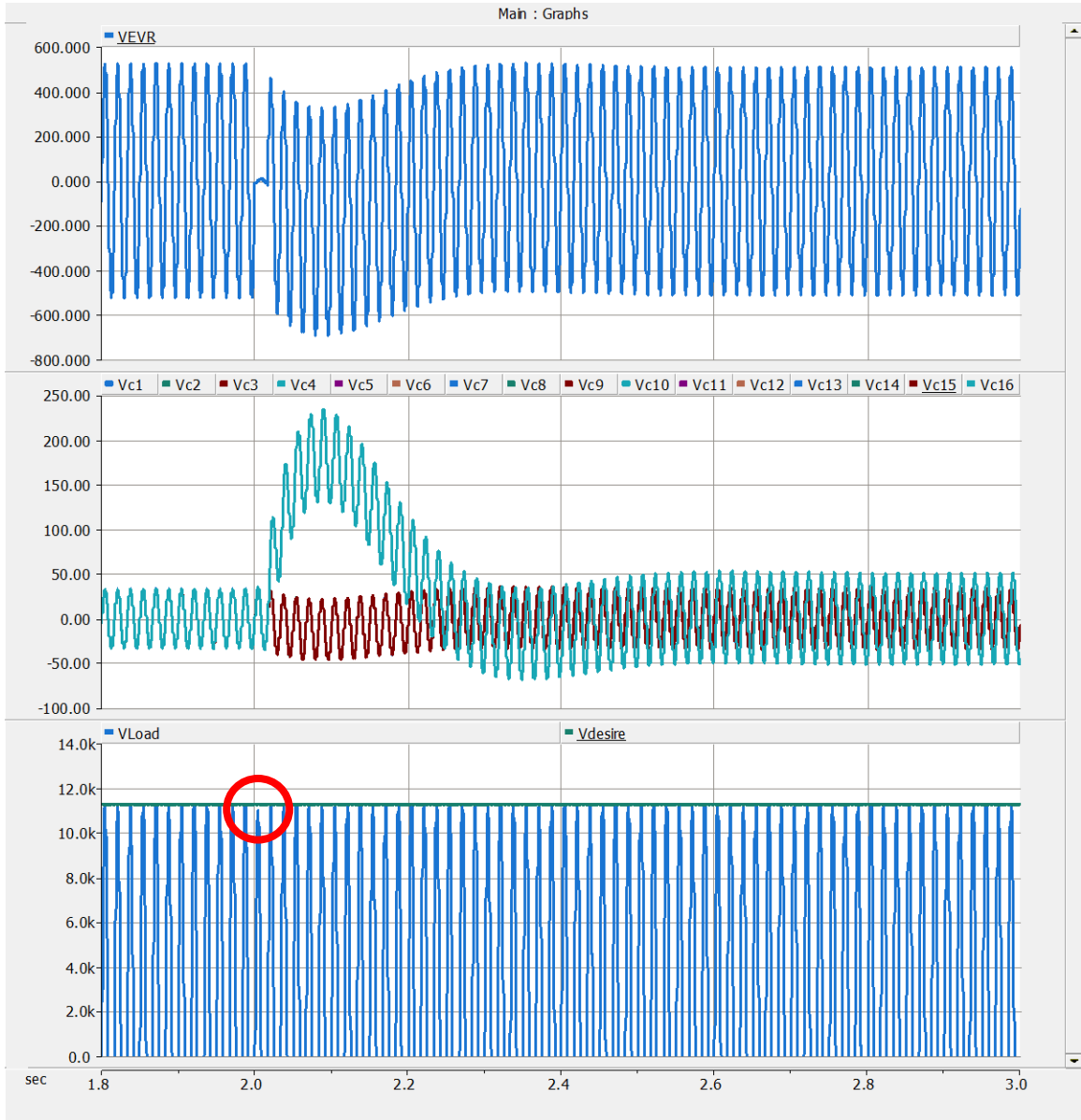
Figure 5.24: The CL-EVR and capacitor voltages during the fault time under the inductive load.
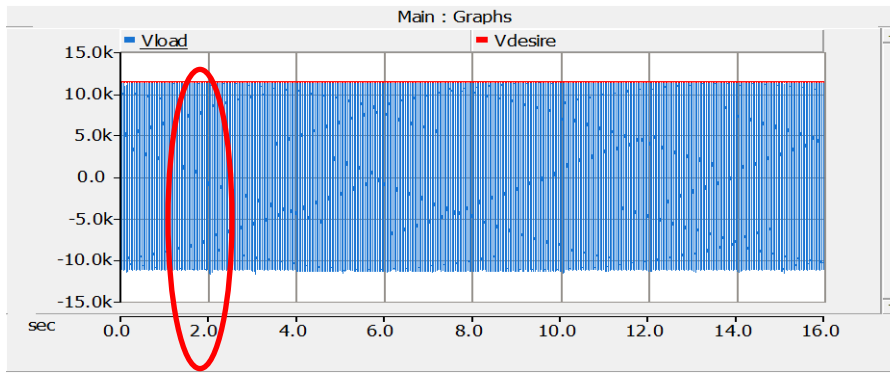
Figure 5.25: The load voltage with fault at 2s under the inductive load.

5.7   Experimental Results

A 33 kVA single-phase CL-EVR was prototyped and constructed and tested. To test the

CL-EVR only, the 8kV nominal voltage was not applied, and the CL-EVR was directly

connected to the load in the manner of Figure 5.1. Also, the experiment was conducted

with a 120 V laboratory source instead of the 400 V source to check the basic operation.

The test verifies whether changing the voltage order to the CL-EVR results in it applying

the ordered voltage to the load. Figure 5.26 shows the measured load voltage oscillogram

when the load voltage order is stepped from level one to level sixteen (120 V) in 16 steps,

and then back from level sixteen to level eight (60 V) with an 11 A resistive load. Figure

5.27 shows the injected voltage for a 2 A inductive load with the same voltage steps. As is

evident, the voltage follows the order between the levels without significant overshoot.

Figure 5.28 gives a more detailed view of the injected voltage for the 2A inductive load

case when the voltage order changes only over one step from level 1 to level 2. Similarly,

Figure 5.29 shows the CL-EVR voltage when switching from level 2 to level 1. As can be

seen, the changeover from one level to the other is achieved smoothly without a significant

transient. Figure 5.30 demonstrates the results for the voltage across the TRIAC, as it is

shown the voltage is around 1.2V close to what is mentioned in the datasheet of the TRIAC.

Figure 5.26: The voltage across the resistive load up-stepped from level 1 to 16 and subsequently down-stepped from level 16 to 8.
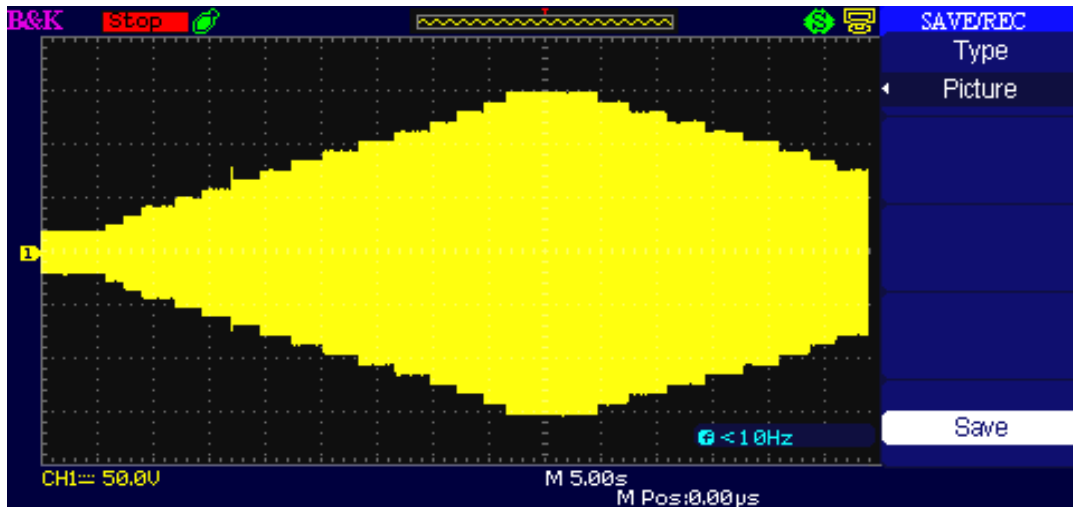
Figure 5.27: The voltage across the inductive load being up-stepped from level 1 to 16 and subsequently down-stepped from level 16 to 8.
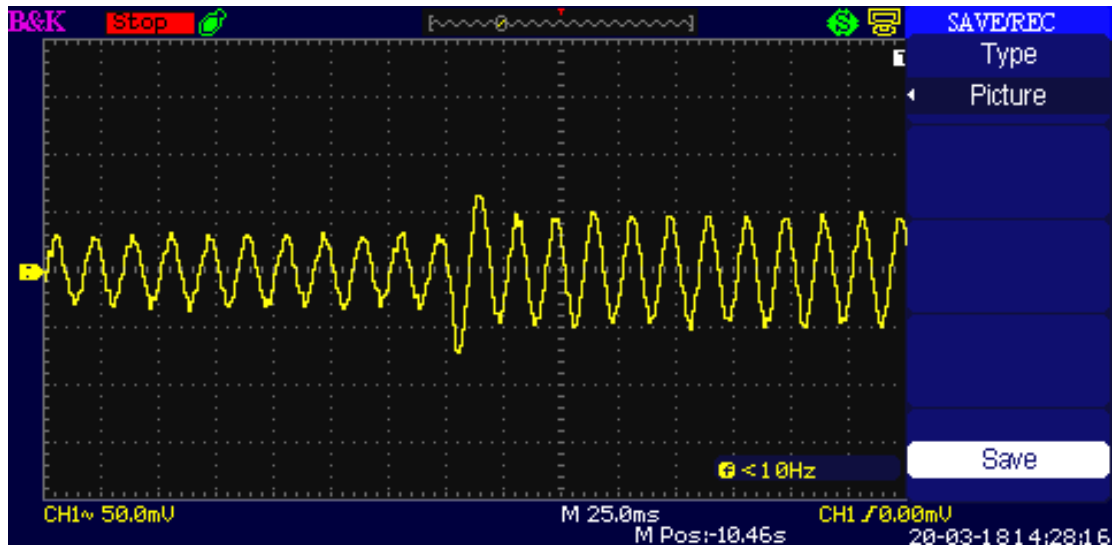
Figure 5.28: The transition from level 1 to level 2 under inductive load.
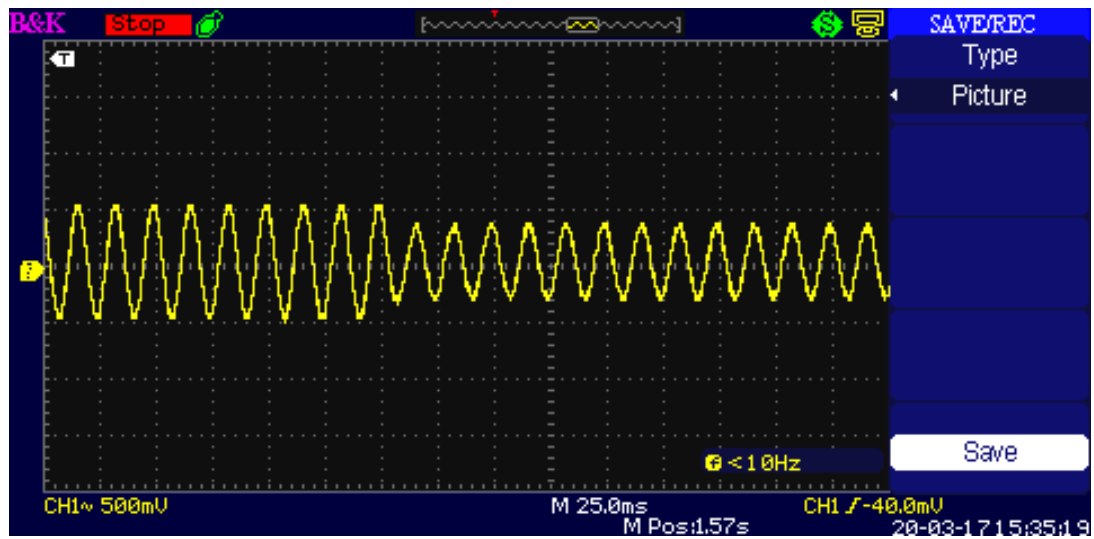
Figure 5.29: The transition from level 2 to level 1 under inductive load.
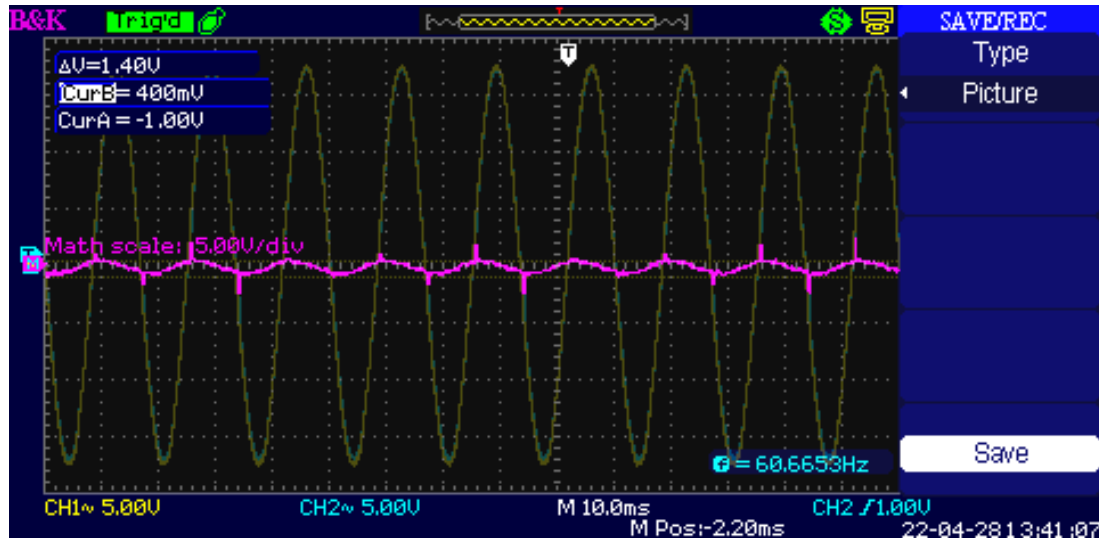
Figure 5.30: The input voltage showed with yellow color and the voltage across the
TRIAC T_{16} when it is on showed with purple color.

5.8   Chapter Conclusion

In this chapter, a new approach for the electronic voltage regulator to be used as a substitute

for the electromechanical tap changer is proposed. The proposed new topology in this

thesis can apply additive or subtractive (aka boost or buck) voltages to compensate for an

increase or decrease in system voltages. This regulator employs a ladder of power

capacitors which are in series and connected across the input voltage to apply different

levels of voltages to a controlled or regulated transformer. Considering this, the proposed

Electronic Voltage Regulator (CL-EVR) can be utilized as a replacement for conventional

electromechanical type on-load tap changers (OLTCs) commonly used in power

transformers and meant to compensate for voltage changes in a system. Electromechanical

tap changers have some significant issues, such as defined time durations when switching

to different taps, as determined by the spring-loaded mechanism's operation; a high

malfunction rate due to mechanical switching when causing arcing, and thereby decreasing

the operating lifetime of transformers. In this CL-EVR instead of electromechanical taps, a combination of capacitors and TRIACs are used at each voltage level to eliminate arcing effects while increasing the speed of the tap changing process. Furthermore, the electronic regulator can improve the load power factor due to the presence of capacitors. Other advantages over conventional OLTC's are the elimination need for a reactor is used, and the elimination of a tapped winding with its numerous taps leads, with a correspondingly higher cost. This will reduce the overall size of the active part of the main transformers and improve efficiency by reducing operating losses.

Any potential inductive load impedance ranges where resonance due to L-C oscillations between the capacitor and inductive loads can occur were identified using phasor analysis. This allowed for the capacitor values to be designed so that resonance is avoided in the normal operating range of the CL-EVR.

The Laplace analysis was performed to consider the transient and steady-state behaviour of the CL-EVR under different loads. This provided a sanity check on the EMT simulation results as the two agreed almost perfectly.

A new failure detection method is included that detects a failed TRIAC to enable the system to continue operating. The failure detection circuit is seamlessly incorporated within the main circuit and has a high-speed detection rate.

Finally, a 33kVA single-phase CL-EVR was prototyped at the laboratory and examined under different load conditions. The experimental results prove that the proposed CL-EVR can provide the different portions of the voltage under different loads properly. The voltage transition from one level to the other is smooth and without any significant transients under the resistive and inductive loads.

Chapter 6: Contributions, Conclusions, and Future Work

In this chapter, a brief overview of this work, the main contributions, and conclusions of the research are given. In the end, some suggestions are provided as directions for future works.

6.1   Contributions and Conclusions

1. A thorough investigation of Electronic Voltage Regulators (CL-EVRs) including electromechanical and solid-state tap changers was conducted. The upsides and downsides of these tap changers were assessed, to improve CL-EVR characteristics.

2. A major missing aspect in the previous academic literature was identified. Missing in the previous work on electro-mechanical tap changers was the analysis of the transient behaviour of the change-over switch. This thesis proposed a new model to predict the transient behaviour of the change-over switch based on two important factors related to transient studies– namely the recovery voltages and the magnitude of the currents in the contacts during change-over operation. The new model utilized Mayer's arc model to simulate the floating condition of the change-over switch while changing from one contact to the other. The proposed model was

validated by theoretical analysis both with and without a tie-in resistor, and they match each other with an error of less than 2.29%.

3. After an in-depth analysis of the electromechanical and solid-state tap changers, it was found that there are yet-to-be solved issues such as pitting on mechanical contacts, arc issues, high maintenance cost, and high malfunction rate. Voltage Source Converters (VSC) based taps injections have been proposed as a solution recently. In this thesis, the previous literature on VSCs was investigated. Finally, a converter-based on-load tap changer (COLTC) was proposed.

4. Based on the EMT simulation results, the proposed COLTC can manage the problems associated with the traditional tap changers. The benefits of the proposed COLTC include less transient voltage and current, no arcing and pitting on mechanical contacts, no need to change-over switch and tie-in resistor, and the ability to provide voltage with different phase angles because of Sinusoidal Pulse Width Modulation (SPWM). Also, the presented COLTC can maintain the load voltage in an acceptable range both under resistive and inductive loads. However, the COLTC has some downsides such as the need for an L-C filter to reduce high-frequency harmonics and the high implementation cost. The proposed converter-based OLTC, can manage the problems corresponding to the traditional OLTCs. Nevertheless, the COLTC has some drawbacks such as high implementation cost, complicated control system, and high voltage stress on the power switches of the VSC.

5. To address the above drawbacks, a much-improved novel capacitive ladder-based electronic voltage regulator (CL-EVR) topology was proposed. The proposed CL-

EVR is free of mechanical contacts and tapped windings. It utilizes a ladder of capacitor and solid-state switches (TRIACs) instead of mechanical taps. The elimination of mechanical taps gets rid of the arcing and pitting on contacts experienced in the case with a traditional OLTC. An H-bridge circuit is included downstream of the capacitive divider so that the voltage to be injected can be applied in an additive or subtractive mode, thereby increasing the voltage adjustment range of the overall CL-EVR. Also, the output of the CL-EVR is purely sinusoidal, so no filtering is required as was the case with COLTC.

6. Electromagnetic Transient (EMT) Simulation is used to design and debug the controls for operation under various loads for a 100 kVA (3-phase) capacitive ladder-type CL-EVR. The simulation results showed that the proposed CL-EVR can maintain the load voltage within a 0.5% deviation from the rated voltage of the load. Also, for the operating load range, the maximum transient voltage across each component is less than the manufacturer's allowable maximum. This was also confirmed with lab tests. For example, the maximum transient voltage across the capacitor in the ladder is 50% less than the rating of the selected capacitor for the experimental test.

7. To sanity-check the EMT simulation results, a thorough theoretical steady-state and Laplace-transform-based transient calculation was performed. The theoretical results matched the EMT simulation results very well, thereby validating the latter.

8. Any potential inductive load impedance ranges where resonance due to L-C oscillations between the capacitor and inductive load can occur were identified

using phasor analysis. This allowed for the capacitor values to be designed so that resonance is avoided in the normal operating range of the CL-EVR.

9. A new failure detection method and isolation controller was proposed that detects a faulted TRIAC and isolates it so that the CL-EVR keeps working post-failure. TRIAC failure detection is initiated when the main winding voltage changes due to a system event (e.g., remote fault) triggering a change of voltage level by the CL-EVR controller. During this time, the proposed method compares the CL-EVR voltage with a pre-defined threshold. if the CL-EVR voltage is larger than the threshold, it indicates that the last conducting TRIAC is faulted and has not turned off. On TRIAC fault detection, the control system sends a "turn-off" signal to a microswitch in series with the failed TRIAC to isolate it so it is no longer in the circuit. Hence, The CL-EVR can still keep working without any interruption, although there is a one-less level for the selectable voltage.

10. The proposed CL-EVR was experimentally tested and investigated. The results proved that the CL-EVR can provide different voltage levels to the load properly. According to the experimental result of the load voltage, the transition from one level to the other is smooth both under the inductive and resistive loads without any significant transient.

6.2   Limitations and Future works

There are some possible paths for continuing this work which are itemized here:

1. The CL-EVR can perfectly work in the 100 kVA rating. However, the load effect on CL-EVR because of the capacitor ladder is an important factor. When the load

current increases, a phase shift will happen, which can negatively affect the voltage regulation. Using different capacitor sizes for each level could be investigated as a solution to more optimally manage the load effect issue.

2. During the field test of the CL-EVR, the H-bridge TRIACs failed to turn on at very low voltages (below 14 V on the 400 V full scale). The problem could be solved by lowering the gate resistor. However, reducing the gate resistor could make the TRIAC more susceptible to failure resulting from a high inrush gate current. The design could be further optimized by investigating other solid-state switch elements such as Insulted Gate Bipolar Transistors (IGBTs) in the H-bridge circuit.

3. The proposed model for the change-over switch transient behaviour can provide a very precise result when the change-over switch starts to move. However, the modelling is not precise as we have not used an arc model to precisely model the situation when an arc is initiated as the contact comes close to its final position. An improved model considering arc initiation could be developed in the future.

4. Another path to future work can be decreasing the failure detection processing time to detect the failed TRIAC faster than the proposed method, which requires at least a cycle.

5. Implementing the proposed CL-EVR in real-time power system simulation tools (e.g. RTDS[5]) could be beneficial to investigating larger system-level impacts of the proposed device.

---

[5] Real time Digital Simulator

6.3 Publications and patents resulting from the thesis

6.3.1 Publications:

1. Abolfazl Babaei, Waldemar Ziomek, Aniruddha M. Gole, "A Multi-Level Inverter Based On-Load Tap Changer Transformer Topology for Harnessing Photo-Voltaic Energy," 2021 IEEE Electrical Power and Energy Conference (EPEC), Toronto, Ontario, October 22-24, 2021.

2. Abolfazl Babaei, Waldemar Ziomek, Aniruddha M. Gole, "A New Approach for the Failure Detection and the Self-healing Process in A Solar-based Tap Changing Transformer," 2022 IEEE International Conference on Electrical, Computer and Energy Technologies (ICECET), Prague, Czech Republic, July 20-22, 2022.

3. Abolfazl Babaei, Waldemar Ziomek, Aniruddha M. Gole, "The Improvement of Power Quality in an ac-ac Direct Matrix Converter by Using Hybrid Filters," 2022 IEEE International Conference on Electrical, Computer and Energy Technologies (ICECET), Prague, Czech Republic, July 20-22, 2022.

4. Abolfazl Babaei, Waldemar Ziomek, Aniruddha M. Gole, "A Comparative Study on Solar-Based Multilevel Inverters as A Substitute for Existing OLTCs," 2022 IEEE Canadian Conference on Electrical and Computer Engineering (CCECE), Halifax, Canada, Septmeber 20-22, 2022.

5. Abolfazl Babaei, Waldemar Ziomek, Aniruddha M. Gole, "Transient characteristics of on-load tap changers during change-over operation," Electric Power Systems Research Journal (ELSEVIER), Volume 197, 2021, 107296, ISSN 0378-7796.

6. Abolfazl Babaei, Waldemar Ziomek, Aniruddha M. Gole, "A Capacitive ladder Based Power Electronic Ac Voltage Regulator," Submitted to IEEE Transactions on Industrial Electronics.

6.3.2 Patents

7. George Partyka, Waldemar Ziomek, Abolfazl Babaei, Greg Parson, Aniruddha M. Gole, "Electronic Voltage Regulator Apparatus and Method," U.S. Patent 17/703,369. March 24, 2022.

8. George Partyka, Waldemar Ziomek, Abolfazl Babaei, Greg Parson, Aniruddha M. Gole, "Electronic Voltage Regulator Apparatus and Method," Canadian Patent Application 3,153,423. March 24, 2022.

References

1. A. Krämer, "On-Load Tap-Changers for Power Transformers –Operation, Principles, Applications and Selection," 2nd edition, Kerschensteiner Verlag, Lappersdorf, Germany, 2014. ISBN 978-3- 931954-47-5.

2. "IEEE Power, Distribution & Regulating Transformers Collection: VuSpec(TM)," in IEEE Power, Distribution & Regulating Transformers Collection: VuSpec(TM) , vol., no..

3. "IEEE Guide for Dry-Type Transformer Through-Fault Current Duration," in IEEE Std C57.12.59-2015 (Revision of IEEE Std C57.12.59-2001), vol., no., pp.1-21, 6 Nov. 2015, doi: 10.1109/IEEESTD.2015.7320937.

4. D. Martin, J. Marks, T. Saha., "Survey of Australian power transformer failures and retirements," IEEE Electrical Insulation Magazine, vol. 33, no. 5, pp. 16-22, 2017.

5. A.G. Kay, "The monitoring and protection of on load tap changers", Condition Monitoring of Large Machines and Power Transformers, IEEE Colloquium, 19 June 1997, London, pp. 5/1 - 5/9, 1997.

6. C. Oates, A. Barlow, V. Levi, "Tap changer for distributed power", 12th Conference on Power Electronics and Applications 2 – 5 September 2007, Aalborg, Denmark, 2007.

7. M.A. Redfern, W.R.C. Handley, "Duty based maintenance for on-load transformer tap changers", Power Engineering Society Summer Meeting, Conference Proceedings, Vol. 3, 15 - 19 July 2001, Vancouver, Canada, pp. 1824 – 1829, 2001.

8. A. Cichoń, "New method for tap changer diagnostics", Nowa metoda diagnostyki stanu technicznego podobciążeniowych przełączników zaczepów", Studia i Monografie, Wydawnictwo Politechniki Opolskiej, z. 259, Opole, 2011.

9. Li Xiaoming, Liao Qingfen, Yin Xianggen and Xie Jianghui, "A new on-load tap changing system with power electronic elements for power transformers," Proceedings. International Conference on Power System Technology, Kunming, China, 2002, pp. 556-559 vol.1, doi: 10.1109/ICPST.2002.1053604.

10. J. H. Harlow and F. A. Stich, "An Arcless Approach to Step-Voltage Regulation," in IEEE Power Engineering Review, vol. PER-2, no. 7, pp. 47-48, July 1982, doi: 10.1109/MPER.1982.5521087.

11. K. A. Krishnamurthy and R. M. Mathur, "Improvements in a Thyristor Controlled Static on-Load Tap-Changer for Transformers," in IEEE Transactions on Power Apparatus and Systems, vol. PAS-101, no. 9, pp. 3091-3096, Sept. 1982, doi: 0.1109/TPAS.1982.317520.

12. M. T. Richardson, G. A. Henry and N. R. Mckennon, "Microcontroller Based Solid State on-Load Tap Changer for Pole Mounted Transformers," SoutheastCon 2021, 2021, pp. 1-4, doi: 10.1109/SoutheastCon45413.2021.9401818.

13. R. Fourie and H. d. T. Mouton, "Development of a MV IGBT based solid-state tap changer," AFRICON 2009, 2009, pp. 1-6, doi: 10.1109/AFRCON.2009.5308128.

14. D. Nadeem, Haroon-ur-Rashid and M. Saeed, "Fully electronic tap changer control," 2013 IEEE Conference on Clean Energy and Technology (CEAT), 2013, pp. 114-117, doi: 10.1109/CEAT.2013.6775610.

15. R. C. Degeneff, "A new concept for a solid-state on-load tap changers," 14th International Conference and Exhibition on Electricity Distribution. Part 1. Contributions (IEE Conf. Publ. No. 438), 1997, pp. 7/1-7/4 vol.1, doi: 10.1049/cp:19970447.

16. Y. H. Chung, G. H. Kwon, T. B. Park and K. Y. Lim, "Dynamic voltage regulator with solid state switched tap changer," CIGRE/IEEE PES International Symposium Quality and Security of Electric Power Delivery Systems, 2003. CIGRE/PES 2003., 2003, pp. 105-108, doi: 10.1109/QSEPDS.2003.159804.

17. P. Bauer and R. Schoevaars, "Bidirectional switch for a solid state tap changer," IEEE 34th Annual Conference on Power Electronics Specialist, 2003. PESC '03., 2003, pp. 466-471 vol.1, doi: 10.1109/PESC.2003.1218336.

18. D. Monroy, A. Gomez-Exposito and E. Romero-Ramos, "Improving the voltage regulation of secondary feeders by applying solid-state tap changers to MV/LV transformers," 2007 9th International Conference on Electrical Power Quality and Utilisation, 2007, pp. 1-6, doi: 10.1109/EPQU.2007.4424122.

19. D. Monroy-Berjillos, A. Gómez-Expósito and A. Bachiller-Soler, "A Lab Setup Illustrating Thyristor-Assisted Under-Load Tap Changers," in IEEE Transactions on Power Systems, vol. 25, no. 3, pp. 1203-1210, Aug. 2010, doi: 10.1109/TPWRS.2009.2039717.

20. Hao Jiang, R. Shuttleworth, B. A. T. Al Zahawi, X. Tian and A. Power, "Fast response GTO assisted novel tap changer," in IEEE Transactions on Power Delivery, vol. 16, no. 1, pp. 111-115, Jan. 2001, doi: 10.1109/61.905608.

21. P. Bauer and S. W. H. De Haan, "Solid state tap changers for utility transformers," 1999 IEEE Africon. 5th Africon Conference in Africa (Cat. No.99CH36342), 1999, pp. 897-902 vol.2, doi: 10.1109/AFRCON.1999.821888.

22. J. de Oliveira Quevedo et al., "Analysis and Design of an Electronic On-Load Tap Changer Distribution Transformer for Automatic Voltage Regulation," in IEEE Transactions on Industrial Electronics, vol. 64, no. 1, pp. 883-894, Jan. 2017, doi: 10.1109/TIE.2016.2592463.

23. R. Echavarria, A. Claudio and M. Cotorogea, "Analysis, Design, and Implementation of a Fast On-Load Tap Changing Regulator," in IEEE Transactions on Power Electronics, vol. 22, no. 2, pp. 527-534, March 2007, doi: 10.1109/TPEL.2006.889938.

24. J. Faiz and B. Siahkolah, "New Controller for an Electronic Tap Changer—Part II: Measurement Algorithm and Test Results," in IEEE Transactions on Power Delivery, vol. 22, no. 1, pp. 230-237, Jan. 2007, doi: 10.1109/TPWRD.2006.881423.

25. S. M. Fernández, S. M. García, C. C. Olay, J. C. Campo Rodríguez, R. V. García and J. V. López, "Electronic Tap Changer for Very High-Power Medium-Voltage Lines With No Series–Parallel Thyristors," in IEEE Transactions on Industrial Electronics, vol. 65, no. 7, pp. 5237-5249, July 2018, doi: 10.1109/TIE.2017.2777380.

26. E. O. Hasan, A. Y. Hatata, E. A. Badran and F. H. Yossef, "Voltage Control of Distribution Systems Using Electronic OLTC," 2018 Twentieth International Middle East Power Systems Conference (MEPCON), 2018, pp. 845-849, doi: 10.1109/MEPCON.2018.8635151.

27. T. Larsson, R. Innanen and G. Norstrom, "Static electronic tap-changer for fast phase voltage control," 1997 IEEE International Electric Machines and Drives Conference Record, 1997, pp. TC3/4.1-TC3/4.3, doi: 10.1109/IEMDC.1997.604265.

28. Y. P. Agalgaonkar, B. C. Pal and R. A. Jabr, "Distribution Voltage Control Considering the Impact of PV Generation on Tap Changers and Autonomous Regulators," in IEEE Transactions on Power Systems, vol. 29, no. 1, pp. 182-192, Jan. 2014, doi: 10.1109/TPWRS.2013.2279721.

29. P. Bauer and S. W. H. de Haan, "Electronic tap changer for 500 kVA/10 kV distribution transformers: design, experimental results and impact in distribution networks," Conference Record of 1998 IEEE Industry Applications Conference. Thirty-Third IAS Annual Meeting (Cat. No.98CH36242), 1998, pp. 1530-1537 vol.2, doi: 10.1109/IAS.1998.730344.

30. R. Bhuyan, A. R. Mor, P. Morshuis, G. C. Montanari and W. Erinkveld, "Analysis of the arcing process in on-load tap changers by measuring the acoustic signature," 2014 IEEE Electrical Insulation Conference (EIC), 2014, pp. 193-197, doi: 10.1109/EIC.2014.6869374.

31. T. B. Shanker, H. N. Nagamani and G. S. Punekar, "Acoustic emission signal analysis of On-Load Tap Changer (OLTC)," 2013 IEEE 1st International Conference on Condition Assessment Techniques in Electrical Systems (CATCON), 2013, pp. 347-352, doi: 10.1109/CATCON.2013.6737525.

32. A. Cichon, T. Borucki, T. Boczar and D. Zmarzly, "Characteristic of acoustic emission signals generated by electric arc in on load tap changer," Proceedings of 2011 International Symposium on Electrical Insulating Materials, 2011, pp. 437-439, doi: 10.1109/ISEIM.2011.6826306.

33. A. Cichoń, T. Boczar, P. Frącz and D. Zmarzły, "Detection of defects in on-load tap-changers using acoustic emission method," 2012 IEEE International Symposium on Electrical Insulation, 2012, pp. 184-188, doi: 10.1109/ELINSL.2012.6251454.

34. Feizifar, B., Usta, O. "Failure Detection of On-Load Tap-Changers Using a New Power-Based Algorithm," Arab J Sci Eng 44, 6967–6976 (2019). https://doi.org/10.1007/s13369-019-03733-w.

35. Li Xiaoming, Liao Qingfen, Yin Xianggen and Xie Jianghui, "A new on-load tap changing system with power electronic elements for power transformers," Proceedings. International Conference on Power System Technology, Kunming, China, 2002, pp. 556-559 vol.1, doi: 10.1109/ICPST.2002.1053604.

36. E. Martinez, I. Fernandez and J. M. Canales, "Thyristor based solid state tap changer for distribution transformers," 2013 IEEE 11th International Workshop of Electronics, Control, Measurement, Signals and their application to Mechatronics, 2013, pp. 1-5, doi: 10.1109/ECMSM.2013.6648942.

37. J. Faiz and B. Siahkolah, "New solid-state onload tap-changers topology for distribution transformers," in IEEE Transactions on Power Delivery, vol. 18, no. 1, pp. 136-141, Jan. 2003, doi: 10.1109/TPWRD.2002.803723.

38. J. Faiz and B. Siahkolah, "New Controller for an Electronic Tap Changer—Part I: Design Procedure and Simulation Results," in IEEE Transactions on Power Delivery, vol. 22, no. 1, pp. 223-229, Jan. 2007, doi: 10.1109/TPWRD.2006.881424.

39. R. C. Degeneff, "A new concept for a solid-state on-load tap changers," 14th International Conference and Exhibition on Electricity Distribution. Part 1. Contributions (IEE Conf. Publ. No. 438), 1997, pp. 7/1-7/4 vol.1, doi: 10.1049/cp:19970447.

40. J. Faiz and B. Siahkolah, "Differences between conventional and electronic tap-changers and modifications of controller," in IEEE Transactions on Power Delivery, vol. 21, no. 3, pp. 1342-1349, July 2006, doi: 10.1109/TPWRD.2005.861323.

41. A. Babaei, W. Ziomek, A M. Gole, "Transient characteristics of on-load tap changers during change-over operation," Electric Power Systems Research, Volume 197, 2021, 107296, ISSN 0378-7796.

42. Joon-Ho Choi and Jae-Chul Kim, "Advanced voltage regulation method at the power distribution systems interconnected with dispersed storage and generation systems," in IEEE Transactions on Power Delivery, vol. 15, no. 2, pp. 691-696, April 2000, doi: 10.1109/61.853006.

43. Tae-Eung Kim and Jae-Eon Kim, "Considerations for the feasible operating range of distributed generation interconnected to power distribution system," IEEE Power Engineering Society Summer Meeting,, 2002, pp. 42-48 vol.1, doi: 10.1109/PESS.2002.1043175.

44. T. Senjyu, Y. Miyazato, A. Yona, N. Urasaki and T. Funabashi, "Optimal Distribution Voltage Control and Coordination With Distributed Generation," in IEEE Transactions on Power Delivery, vol. 23, no. 2, pp. 1236-1242, April 2008, doi: 10.1109/TPWRD.2007.908816.

45. S. Agarwal and S. R. Deore, "Level shifted SPWM of a seven-level cascaded multilevel inverter for STATCOM applications," 2015 International Conference on Nascent Technologies in the Engineering Field (ICNTE), 2015, pp. 1-7.

46. Y. Cheng, C. Qian, M. L. Crow, S. Pekarek and S. Atcitty, "A Comparison of Diode-Clamped and Cascaded Multilevel Converters for a STATCOM With Energy Storage," in IEEE Transactions on Industrial Electronics, vol. 53, no. 5, pp. 1512-1521, Oct. 2006.

47. S. Choudhury, S. Nayak, T. P. Dash and P. K. Rout, "A comparative analysis of five level diode clamped and cascaded H-bridge multilevel inverter for harmonics reduction," 2018 Technologies for Smart-City Energy Security and Power (ICSESP), 2018, pp. 1-6.

48. A. Babaei, A. Akbari, A. B. Vandaei and H. Rezaei, "A Multilevel Inverter with High Efficiency, High Stability, and Low Cost," 2019 5th Conference on Knowledge Based Engineering and Innovation (KBEI), 2019, pp. 899-904.

49. A. Babaie, B. Karami and A. Abrishamifar, "Improved equations of switching loss and conduction loss in SPWM multilevel inverters," 2016 7th Power Electronics and Drive Systems Technologies Conference (PEDSTC), 2016, pp. 559-564.

50. A. Babaei, I. Kaffashan and A. Abrishamifar, "An Improved Threefold Interleaved PFC Circuit with Better Voltage Profile and Optimizing Current-Sharing Method," in IEEE Canadian Journal of Electrical and Computer Engineering, vol. 44, no. 2, pp. 253-260, Spring 2021.

51. A. Babaei, I. Kaffashan and A. Abrishamifar, "An Optimized Zero-Current, Zero-Voltage, and Three-Level DC–DC Converter," in IEEE Canadian Journal of Electrical and Computer Engineering, vol. 44, no. 2, pp. 216-222, Spring 2021, doi: 10.1109/ICJECE.2020.3037638.

52. A. Babaei, F. Poormohammadi, A. Abrishamifar, " An Improved Inverter for Renewable Energy Applications with Solid State Transformers", 4th International Conference on Science and Engineering, July 2018, Rome, Italy.

53. A. Babaei, H. Rezaei and A. B. Vandaei, "An Improved Method for Reliability Calculation of Multilevel Inverters," 2019 5th Conference on Knowledge Based Engineering and Innovation (KBEI), Tehran, Iran, 2019, pp. 372-377.

54. H. Rezaei and A. Babaei, "Thermal analysis of inverters and high frequency transformers in the DC-DC converters," 2017 IEEE 4th International Conference on Knowledge-Based Engineering and Innovation (KBEI), Tehran, 2017, pp. 0125-0130.

55. S. Ahmad, F. I. Bakhsh and M. S. Jamil Asghar, "A novel DC-to-AC controlled multi-level inverter," IMPACT-2013, 2013, pp. 315-319, doi: 10.1109/MSPCT.2013.6782144.

56. M. Anzari, J. Meenakshi and V. T. Sreedevi, "Simulation of a transistor clamped H-bridge multilevel inverter and its comparison with a conventional H-bridge multilevel inverter," 2014 International Conference on Circuits, Power and Computing Technologies [ICCPCT-2014], 2014, pp. 958-963, doi: 10.1109/ICCPCT.2014.7054952.

57. S. S. Barah and S. Behera, "An Optimize Configuration of H-Bridge Multilevel Inverter," 2021 1st International Conference on Power Electronics and Energy (ICPEE), 2021, pp. 1-4, doi: 10.1109/ICPEE50452.2021.9358533.

58. N. Benaifa, H. Bierk, B. Ajayi and E. Nowicki, "Parallel operated inverters as a multilevel case," 2008 Canadian Conference on Electrical and Computer Engineering, 2008, pp. 002003-002006, doi: 10.1109/CCECE.2008.4564896.

59. R.Ekström,K.Thomas,andM.Leijon,"Fast solid-state on-load tap change using two current-controlled voltage-source inverters," IET Power Electron., vol. 7, no. 10, pp. 2610–2617, 2014.

60. A. Hota, V. Sonti, S. Jain and V. Agarwal, "Common Mode Voltage Elimination in Single-Phase Multilevel Inverter using a 3rd Leg," 2021 International Conference on Sustainable Energy and Future Electric Transportation (SEFET), 2021, pp. 1-5, doi: 10.1109/SeFet48154.2021.9375643.

61. H. Chen and D. Divan, "Design of a 10-kV·A Soft-Switching Solid-State Transformer (S4T)," in IEEE Transactions on Power Electronics, vol. 33, no. 7, pp. 5724-5738, July 2018.

62. A. Mittal, K. Janardhan and A. Ojha, "Multilevel inverter-based Grid Connected Solar Photovoltaic System with Power Flow Control," 2021 International Conference on Sustainable Energy and Future Electric Transportation (SEFET), 2021, pp. 1-6, doi: 10.1109/SeFet48154.2021.9375753.

63. A. Kahwa, H. Obara and Y. Fujimoto, "Design of 5-level reduced switches count H-bridge multilevel inverter," 2018 IEEE 15th International Workshop on Advanced Motion Control (AMC), 2018, pp. 41-46, doi: 10.1109/AMC.2019.8371060.

64. S. Senthil and K. Ravi, "A New Interconnection Of Micro Grid Distributed Energy Sources Using Space Vector Multilevel Inverter," 2019 International Conference on Computation of Power, Energy, Information and Communication (ICCPEIC), 2019, pp. 028-033, doi: 10.1109/ICCPEIC45300.2019.9082351.

65. S. Vijayalakshmi et al., "A Hybrid Multilevel Inverter for Electric Vehicle Applications," 2021 2nd International Conference for Emerging Technology (INCET), 2021, pp. 1-5, doi: 10.1109/INCET51464.2021.9456364.

66. P. Karuppanan and K. K. Mahapatra, "FPGA based cascaded multilevel pulse width modulation for single phase inverter," 2010 9th International Conference on Environment and Electrical Engineering, 2010, pp. 273-276, doi: 10.1109/EEEIC.2010.5489988.

67. A. Prayag and S. Bodkhe, "A comparative analysis of classical three phase multilevel (five level) inverter topologies," 2016 IEEE 1st International Conference on Power Electronics, Intelligent Control and Energy Systems (ICPEICES), 2016, pp. 1-5, doi: 10.1109/ICPEICES.2016.7853567.

68. H. Jafari, M. Hassanifar, D. Nazarpour and S. Golshannavaz, "A New Hybrid Three-Phase Multilevel Inverter Devoted to Electric Drive with Constant Volt per Hertz Control," 2021 12th Power Electronics, Drive Systems, and Technologies Conference (PEDSTC), 2021, pp. 1-6, doi: 10.1109/PEDSTC52094.2021.9405935.

69. S. Maurya, D. Mishra, K. Singh, A. K. Mishra and Y. Pandey, "An Efficient Technique to reduce Total Harmonics Distortion in Cascaded H- Bridge Multilevel Inverter," 2019 IEEE International Conference on Electrical, Computer and Communication Technologies (ICECCT), 2019, pp. 1-5, doi: 10.1109/ICECCT.2019.8869424.

70. Abolfazl Babaei, Waldemar Ziomek, Aniruddha M. Gole, "A Multi-Level Inverter Based On-Load Tap Changer Transformer Topology for Harnessing Photo-Voltaic Energy," 2021 IEEE Electrical Power and Energy Conference (EPEC), Toronto, Ontario, October 22-24,2021.

71. M. Gazdović and T. Šimović, "Digitalization of regulation unit selection process in power transformer design," 2018 41st International Convention on Information and Communication Technology, Electronics and Microelectronics (MIPRO), 2018, pp. 1495-1500, doi: 10.23919/MIPRO.2018.8400269.

72. J. Lin et al., "Research on Vibration Signal of Transformer On- load Tap Changer Based on Kurtosis and Tunable Q-factor Wavelet Transform," 2021 IEEE 4th International Electrical and Energy Conference (CIEEC), 2021, pp. 1-4, doi: 10.1109/CIEEC50170.2021.9510855.

73. S. M. Al-Ameri, A. Allawy Alawady, M. F. Mohd Yousof, M. Saufi Kamarudin and H. A. Illias, "The Effect of Tap Changer Coking and Pitting on Frequency Response Analysis Measurement of Transformer," 2021

IEEE International Conference on the Properties and Applications of Dielectric Materials (ICPADM), 2021, pp. 21-24, doi: 10.1109/ICPADM49635.2021.9493956.

74. X. Quan, Y. Li, Y. Zhiyong, X. Shunkai, Y. Shan and Z. Chunhang, "Research on Characteristics of Thyristors Applied to On-Load Tap-Changer," 2020 Asia Energy and Electrical Engineering Symposium (AEEES), 2020, pp. 291-295, doi: 10.1109/AEEES48850.2020.9121463.

75. Y. Bing, Z. Lin, L. Haofan and Y. Yong, "Analysis of Time Domain Characteristic of Transformer On-load Tap-changer," 2021 6th International Conference on Integrated Circuits and Microsystems (ICICM), 2021, pp. 390-393, doi: 10.1109/ICICM54364.2021.9660290.

76. J. C. Castro, G. S. Lagos and O. A. Gonzalez, "Simulation and measuring transients in On-Load Tap Changers," in IEEE Latin America Transactions, vol. 15, no. 10, pp. 1901-1907, Oct. 2017, doi: 10.1109/TLA.2017.8071234.

77. L. Bao, Y. Yuan, Y. Lei, Q. Zhu, W. Zhang and L. Zhao, "Simulation and Experimental Study of Switching Transient Process of On-load Tap Changer of Converter Transformer," 2020 IEEE International Conference on High Voltage Engineering and Application (ICHVE), 2020, pp. 1-4, doi: 10.1109/ICHVE49031.2020.9279460.

78. L. Wang, T. Yeh, W. Lee and Z. Chen, "Analysis of a Commercial Wind Farm in Taiwan Part II: Different Current-Limit Reactors and Load Tap Changers on System Performance," in IEEE Transactions on Industry Applications, vol. 47, no. 2, pp. 954-964, March-April 2011, doi: 10.1109/TIA.2010.2091373.

79. Jae-Hyeong Suh, Bum-Seok Suh and Dong-Seok Hyun, "A new snubber circuit for high efficiency and overvoltage limitation in three-level GTO inverters," in IEEE Transactions on Industrial Electronics, vol. 44, no. 2, pp. 145-156, April 1997, doi: 10.1109/41.564152.

80. 0.Mayr," Beitrage zur Theorie des Statischen und des, Dynamischen Lichtbogens," Archiv für Elektrotechnik 37 (12) (1943) 588–608.

81. A.M.Cassie, "Arc rupture and circuit severity : A new theory," CIGRE Rep.102,1939.

82. P.H. Schavemaker and L. Van der Sluis,"The Arc Model Blockset," Proceedings of the Second IASTED International Conference POWER AND ENERGY SYSTEMS (EuroPES) June 25-28, 2002, Crete, Greece.

83. George Partyka, Waldemar Ziomek, Abolfazl Babaei, Greg Parson, Aniruddha M. Gole, "Electronic Voltage Regulator Apparatus and Method," U.S. Patent 17/703,369. March 24, 2022.

84. George Partyka, Waldemar Ziomek, Abolfazl Babaei, Greg Parson, Aniruddha M. Gole, "Electronic Voltage Regulator Apparatus and Method," Canadian Patent Application 3,153,423. March 24, 2022.